

Recent developments and research needs in turbulence modeling of hypersonic flows

Pratikkumar Raje,¹ Eric Parish,² Jean-Pierre Hickey,³ Paola Cinnella,⁴ and Karthik Duraisamy¹

¹*University of Michigan*

²*Sandia National Labs*

³*University of Waterloo*

⁴*Sorbonne University*

(*Electronic mail: praje@umich.edu)

(Dated: 19 December 2024)

Hypersonic flow conditions pose exceptional challenges for Reynolds-Averaged Navier-Stokes (RANS) turbulence modeling. Critical phenomena include compressibility effects, shock/turbulent boundary layer interactions, turbulence-chemistry interaction in thermo-chemical non-equilibrium, and ablation-induced surface roughness and blowing effects. This comprehensive review synthesizes recent developments in adapting turbulence models to hypersonic applications, examining approaches ranging from empirical modifications to physics-based reformulations and novel data-driven methodologies. We provide a systematic evaluation of current RANS-based turbulence modeling capabilities, comparing eddy viscosity and Reynolds stress transport formulations in their ability to predict engineering quantities of interest such as separation characteristics and wall heat transfer. Our analysis encompasses the latest experimental and direct numerical simulation datasets for validation, specifically addressing two- and three-dimensional equilibrium turbulent boundary layers and shock/turbulent boundary layer interactions across both smooth and rough surfaces. Key multi-physics considerations including catalysis and ablation phenomena along with the integration of conjugate heat transfer into a RANS solver for efficient design of a thermal protection system are also discussed. We conclude by identifying the critical gaps in the available validation databases and limitations of the existing turbulence models and suggest potential areas for future research to improve the fidelity of turbulence modeling in the hypersonic regime.

I. INTRODUCTION

The development of hypersonic vehicles, including aircraft, missiles, glide vehicles, reusable launch vehicles, and spacecraft, is at the forefront of aerospace and defense research. Hypersonic vehicles are designed to operate at Mach number greater than 5 through the planetary atmosphere and they have the potential to transform military capabilities, space exploration, and commercial aviation. A hypersonic vehicle experiences a wide spectrum of flow regimes along its flight trajectory, ranging from subsonic to hypersonic speeds, continuum to free-molecular conditions, and laminar to turbulent flow behavior. These flow conditions are generally characterized using Mach (Ma : vehicle speed/sound speed), Knudsen (Kn : molecular mean free path/reference length), and Reynolds (Re : inertial/viscous forces) numbers. Moreover, high-temperature effects at hypersonic speeds lead to thermochemical non-equilibrium and result in widely varying Damköhler numbers (Da : flow time/chemical reaction times). This review focuses on the modeling of hypersonic turbulent flows in the continuum regime as the vehicle design is generally based on such flow conditions because of the associated extreme aerothermal loads. The complex nature of these flows presents a formidable challenge for accurate physical modeling and numerical analysis and demands sophisticated techniques and significant computational resources.

The complexity of modeling hypersonic turbulent flows relevant to practical applications arises from several unique physical phenomena that are not present or are significantly less pronounced at lower speeds. These include strong compressibility effects; the presence of strong shock waves that lie

close to the vehicle body and the associated shock/turbulent boundary layer interactions i.e. SBLIs; significantly high temperatures due to extreme viscous dissipation within the turbulent boundary layers and strong shock waves leading to chemical and thermal non-equilibrium and the associated turbulence/chemistry interactions i.e. TCI; and surface reactions including ablation and the associated ablative particle-flow interaction. Intense aerothermodynamic heating, unsteady pressure loads, and high skin-friction drag are the important global manifestations of the aforementioned complex physical phenomena crucial for engineering design considerations. Additionally, a better understanding of the flow-field in terms of locations of shock waves, expansion fans, turbulent boundary and free-shear layers, and separated regions including shock-induced recirculation bubbles, especially at off-design conditions, is critical for the successful and safe operation of hypersonic vehicles. For example, the shock wave from the engine cowl impinging on the pylon holding a dummy scramjet engine and shock waves impinging on the vertical tail caused severe heating and structural damage to the X-15 aircraft during its final hypersonic flight¹. Accurate prediction of these complex hypersonic flow-fields and the engineering quantities of interest (QoIs) is a significantly complex and challenging task for the Computational Fluid Dynamics (CFD) community.

The limitations of the present-day computational resources restrict the Direct Numerical Simulation (DNS)² and/or Large eddy simulations (LES)³ to grid resolutions that cannot fully resolve the salient structures present in practical engineering applications^{4,5}. A variety of methods like the wall-modeled LES (WMLES)⁶ and detached eddy simulations (DES)⁷ are developed to efficiently handle the near-wall turbulence, how-

ever, Reynolds-averaged Navier-Stokes (RANS) remains the primary workhorse for numerical predictions of practical flows in the aerospace industry. In fact, RANS-based CFD plays an important role in obtaining certification from governing regulatory bodies. In the RANS approach, the mean flow field is computed, and the effect of turbulence on the mean flow is introduced using a turbulence model. RANS requires considerably coarser grid sizes than DNS and LES and is favored in the standard engineering design process because of significantly shorter turnaround times. Turbulence modeling is a crucially important aspect of the RANS-based CFD techniques as it considerably influences predictions for aerodynamic forces, heat transfer rates, and chemical reactions.

The modeling challenges posed by the hypersonic turbulent flows are rooted in the complexity of the strain field and the high rates of change to which the mean flow as well as the turbulence fields are subjected. Additionally, cold-wall conditions, characterized by the ratio of wall temperature to the adiabatic wall (or recovery) temperature i.e. T_w/T_{aw} , are common in hypersonic flight vehicles and wind tunnel experiments. This occurs because of transient heating of the vehicle/model, active cooling or ablation of the surface, and/or radiative cooling of the surface. Strong wall cooling increases the significance of compressibility effects, impacts near-wall turbulence characteristics, and may affect SBLI properties⁸. Moreover, the surfaces of hypersonic vehicles, e.g. ballistic and maneuverable reentry vehicles, become rough, generally characterized by the dimensionless surface roughness height k_s^+ , in key aerothermal heating areas due to the ablation loss of the heat shield. This leads to an increased heat transfer at the wall which in turn accelerates the ablation process. The ablation process leads to the thermal decomposition of the materials by pyrolysis reactions. The pyrolysis products are then outgassed into the boundary layer, resulting in the blowing phenomenon. Unlike surface roughness, blowing effects on the boundary layer decrease the heat load. Thus, the ablation process critically affects the aerothermal loads in the presence of roughness and blowing effects, and modeling these effects is a significantly challenging task⁹.

Marvin¹⁰ and Marvin and Coakley¹¹ briefly discuss turbulence modeling for supersonic and hypersonic flows and evaluate the performance of several zero-, two-equation, and Reynolds stress transport models (RSTMs) against the experimental data for a number of hypersonic attached boundary layer and separated SBLI flows. Roy and Blottner¹² present a comprehensive review of the performance of a total of 18 one- and two-equation Boussinesq hypothesis-based eddy viscosity models (EVMs) including Spalart-Allmaras (SA)¹³ and the variants of $k-\epsilon$ and $k-\omega$ models against the extended hypersonic SBLI experimental database of Settles and Dodson¹⁴ consisting of nine experiments on five different geometries. Marvin *et al.*¹⁵ present a compilation of experimental validation database from 10 experiments on six different geometries along with predictions obtained using $k-\epsilon$, $k-\omega$, and SA models. However, these works consider only two-dimensional (2D)/axisymmetric hypersonic wall-bounded flows. On the other hand, performance assessment of turbulence models for three-dimensional (3D) SBLIs is limited^{16,17}.

Smits *et al.*¹⁸ reviews the status of basic research in computational methods for hypersonic turbulent flows including RANS as well as DNS, LES, and RANS-LES hybrid approaches. Georgiadis *et al.*¹⁹ provides an assessment of the “state-of-practice” in RANS with a focus on the two-equation $k-\epsilon$ and $k-\omega$ family of models for predicting hypersonic propulsion flowpaths including laminar-to-turbulent boundary layer transition, SBLIs, and modeling of the combustor and exhaust system in the context of a scramjet engine. A number of works^{20,21} provide an assessment of the standard turbulence models in predicting the hypersonic zero-pressure-gradient (ZPG) turbulent boundary layers (TBLs) and SBLIs at different wall temperature conditions. Interestingly, there is a shift in the attention and recent works focus on evaluating the performance of these models and the compressibility corrections in predicting ZPG hypersonic TBLs at cold wall conditions^{22–24}. The works discussed above generally evaluate the performance of Cebeci-Smith²⁵ and Baldwin-Lomax²⁶ zero-equation models, SA one-equation model, and $k-\epsilon$ and $k-\omega$ model variants including Menter SST $k-\omega$ ²⁷ two-equation EVMs with and without the classical compressibility corrections. However, these works consider the hypersonic flow regime where calorically perfect gas models are appropriate. A recent work⁸ performs an *a priori* assessment of the classical closures and compressibility corrections used with Menter SST $k-\omega$ model using DNS^{28,29} for ZPG TBLs at Mach numbers up to about 12.5 with different levels of wall cooling including high enthalpy conditions with thermochemical non-equilibrium.

For hypersonic flows at high-enthalpy conditions, conversion of kinetic energy into internal energy can lead to sufficiently high temperatures to induce chemical reactions and/or thermal non-equilibrium effects that greatly influence surface forces and heat transfer³⁰. Depending on the flow Damköhler number, i.e. the ratio of the flow characteristic time to the characteristic times of chemical reactions or thermal relaxation, the flow can be considered as chemically (thermally) frozen, in chemical (thermal) equilibrium or in non-equilibrium conditions. The former case occurs when thermochemical processes are very slow compared to the flow residence time ($Da \rightarrow 0$), so that the advancement of such processes is essentially negligible; on the opposite side, when the reaction or thermal relaxation occurs on very fast time scales ($Da \rightarrow \infty$), the chemical composition and thermophysical flow properties change instantaneously as the flow conditions change. In many practical cases, the flow is characterized by small but non-negligible Damköhler numbers, leading to nonequilibrium effects. In such cases, the governing equations are supplemented with additional transport equations describing the evolution of the chemical species/ions and/or the energies associated with the internal molecular degrees of freedom of polyatomic molecules^{1,31}, and most typically energies associated with vibrational modes. The Reynolds-averaged counterparts of the chemistry/vibrational energies equations involve additional unclosed terms. They are generally modeled using rough gradient approximations based on the introduction of constant nondimensional turbulent transport parameters (e.g. constant turbulent Schmidt numbers

for the species and constant vibrational Prandtl numbers for the vibrational energy, which may be highly influential on the results³². More sophisticated, nonlinear representations have been attempted with some success^{33,34}. Conducting experiments in these conditions is generally impractical or impossible, because of the extreme thermodynamic conditions and huge amounts of electric power needed to operate high-enthalpy wind tunnels³⁵. On the other hand, numerical simulations are also very challenging, depending on the complexity of the thermochemical models in use, and on the range of physical space and time scales to be simulated. Only recently, DNS data are beginning to be available^{28,29,36}, providing valuable insights into the validity of modeling assumption. The picture is further complicated if shock waves are present, promoting non-equilibrium conditions, for which experimental or high-fidelity data for turbulent high-enthalpy conditions are very scarce³⁷⁻³⁹.

This review paper aims to provide a comprehensive overview of the latest advancements in turbulence modeling for hypersonic flows. We limit our scope to the modeling of fully turbulent hypersonic boundary layer flows and do not consider transition modeling, which is also critically important in practical hypersonic flows. The performance of various turbulence modeling approaches for hypersonic flows, including zero-, one-, and two-equation eddy viscosity models, as well as RSTMs, Explicit Algebraic Reynolds Stress Models (EARSMs), and Non-Linear EVMs (NLEVMs) is discussed at length. This includes the generalization of low-speed models using compressibility corrections, heat flux modeling (e.g. variable turbulent Prandtl number models), etc. for hypersonic flows. The capabilities and limitations of these models in predicting key flow features and QoIs, such as shock-induced separations, wall pressure, surface heat transfer rates, and skin friction are highlighted. Furthermore, the ongoing challenges in hypersonic turbulence modeling, including the need for an improved physical understanding of compressibility effects on turbulence are discussed. We note here that the discussion does not involve turbulence models using wall functions, but includes the models where integration of the governing equations to the wall is performed.

The effects of thermochemical non-equilibrium relevant to high enthalpy flows expected during hypersonic flights on turbulence modeling are discussed. This includes the additional Favre-averaged species transport and vibrational energy equations and the modeling of unclosed terms therein. The available validation experimental dataset and DNS studies in the hypersonic regime including equilibrium TBLs and SBLIs over smooth and rough surfaces are provided. The emergence of machine learning and data-driven techniques has opened new avenues for turbulence modeling⁴⁰. These approaches leverage high-fidelity simulation data and experimental results to improve model accuracy and generalizability. The role of machine learning and data-driven approaches in turbulence modeling for hypersonic flows and key insights in developing reliable data-driven models are discussed. Key multiphysics considerations are also discussed, including ablation and the conjugate heat transfer for efficient thermal protection system design. By examining the developments in the

field, the paper seeks to highlight progress, identify persistent challenges, and suggest potential future research directions. As the field continues to evolve rapidly, driven by renewed interest in hypersonic flight technologies, a thorough understanding of the current state-of-the-art in turbulence modeling is essential for advancing the design and analysis capabilities for next-generation hypersonic vehicles.

The paper is organized as follows. Section II provides the governing Favre-averaged equations for calorically and thermally perfect gases. Section III gives a detailed discussion on turbulence modeling specifically for hypersonic flows. Eddy-viscosity models including linear EVMs (LEVMs), NLEVMs, and EARSMs along with the advanced RSTMs are covered. The performance of these modeling strategies in predicting attached and separated TBL flows is discussed in detail. Modeling for the thermo-chemical non-equilibrium effects in the hypersonic regime is also presented. Various modeling improvement strategies including ad-hoc fixes and physics-based corrections to the standard turbulence models for hypersonic flows to improve separation size and wall heat transfer predictions are discussed in Section IV. Critical modeling challenges pertinent to hypersonic flows are addressed in Section V. This includes modeling in the presence of shock/turbulence interaction along with modeling for equilibrium hypersonic TBLs especially at cold wall conditions and SBLIs. Advanced topics like the modeling for surface roughness and blowing effects and thermochemical non-equilibrium effects relevant to hypersonic conditions are also discussed along with key insights into multiphysics considerations including ablation and conjugate heat transfer. Section VI provides the available validation datasets from the experiments and DNS studies performed to date in the hypersonic regime. The current limitations and unresolved issues in turbulence modeling for hypersonic flows are addressed in Section VII along with key insights on data-driven models. Finally, the paper concludes with a summary of key findings and perspectives on future directions in Section VIII.

II. GOVERNING EQUATIONS

In this section, we limit our discussion to calorically and thermally perfect gases for simplicity. Also, nearly all the available hypersonic experimental databases are limited to low-enthalpy conditions (see Section VI), and turbulence model validation using perfect gas assumption is standard practice. However, temperatures in a hypersonic flow field can reach extremely high values inducing non-equilibrium effects including molecular dissociation, ionization, thermochemical reactions, radiation, and surface reactions such as ablation. The complex challenges of modeling these non-equilibrium effects and their profound implications for turbulence modeling will be addressed in Sections III A 5 and V E. In this review, our focus is confined to continuum flows, where the mean free path of gas molecules is small compared to the characteristic flowfield scale. The equations governing the hypersonic flows under these conditions are the Navier-Stokes (NS) equations describing the conservation of mass,

momentum, and total energy supplemented by an equation of state. However, as we are interested in the mean behavior of these flows, it is customary to use Reynolds decomposition and express all the instantaneous quantities as the sum of mean and fluctuating parts. For the compressible flows, an established practice is to use Reynolds time-averaging for the density and pressure whereas Favre-averaging (also called density-weighted- or mass-averaging) for the velocity and energy (temperature) variables. The NS equations are then transformed into the Favre-averaged Navier-Stokes equations using the RANS formalism. Using the Einstein summation convention, these mean equations which account for density and temperature fluctuations together with the velocity and pressure fluctuations in a hypersonic flow field are given by

Conservation of mass,

$$\frac{\partial \bar{\rho}}{\partial t} + \frac{\partial}{\partial x_i} (\bar{\rho} \tilde{u}_i) = 0 \quad (1)$$

Conservation of momentum,

$$\frac{\partial}{\partial t} (\bar{\rho} \tilde{u}_i) + \frac{\partial}{\partial x_j} (\bar{\rho} \tilde{u}_j \tilde{u}_i) + \frac{\partial (-\tau_{ij})}{\partial x_j} = -\frac{\partial \bar{p}}{\partial x_i} + \frac{\partial \bar{\sigma}_{ij}}{\partial x_j} \quad (2)$$

Conservation of total energy,

$$\begin{aligned} \frac{\partial \bar{\rho} \tilde{E}}{\partial t} + \frac{\partial}{\partial x_j} (\bar{\rho} \tilde{H} \tilde{u}_i) + \frac{\partial (-\tau_{ij}) \tilde{u}_i}{\partial x_j} \\ = \frac{\partial}{\partial x_j} \left[-q_{L_j} - q_{T_j} + \overline{\sigma_{ji} u_i''} - \overline{\rho u_j'' \frac{1}{2} u_i'' u_i''} \right] + \frac{\partial (\bar{\sigma}_{ij} \tilde{u}_i)}{\partial x_j} \end{aligned} \quad (3)$$

Equation of state,

$$\bar{p} = \bar{\rho} R \tilde{T}, \quad (4)$$

where ρ = density, u = velocity, p = pressure, T = temperature, and R = specific gas constant. Here, $(\bar{\cdot})$, $(\tilde{\cdot})$, and $(\cdot)''$ represent Reynolds time-averaged, Favre-averaged, and Favre fluctuating quantities, respectively. The averaged specific total energy and total enthalpy are given by

$$\begin{aligned} \tilde{E} &= \tilde{e} + \frac{1}{2} \tilde{u}_i \tilde{u}_i + k \\ \tilde{H} &= \tilde{E} + \frac{\bar{p}}{\bar{\rho}} = \tilde{h} + \frac{1}{2} \tilde{u}_i \tilde{u}_i + k, \end{aligned} \quad (5)$$

where k is the turbulence kinetic energy (TKE). The specific heats C_p and C_v are constant for a perfect gas and the averaged specific internal energy and enthalpy are given by

$$\tilde{e} = C_v \tilde{T}, \quad \tilde{h} = C_p \tilde{T}. \quad (6)$$

The averaged viscous stresses are described by,

$$\bar{\sigma}_{ij} = \tilde{\mu} \left(\frac{\partial \tilde{u}_i}{\partial x_j} + \frac{\partial \tilde{u}_j}{\partial x_i} - \frac{2}{3} \frac{\partial \tilde{u}_k}{\partial x_k} \delta_{ij} \right) \quad (7)$$

and the molecular viscosity is generally given by the Sutherland relation of the form $\tilde{\mu} = A \tilde{T}^n / (B + \tilde{T})$, where n, A , and B

are constants that depend on the gas or Keyes law. The laminar heat flux is given by

$$q_{L_j} = -\frac{\tilde{\mu} C_p}{Pr} \frac{\partial \tilde{T}}{\partial x_j}, \quad (8)$$

and Pr is the Prandtl number. Additional assumptions are made in the course of deriving the above equations, and these are the neglect of turbulent fluctuations of the dynamic viscosity, the thermal conductivity, and the specific heats.

All terms appearing in the Eqns. (1)-(3) are closed except for those resulting from turbulent fluctuations, represented by the blue underlined terms. These terms describe the average effect of turbulence on the mean flow. The blue underlined terms in Eqns. (2) and (3) include the unclosed terms in the form of the Reynolds stresses $\tau_{ij} = -\overline{\rho u_j'' u_i''}$ and turbulent heat flux $q_{T_j} = \overline{\rho u_j'' h''}$. The unclosed terms $(\overline{\sigma_{ji} u_i''})$ and $(\overline{\rho u_j'' \frac{1}{2} u_i'' u_i''})$ in Favre-averaged energy Eqn. (3) characterize the molecular diffusion and turbulent transport of TKE, respectively and they also appear in the Favre-averaged TKE transport equation (see Eqn. (21)). Notably, the gradients of Reynolds stresses in the Favre-averaged momentum Eqn. (2) play a significant role in determining the separation characteristics like separation location and length in case of flows involving shock-induced separations. On the other hand, the gradient of the turbulent heat-flux vector in the Favre-averaged total energy Eqn. (3) is crucial for the correct prediction of wall heat transfer rates. Hence, accurate representation of these turbulent quantities is key to correctly predicting the hypersonic flow field and the engineering QoIs. The goal of turbulence modeling is to develop appropriate closures for these unclosed terms by relating them to known mean flow quantities such as velocity and temperature.

III. TURBULENCE MODELING FOR HYPERSONIC FLOWS

Historically, turbulence models used to predict compressible flows have involved simple extensions of incompressible models using density-weighted averages. Variable density extensions of the existing incompressible turbulence models are obtained by invoking Morkovin's hypothesis. This hypothesis asserts that compressibility or Mach number only affects the turbulence, at least the velocity correlations, through variations in mean density $\bar{\rho}$ alone and that density and temperature fluctuations have negligible effect on the turbulence. Morkovin's hypothesis with density-weighted averaging effectively isolates the turbulence dynamics from the compressibility effects by focusing on how the turbulence would behave if the density were constant. It implies the structural similarity between compressible and incompressible turbulent flows and provides a foundation for applying incompressible modeling approaches to compressible flows.

DNS studies of Refs. 41 and 42 have confirmed the validity of Morkovin's hypothesis for the mean velocity and mean temperature fields in the case of ZPG TBLs at hypersonic speeds (freestream Mach numbers ranging up to 14)

with varying wall temperatures (wall-to-recovery temperature ratio between 0.18 and 1.0). Similar conclusions are drawn from the Mach 6.7⁴³⁻⁴⁶, Mach 7.2^{47,48}, and Mach 11⁴⁹ experimental studies of ZPG flat plate TBLs. Furthermore, DNS studies of Ref. 50 have also shown the applicability of the hypothesis for predicting the turbulence field itself for flat-plate TBLs up to a Mach number of at least 10 at adiabatic as well as cold wall conditions. However, the hypothesis is likely to become invalid under nonequilibrium conditions e.g. SBLIs. As the Mach numbers increase in the hypersonic regime, significant compressibility effects are introduced which are not adequately captured by the hypothesis. Additional terms such as those related to the dilatation dissipation, pressure work, pressure dilatation, etc. are generally added to the turbulence models or the incompressible model coefficients are modified to account for compressibility effects.

Most of the research efforts in turbulence modeling have focused on improving the Reynolds stress tensor closures. Hypersonic ZPG TBLs have unequal distribution of Reynolds normal stresses across the boundary layer thickness. Moreover, these TBLs interact with the shock waves in complex ways, leading to rapid distortion of the turbulence structure. A shock wave has strong directionality, i.e. it alters the flow quantities differently between the shock-normal and shock-transverse directions. This results in significant anisotropy in the Reynolds stresses. Reynolds stress tensor can be written in terms of its isotropic form and the deviations from isotropy as,

$$\tau_{ij} = -\overline{\rho u_i'' u_j''} = \underbrace{\left(\tau_{ij} + \frac{2}{3} \bar{\rho} k \delta_{ij} \right)}_{\text{deviatoric}} - \underbrace{\frac{2}{3} \bar{\rho} k \delta_{ij}}_{\text{isotropic}}. \quad (9)$$

The departure from the isotropic state provides a measure of the Reynolds stress anisotropy state, i.e. deviation from the normal stress isotropy. The deviatoric or the anisotropy part of the Reynolds stress tensor i.e. τ_{ij}^{dev} can be equivalently expressed in terms of the Reynolds stress anisotropy tensor a_{ij} - a traceless and symmetric tensor - as,

$$a_{ij} = \frac{-\tau_{ij}^{dev}}{\bar{\rho} k}. \quad (10)$$

The Reynolds stress tensor can be written as,

$$\tau_{ij} = -\bar{\rho} k \left(a_{ij} + \frac{2}{3} \delta_{ij} \right). \quad (11)$$

Thus, the closure for Reynolds stress tensor amounts to constructing a representation for the anisotropy tensor a_{ij} . The Reynolds stress tensor is linearly or non-linearly related to the mean strain-rate and/or vorticity tensors via μ_T in eddy-viscosity models, whereas transport equations for individual Reynolds stress components are solved in the case of Reynolds stress transport models. EVMs are generally the preferred choice while a very limited amount of work exists on RSTMs for hypersonic flow predictions.

The turbulent heat flux vector is another important unclosed term in the Favre-averaged total energy Eqn. (3). It is most

commonly modeled by invoking the Reynolds analogy. A gradient diffusion approximation is generally used, similar to the eddy viscosity concept for momentum transfer. This is expressed as

$$q_{Tj} = -\frac{\mu_T C_p}{Pr_t} \frac{\partial \tilde{T}}{\partial x_j}, \quad (12)$$

where Pr_t is the turbulent Prandtl number. Morkovin's hypothesis, which assumes negligible total temperature fluctuations across an equilibrium TBL, leads to $Pr_t = 1$ for adiabatic wall conditions. Generally, a constant value of 0.9 (0.89 in some works) for Pr_t is used.

A. Modeling capabilities and limitations for hypersonic flows

The most popular and widely used class of turbulence models is the eddy-viscosity models that introduce closures for a_{ij} using the concept of eddy-viscosity μ_T . A generalized expansion of a_{ij} is given by the linear combination of the basis tensor $T_{ij}^{(\lambda)}$ ⁵¹

$$a_{ij} = \sum_{\lambda} \beta^{(\lambda)} T_{ij}^{(\lambda)}. \quad (13)$$

On dimensional grounds, a_{ij} is assumed to be a function of $S_{ij}^* = \tau S_{ij}^D$ and $\Omega_{ij}^* = \tau \Omega_{ij}$, where $\tau = \varepsilon/k = 1/(C_{\mu} \omega)$ represents the turbulent time scale with ε, ω being the dissipation rate of TKE and dissipation per unit TKE (or specific dissipation), respectively and C_{μ} is a model coefficient. Here, $S_{ij}^D = S_{ij} - (1/3) S_{kk} \delta_{ij}$ is the deviatoric part of the strain-rate tensor $S_{ij} = (1/2)(\partial \tilde{u}_i / \partial x_j + \partial \tilde{u}_j / \partial x_i)$ and $\Omega_{ij} = (1/2)(\partial \tilde{u}_i / \partial x_j - \partial \tilde{u}_j / \partial x_i)$ is the vorticity (or rotation) tensor. The scalar coefficients β 's may be functions of the invariants of S_{ij}^* and Ω_{ij}^* and λ is the number of linearly independent basis tensors. It follows from the Cayley-Hamilton theorem that the number of independent invariants is two and $\lambda = 3$ for two-dimensional flows, whereas there are five independent invariants and $\lambda = 10$ for three-dimensional flows. Using Eqns. (11) and (13), the Reynolds stress tensor τ_{ij} can be expressed as

$$\tau_{ij} = -\bar{\rho} k \sum_{\lambda} \beta^{(\lambda)} T_{ij}^{(\lambda)} - \frac{2}{3} \bar{\rho} k \delta_{ij}. \quad (14)$$

Thus, the task of formulating a model for the Reynolds stress is reduced to that of determining β 's as the basis tensors T_{ij} are known functions of S_{ij}^* and Ω_{ij}^* . In the EVM framework, eddy-viscosity is constructed from turbulence scalars, and a general expression for the eddy-viscosity hypothesis can be written as

$$\tau_{ij} = 2\mu_T S_{ij}^D - \frac{2}{3} \bar{\rho} k \delta_{ij} - \bar{\rho} k a_{ij}^{(NL)}, \quad (15)$$

where superscript "NL" refers to the non-linear (quadratic and higher) contributions added to the linear part in the definition of τ_{ij} . Eddy viscosity accounts for the momentum transfer and energy dissipation due to turbulent fluctuations. Unlike the molecular viscosity μ , eddy viscosity μ_T is a hypothetical property of the flow that needs to be modeled.

Depending on whether the non-linear contributions are considered or not in Eqn. (15), the EVMs can be categorized into Boussinesq hypothesis-based models (also called Linear Eddy-Viscosity Models or LEVMs) and Extended Boussinesq hypothesis-based models. Furthermore, μ_T is modeled in terms of length and velocity scales of turbulence based on dimensional grounds. The way these turbulence scales are determined defines the type of eddy viscosity model to be used. If both the scales are determined algebraically from mean flow data, the models are referred to as zero-equation or algebraic models. If the length scale is determined algebraically, but the velocity scale is determined from a field equation such as the TKE equation, or alternatively, a transport equation for some form of μ_T is directly solved, the model is referred to as a one-equation model. If both the scales are determined from field equations, the resulting model is called a two-equation model. Zero-, one-, and two-equations-based LEVMs exist but the extended Boussinesq hypothesis is generally used in a two-equation modeling framework.

1. Boussinesq hypothesis-based models

Boussinesq eddy-viscosity hypothesis⁵² linearly relates the deviatoric part of the Reynolds stress tensor to the traceless mean strain rate tensor S_{ij}^D via the eddy-viscosity μ_T ,

$$\tau_{ij} = 2\mu_T S_{ij}^D - \frac{2}{3}\bar{\rho}k\delta_{ij}. \quad (16)$$

It is the most commonly used approach to model the Reynolds stress tensor. However, it does not accurately represent the Reynolds stress tensor, and the key deficiencies of this constitutive relation influential in hypersonic flows predictions are :

- It cannot correctly predict Reynolds stress anisotropy, a key feature in hypersonic SBLI flows. Application of the thin-shear-layer approximations to Eqn. (16) yields purely isotropic normal stresses i.e. $\tau_{xx} = \tau_{yy} = \tau_{zz} = -(2/3)\bar{\rho}k$, which is inaccurate even for a non hypersonic ZPG TBL.
- Turbulent transport of momentum is determined by a single scalar μ_T , so at most one Reynolds stress component (generally, the shear stress) can be represented accurately.
- It is not a realizable model and breaks down in the presence of shock waves. As τ_{ij} is proportional to mean strain rates, it increases monotonically with mean velocity gradients thereby significantly overestimating Reynolds stresses at shock waves. Limiting functions or damping factors are generally used to prevent excessive turbulence production or dissipation rates in the vicinity of shock waves.

Despite these shortcomings, this modeling framework remains the most popular group of models in aerospace-related CFD. This is because the extremely complex geometries and

the associated meshing problems involved in such applications favor the simplicity and economy of these models for engineering predictions.

Zero-equation models are the simplest and most economical models as they do not involve solving additional transport equations. These models directly model μ_T using theoretical/empirical algebraic relations. Baldwin–Lomax (BL) model is the stand-out zero-equation model in hypersonic applications involving flow separation, which formulates μ_T into a two-layer structure. The inner layer part is based on the mixing length model with a van Driest viscous damping correction while the outer layer uses a function of the maximum value of the mean vorticity and total velocity difference. It was initially developed based on the Cebeci–Smith (CS) model with modifications that avoid the necessity for calculating the edge of the boundary layer. BL model shows disparities in mean profiles with DNS, especially for the temperature, under diabatic (cold or heated wall) conditions for ZPG hypersonic TBLs⁵³. In general, it tends to overpredict separation regions and wall heat-transfer rates when applied to two-dimensional and axisymmetric SBLIs^{54–56}. It gives incorrect surface pressure and wall heat-transfer rates for three-dimensional crossing SBLIs^{17,57,58}. Modifications especially for hypersonic flows in terms of employing well-established relations for compressible turbulent mean flows including the velocity transformation and algebraic temperature–velocity relation⁵³, adjusting the model coefficients to take into account compressibility and pressure gradient effects^{55,58–60}, show significant improvements over the original model for a range of hypersonic flow applications including SBLIs.

The use of zero-equation models to provide a length scale for the TKE equation has been explored for hypersonic applications. For example, the McDonald-Camarata model⁶¹ with TKE-equation failed to improve the solution provided by the zero-equation model for a Mach 7.4 hypersonic inlet⁶². One equation models like SA, Goldberg R_T ⁶³, and Menter’s one-equation model⁶⁴ solve for μ_T (or some form of it) directly without dimensionally relating it with the turbulence scales. Variable density extensions of these models have been applied for hypersonic flow predictions. The standard SA model without any corrections generally underpredicts the separation size but may give good predictions for surface heat transfer rates^{63,65}. The R_T model has been shown to perform better than the SA model in hypersonic SBLIs predicting the correct extent of the separation region and heat-transfer rates for a Mach 9.22 flow over 38° cooled ramp. Also, the R_T model does not require the calculation of wall distance, unlike the SA model. However, the performance of this model has not yet been tested widely for hypersonic boundary layer applications. On the other hand, Menter’s one-equation model, derived from the k - ϵ model, performs poorly in predicting the separation and heat transfer rate for hypersonic SBLIs⁶³.

In two-equation turbulence models the transport equations are solved for two turbulent fields that are directly related to the length and velocity scales. Unlike the zero- and one-equation models, these models do not require the specification of empirical turbulence scales that must be adjusted in an ad-hoc fashion from one flow to the other. Hence, these models

represent the simplest level of Reynolds stress closure that can be formulated in a geometry-independent fashion. The TKE is generally the standard choice for the velocity scale whereas ε or ω are widely used to form the length scale. The standard k - ε and k - ω models, however, show discrepancies for surface heat transfer for ZPG hypersonic TBLs, especially at cold wall conditions, while reasonably predicting skin-friction and mean flow profiles. These models significantly underpredict the separation while grossly overpredicting peak heat transfer and skin-friction for hypersonic SBLIs. The widely popular Menter SST k - ω , a combination of k - ω and k - ε models, also performs poorly in predicting surface heat transfer for hypersonic TBL attached and separated flows. The performance of Menter SST model in predicting SBLIs greatly depends on the choice of sensitizing μ_T i.e. using vorticity or strain-rate invariants and production limiters.

Other choices for the auxiliary equations to determine velocity and length scale exist, for example, $q = \sqrt{k}$, enstrophy ζ i.e. the R.M.S. fluctuating vorticity ($\zeta \sim \omega^2$), and integral length scale l . Refs. 66–68 apply the k - ζ model⁶⁹ to Mach 5 and Mach 9.2 SBLIs involving attached and separated flows. The model is free of damping and wall functions like the k - ω models. The model predictions for separation length agree well with experiments while skin friction is underpredicted and peak heat transfer is significantly overpredicted for these cases. Coakley's q - ω ⁷⁰ and Smith's k - l ⁷¹ models generally result in smaller separation and overprediction of heat transfer for hypersonic SBLIs. Such models with scale-determining equations other than k and ε or ω , however, have not been pursued to any great extent for hypersonic flows.

2. Extended Boussinesq hypothesis-based models

This class of models includes non-linear contributions to represent the Reynolds stress tensor in addition to the linear part, as given by Eqn. (15). The higher order representation allows for a more general coupling between the mean-field and τ_{ij} , compared to the models based on the Boussinesq hypothesis. Non-linear eddy-viscosity models (NLEVMs) and Explicit algebraic Reynolds stress models (EARSMs) fall under this category. Despite the formal functional equivalence between NLEVMs and EARSMs, fundamental differences exist in their origin, precisely in the way the expansion coefficients β 's are obtained. In the case of NLEVMs, the expansion coefficients are determined based on calibrations with experimental or numerical data, and on some physical consistency constraints. On the other hand, in the case of EARSMs, the expansion coefficients are derived from the full differential Reynolds stress equations under weak equilibrium assumption. These models are developed to improve the predictions of Reynolds stress fields by employing either quadratic, cubic, or higher-order expansions of the Reynolds stresses in terms of the strain and vorticity tensors. Also, the turbulent eddy viscosity is additionally sensitized to the mean strain and vorticity tensors. Generally, a quadratic expansion of the Reynolds stresses is found to be sufficient to predict anisotropy in normal Reynolds stresses⁷², while cubic and higher-order terms

are needed to predict streamline curvature, including swirl effects. NLEVMs and EARSMs are generally used with the family of k - ε or k - ω models by replacing the Boussinesq hypothesis. The model development generally involves a straightforward compressibility extension of the incompressible model forms and most of the models neglect compressibility corrections.

Application of the compressible form of NLEVMs to hypersonic flows is seriously limited in the literature. Goldberg *et al.*⁶³ apply a cubic k - ε model wherein Reynolds stresses are modeled using the mean strain and vorticity relations from the quadratic model of Shih *et al.*⁷³ with the cubic extension proposed by Lien and Leschziner⁷⁴ to predict several hypersonic SBLIs. The model predicts correct trends of wall heat transfer including the peak when applied to Mach 8.03 curved compression surface, with experimental data by Holden⁷⁵ (cooled wall). However, it significantly overpredicts surface heat transfer while underpredicting separation size with incorrect peak pressure location for Mach 9.22 flow over a 38° cooled ramp of Coleman and Stollery⁷⁶. For a Mach 8.3 flow in a wedge inlet configuration involving complex three-dimensional crossing SBLI, the model grossly overpredicts surface heat transfer while giving good surface pressure prediction. Zhang *et al.*⁷⁷ apply the cubic k - ε model of Craft *et al.*^{78,79} with low-Reynolds-number effects to Mach 7.05 SBLIs with fully attached and fully separated flows. The model predicts reasonably correct surface pressure distributions for these cases while significantly overpredicting peak heat transfer rates.

EARSMs can be considered as the approximations of Reynolds stress transport models. They are numerically simpler and more economical than Reynolds stress transport closures and provide higher accuracy compared to LEVM and are therefore gaining popularity. The modeling strategy followed in deriving an EARSM involves a mathematically sound transfer of desirable model properties inherent to the elaborate RSTMs to a less elaborate modeling framework. Thus, EARSMs can be considered as an intermediate level between RSTMs and LEVMs. Specifically, these models neglect the advection and diffusion terms in the exact transport equation for a_{ij} which yields an algebraic expression that can be written as,

$$-\frac{\tau_{ij}}{\rho k}(P - \varepsilon) = P_{ij} - \varepsilon_{ij} + \Pi_{ij} \quad (17)$$

Here, P and ε represent the TKE production and dissipation, respectively. On the other hand, P_{ij} represents the production of Reynolds stresses, Π_{ij} and ε_{ij} , respectively, the pressure-strain correlation representing the mechanism of turbulence redistribution and relaxation, and the dissipation rate tensor. Depending on the choice of the models for ε_{ij} and Π_{ij} , the expansion coefficients β 's in Eqn. (14) can be obtained.

The EARSM of Wallin and Johansson⁸⁰ (WJ-EARSM) is one of the few EARSMs developed for compressible flows that have been used to predict hypersonic flows. WJ-EARSM is based on a recalibrated compressible form of the general linear model of the Launder, Reece, and Rodi RSTM rapid pressure-strain rate model. It uses wall-damping functions

derived from the van Driest damping function to obtain the correct near-wall limits of the anisotropies. The new near-wall treatment ensures realizability for the individual stress components. The model accounts for three-dimensionality in the mean flow description of the stress anisotropy. WJ-EARSM represents a fully explicit and self-consistent algebraic relation and consists of a quartic expansion of the Reynolds stresses for a general three-dimensional mean flow. The model gives substantially improved predictions for the separation in case of the Schulein⁸¹ Mach 5 impinging oblique SBLI flows with 10° and 14° shock generators compared to the standard $k-\omega$ and $k-\epsilon$ models using Boussinesq hypothesis^{80,82,83}. Vemula and Sinha⁸³ propose improvements to the WJ-EARSM model to correctly predict the amplification of Reynolds stresses across shocks of varying strengths using linear interaction analysis and DNS results for canonical shock/turbulence interactions (STIs) at a range of Mach numbers. Vemula and Sinha⁸³ applied the shock-unsteadiness (SU) modification of Sinha *et al.*⁸⁴ to WJ-EARSM production term and obtained better predictions for surface pressure and skin-friction for Schulein's⁸¹ 10° and 14° cases with separations whereas the SU modified and original model gave similar results for the 6° case and predicted a small separation in contrast to the experiments.

Raje and Sinha⁸⁵ use the EARSM by Rung *et al.*⁸⁶ to augment the standard SST $k-\omega$ model for high-speed flows. Rung *et al.* EARSM is a realizable quadratic eddy viscosity model and is an improved version of the EARSM by Gatski and Speziale⁸⁷. It enjoys the desirable properties inherent to the elaborate second-moment closure of Speziale, Sarkar, and Gatski⁸⁸. The model is developed for compressible flows and it adopts the compressibility correction in the form of Sarkar's pressure-dilatation model. The Rung EARSM with the SST model gives poor predictions for the separated Mach 8 compression corner and Mach 5 impinging oblique SBLI cases and the EARSM does not improve upon the standard SST model predictions. Raje and Sinha⁸⁵ propose modifications to the structure parameter a_1 (defined as the ratio between Reynolds shear stress and TKE) using the log-layer analysis of EARSM. The structure parameter a_1 , which is generally taken to be equal to 0.31 in the Menter SST $k-\omega$ model, is made a function of the mean velocity field in the form of the magnitude of the deformation rate tensor. Furthermore, to limit any unphysical high values of a_1 in the shock regions, a limiter to a_1 is proposed using an analysis of the SU model at a shock wave. The proposed a_1 is not a constant, unlike the standard SST model, but responds to the changes in strain rate and vorticity magnitude with an added effect of unsteady shock oscillations in response to incoming turbulent fluctuations. The eddy viscosity formulation is modified using the new a_1 definition and deformation rate tensor and the resulting model is called SUQ-SST model. The model is applicable to high-speed turbulent boundary layers including shock waves. The SUQ-SST model consistently predicts the separation shock location and separation bubble size and provides improved surface pressure and skin distributions compared to the baseline model for a range of hypersonic separated flow cases including compression corner and impinging oblique

SBLI. However, the model overpredicts surface heat transfer for these cases.

3. Reynolds stress transport models

Reynolds stress transport models (RSTMs), also called Differential Reynolds stress models, consist of transport equations for all the components of the Reynolds stress tensor without recourse to the eddy viscosity concept. They constitute the highest level of RANS-based turbulence models. These models have the natural potential to deal with the dynamics of inter-component energy transfer, and account for the effects of stresses increase or decrease due to curvature, acceleration or deceleration, swirling flow, and so on. In the case of three-dimensional mean flows, they require the solution of six highly coupled, non-linear partial differential equations and at least one equation for the turbulence dissipation rate. Thus, Reynolds stress transport models are mathematically more complex, pose greater numerical challenges, and require higher computational costs than the eddy viscosity models. The transport equations for the Reynolds stress tensor can be mathematically derived from the momentum equations. The Favre-averaged Reynolds stress tensor transport equation can be written as

$$\frac{\partial}{\partial t}(\bar{\rho}\tau_{ij}) + \frac{\partial}{\partial x_k}(\bar{\rho}\tilde{u}_k\tau_{ij}) = P_{ij} + \Pi_{ij} - \epsilon_{ij} + M_{ij} + D_{ij}, \quad (18)$$

where

$$\begin{aligned} P_{ij} &= -\bar{\rho}\tau_{ik}\frac{\partial\tilde{u}_j}{x_k} - \bar{\rho}\tau_{jk}\frac{\partial\tilde{u}_i}{x_k}; \\ \Pi_{ij} &= p'\left(\frac{\partial u''_i}{\partial x_j} + \frac{\partial u''_j}{\partial x_i}\right) = \phi_{ij} + \frac{2}{3}\phi_p\delta_{ij} + D_{ij}^{(p)}; \\ \phi_{ij} &= p'\left(\frac{\partial u''_i}{\partial x_j} + \frac{\partial u''_j}{\partial x_i} - \frac{\partial u''_k}{\partial x_k}\delta_{ij}\right); \quad \phi_p = p'\frac{\partial u''_k}{\partial x_k}\delta_{ij}; \\ \epsilon_{ij} &= \overline{\sigma'_{ik}\frac{\partial u''_j}{\partial x_k}} + \overline{\sigma'_{jk}\frac{\partial u''_i}{\partial x_k}}; \\ M_{ij} &= \overline{u''_i\left(\frac{\partial\bar{\sigma}_{jk}}{\partial x_k} - \frac{\partial\bar{p}}{\partial x_j}\right)} + \overline{u''_j\left(\frac{\partial\bar{\sigma}_{ik}}{\partial x_k} - \frac{\partial\bar{p}}{\partial x_i}\right)}; \\ D_{ij} &= D_{ij}^{(u)} + D_{ij}^{(p)} + D_{ij}^{(\mu)} = -\frac{\partial}{\partial x_k}\left(\bar{\rho}u''_i u''_j u''_k\right) - \\ &\frac{\partial}{\partial x_k}\left(\delta_{ik}\overline{p'u''_j} + \delta_{jk}\overline{p'u''_i}\right) + \frac{\partial}{\partial x_k}\left(\overline{\sigma'_{ik}u''_j} + \overline{\sigma'_{jk}u''_i}\right). \end{aligned} \quad (19)$$

The terms on the R.H.S. of Eqn. (18) represent the production, pressure-strain redistribution, dissipation (destruction), turbulent mass flux contribution (direct compressibility effects), and turbulent transport (triple velocity correlation + pressure diffusion) and viscous diffusion, respectively. Apart from the production term, which is exact, all other terms need to be modeled. In most RSTMs, direct compressibility effects in terms of M_{ij} and ϕ_p are neglected. The dissipation ϵ_{ij} is usually modeled using an algebraic approach, where a single scalar equation is solved for the dissipation rate of TKE (ϵ

or ω) and an algebraic expression distributes this scalar on the different components of ε_{ij} , using an appropriate tensorial representation. For example, the destruction term is generally modeled using the Kolmogorov hypothesis of local isotropy as

$$\varepsilon_{ij} = \frac{2}{3} \bar{\rho} \varepsilon \delta_{ij} = \frac{2}{3} C_\mu \bar{\rho} k \omega \delta_{ij}. \quad (20)$$

The diffusion term is generally modeled using a gradient diffusion model while the processes of turbulent diffusion by pressure fluctuations are usually neglected. The redistribution tensor Π_{ij} generally exerts a major influence on the model performance and has received the greatest amount of attention. Modeling strategies for Π_{ij} typically consist of some that attempt to model Π_{ij} as a whole and others that model the deviatoric part ϕ_{ij} and pressure diffusion $D_{ij}^{(p)}$ separately. The classical approach is to split the model for ϕ_{ij} into slow and rapid parts. The slow pressure-strain term is also referred to as the return-to-isotropy term and represents turbulence-turbulence interaction. The rapid pressure-strain term (ϕ_{ij}^r) responds directly to the change in mean velocity gradients and is of the same form as of production term in Eq. (18). It tends to redistribute the energy from the Reynolds stress component, where the production is significantly large compared to other components, consequently reducing the anisotropy in Reynolds stresses.

Wilcox⁸⁹ apply the Wilcox Stress- ω model to a Mach 11 SBLI with cold wall $T_w/T_{aw} = 0.2$. The Wilcox model by design is similar to the Launder-Reece-Rodi (LRR) model for the pressure strain correlation model but uses ω instead of ε for the scale-determining equation and does not use a wall-reflection term. The model predicts a smaller separation than experiments. For a Mach 7, 35° cylinder-flare configuration with $T_w/T_{aw} = 0.4$, the model still predicts a smaller separation and also significantly higher peak heat transfer rates compared to the experiments. The model results are similar to Wilcox 2006 k - ω model. The deficiencies in the predictions were attributed to the deficiencies in modeling the scale-determining equation and modeling of pressure-strain correlation. Refs. 90 and 91 apply the Speziale-Sarkar-Gatski/Launder-Reece-Rodi (SSG/LRR)- ω model by Einfeld and Brodersen⁹² to Mach 6.35 compression corner fully attached (15° ramp angle) and separated flows (40° ramp angle). The SSG/LRR-omega model is a combination of the two previously existing models: the Speziale, Sarkar, and Gatski (SSG) model using an ε -based length-scale equation is employed in the far field and coupled to the ω -based Launder, Reece, and Rodi (LRR) model in its modified Wilcox version for the near-wall region. The development of the SSG/LRR-omega model follows the ideas used by Menter for the SST k - ω model. A good agreement with experiments is obtained for the separation size along with the surface pressure distribution and peak heat transfer on the ramp for both cases. For a three-dimensional two-ramp Mach 7.5 intake at slightly off-design conditions of Mach 7.7, the SSG/LRR- ω model predicts the pressure coefficient and the Stanton number of the lower intake wall along the center line in good agreement with the experiments. The

flow partially relaminarizes while expanding and turning inward into the interior engine section, which is predicted well by the model. Gerolymos *et al.*⁹³ assembles a working model by combing the different closures for the ε_{ij} , ϕ_{ij} , $D_{ij}^{(u)}$, and $D_{ij}^{(p)}$ terms and neglect the direct compressibility effects i.e. M_{ij} and ϕ_p . The model uses the Launder-Sharma modified dissipation rate ε transport equation but with a tensorial diffusion coefficient. Comparisons with Gerolymos and Vallet (GV RSM)⁹⁴ and the low-Reynolds number Reynolds stress model WNF (wall normal free)-LSS (Launder-Shima-Sharma)-HL (Hanjalic-Launder) RSM⁹⁵ are done for Schulein's Mach 5, 14° fully separated case. The WNF-LSS-HL RSM underestimates the recirculation zone whereas the new and old GV models give improved predictions of the upstream influence but underestimate the height of the recirculation zone. All these models fail to predict the correct shape of wall friction in the reattachment flow region.

4. Modeling of scale determining equations

A majority of the widely used EVMs, e.g. family of k - ε and k - ε models, use TKE to represent the velocity scale. The value of TKE directly represents the strength of the turbulence in the flow. The TKE transport equation for compressible flows is given by

$$\frac{\partial \bar{\rho} k}{\partial t} + \frac{\partial \bar{\rho} \tilde{u}_j k}{\partial x_j} = P_k - \bar{\rho} \varepsilon + D + T + \Pi^t + M + \Pi^d, \quad (21)$$

where

$$\begin{aligned} P_k &= \tau_{ij} \frac{\partial \tilde{u}_i}{\partial x_j}; \bar{\rho} \varepsilon = \overline{\sigma'_{ji} \frac{\partial u_i''}{\partial x_j}}; D = \frac{\partial}{\partial x_j} \left(\overline{\sigma'_{ji} u_i''} \right); \\ T &= -\frac{\partial}{\partial x_j} \left(\overline{\rho u_j'' \frac{1}{2} u_i'' u_i''} \right); \Pi^t = -\frac{\partial}{\partial x_j} \left(\overline{p' u_j''} \right); \\ M &= \overline{u_i''} \left(\frac{\partial \overline{\sigma_{ji}}}{\partial x_j} - \frac{\partial \bar{p}}{\partial x_i} \right); \Pi^d = \overline{p' \frac{\partial u_i''}{\partial x_i}}. \end{aligned} \quad (22)$$

The terms on the L.H.S. in Eqn. (21) represent the rate of change and transport by convection, respectively, and the terms on the R.H.S. represent Production P_k , Dissipation $\bar{\rho} \varepsilon$, Viscous Diffusion D , Turbulent Transport (triple velocity correlation term) T , Pressure Diffusion Π^t , mass flux contributions M , and pressure dilatation Π^d . The dissipation can be effectively split into solenoidal and dilatation parts i.e. $\bar{\rho} \varepsilon = \bar{\rho} (\varepsilon_s + \varepsilon_d)$ that represent fluctuating vorticity and divergence of fluctuating velocity, respectively. The solenoidal dissipation rate ε_s can be thought of as the dissipation due to the regular process of energy cascading to the smaller scales and in the absence of dilatational effects it can be considered to be equivalent to the “incompressible” dissipation rate. The dilatational dissipation ε_d (also referred to as compressible dissipation) is due to the non-divergent nature of the velocity fluctuations and it is an extra compressibility effect. The most commonly used approach to model unclosed terms in the TKE equation (21) is to generalize the low-speed closure approximations for the

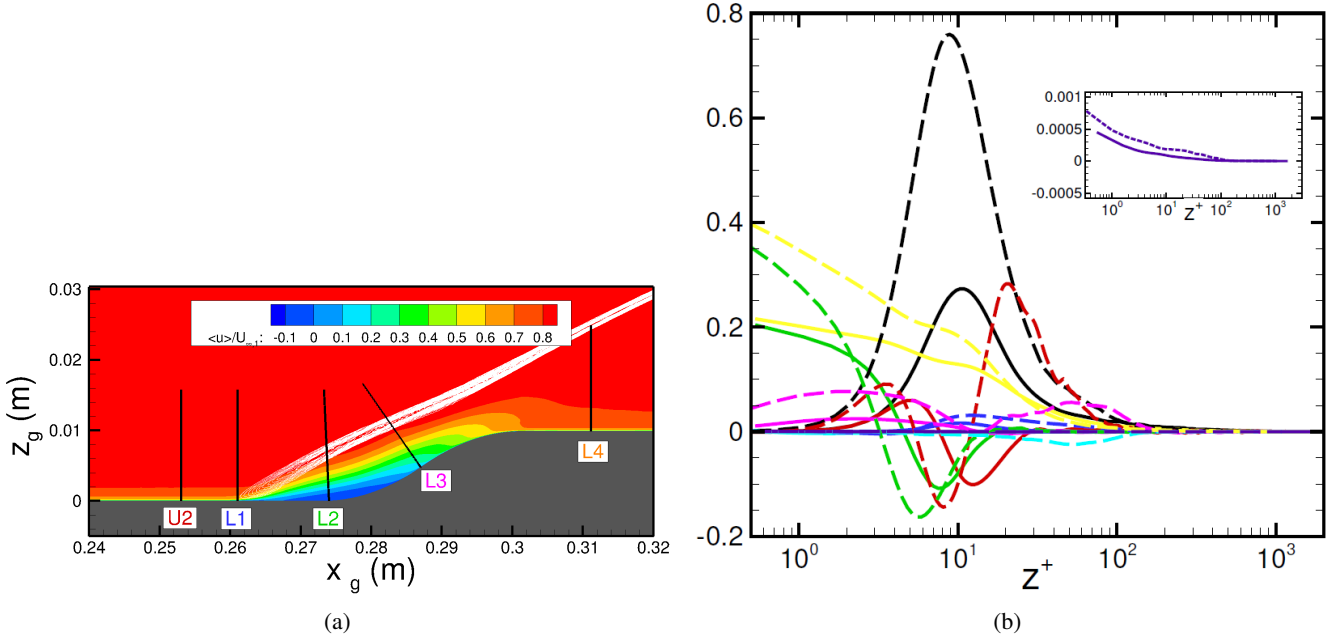


FIG. 1: (a) Mean flow-field over the forward-facing geometry with wall curvature showing SBLI (reproduced from Ref. 96) and (b) TKE budget : Solid lines represent the wall-normal variation of TKE budget terms at U_2 location and dashed lines represent corresponding quantities at L_1 location. Color code : Black - P_k , Yellow - ϵ_s , Violet - ϵ_d , Green - D , Red - T , Magenta - $-\Pi^l$, Blue - M , and Cyan - $-\Pi^d$ (data from the DNS of Ref. 97 taken from Ref. 96).

corresponding incompressible analogs. The terms ϵ_d , M , and Π^d are exactly zero for the incompressible flows and hence are generally neglected even for hypersonic flows. The pressure diffusion term Π^l is also neglected in many works. On the other hand, the terms D and T are modeled using a gradient diffusion hypothesis as $(\tilde{\mu} + \mu_T / \sigma_k) \partial k / \partial x_j$, where σ_k is a model constant. However, these neglected terms can become significant under non-equilibrium conditions such as in the SBLI regions.

Figure 1(a) shows the mean flow for a forward-facing geometry with wall curvature obtained using a recent DNS⁹⁷ with an inflow Mach 4.9 at mild cold wall conditions $T_w / T_{aw} = 0.91$ and an approximate friction Reynolds number of 1000 immediately before the onset of wall curvature. The turbulent boundary layer fully separates at these geometric and flow conditions and SBLI is evident. Compared to the undisturbed boundary layer at location U_2 , TKE budget at L_1 corresponding to the SBLI region shows that contributions due to all the terms on the R.H.S. of Eqn. (21) increase. Production of TKE increases significantly and the terms T , D , Π^l , and ϵ_s become appreciable. Dilatation dissipation ϵ_d and pressure dilatation Π^d remain comparatively smaller for this case. In the separated regions L_2 and L_3 , the budget terms also become significant in the separated shear layer over the separation bubble in addition to post-shock regions. Thus, the usually neglected terms in the TKE transport equation can be expected to become considerable under strong nonequilibrium conditions. The turbulent fluctuations can become locally supersonic relative to the surrounding flow, likely creating local shocklets that may become the source of significant dilatational dissipa-

tion and entropy production.

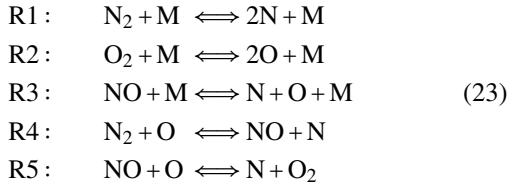
The choice of length-scale determining equation plays a crucial role in determining the predictive capabilities of turbulence models. The most popular and widely used turbulence variable alongside TKE to construct the length-scale in the two-equation modeling framework and RSTMs is the turbulence dissipation rate ϵ or specific dissipation rate ω . The choice between these variables significantly affects the near-wall treatment, wall and far-field boundary conditions, far-field behavior, and model performance. An ϵ -based model is preferred away from the wall to avoid the high sensitivity to freestream turbulence observed in ω -based models. However, the exact ϵ -equation requires a lot of ad hoc modeling, substantially more than the TKE transport equation. Most of the terms in the ϵ -equation are highly empirical and tuned for specific flow cases. As a result, there are numerous variants of the k - ϵ models, with major differences primarily in the near-wall modeling of the ϵ -equation and the eddy-viscosity relation. Conversely, ω -based models offer advantages near walls, allowing integration up to the wall without additional damping functions. However, they struggle in regions of strong SBLIs, where equilibrium conditions are disrupted. Both ϵ - and ω -based models exhibit deficiencies in non-equilibrium near-wall regions, which can lead to excessive length scale predictions in the separated flows, thereby significantly overestimating wall heat-transfer rates, particularly in reattachment regions. Moreover, advanced turbulence models such as NLEVMs, EARSMs, and RSTMs inherit these errors, which can undermine their superior theoretical foundation. Consequently, these advanced models may fail to improve upon

standard two-equation models and, in some cases, even underperform in predicting basic wall-bounded flows.

5. Favre-averaged equations for flows in thermochemical nonequilibrium

High-enthalpy hypersonic flows may incur chemical or thermal nonequilibrium effects, or both. Proper modeling of such phenomena requires a precise picture of the intimate nature of molecules with their different modes of storing energies (translational, rotational, vibrational, and electronic) and their quantum behavior^{1,31,98}. Nevertheless, because of computational limitations, sophisticated “state-to-state” models involving detailed reaction kinetics (i.e. hundreds of species and thousands of intermediate reactions) can be used only for basic systems, and simplified thermochemical models are hence adopted in practice⁹⁹.

In the case of chemical non-equilibrium the fluid is modeled as a reacting mixture of chemical species, corresponding to the reactants and products of chemical reactions. The number of species to be considered depends on the chemical model adopted for air, which may undergo dissociation, recombination, and ionization of the component species, depending on the flight conditions and altitude (see Ref. 1). Chemistry models can vary in complexity, according to the number of chemical species and global or partial reactions used to describe the mixture. In complex configurations, air is often modelled as a five-species mixture of N_2 , O_2 , NO , O and N that undergoes seventeen dissociation/recombination reactions³¹:



being M any of the five species considered. The reader is referred to Ref. 31 for details.

The flow dynamics is generally described by the conservation equations for the mass, momentum, and energy of the mixture, which still take the form (1)-(3), and by supplementing them with transport equations for the chemical species. Because the sum of the masses of all species must equal the mass of the mixture, $N - 1$ additional equations are needed, N being the total number of species, with boundary conditions accounting for the catalytic or non-catalytic nature of the solid walls, i.e. for the presence of various degrees of chemical equilibrium between the flow and the wall.

In this paper, we are interested more specifically into the Favre-averaged form of the species transport equations:

$$\frac{\partial \bar{\rho} \tilde{Y}_n}{\partial t} + \frac{\partial (\bar{\rho} \tilde{Y}_n \tilde{u}_j)}{\partial x_j} = - \frac{\partial \bar{\rho} Y_n u_{nj}^D}{\partial x_j} + \bar{\omega}_n + \frac{\partial \overline{\rho u_j'' Y_n''}}{\partial x_j}, \tag{24}$$

Y_n being the mass fraction, u_{nj}^D the diffusion velocity and $\bar{\omega}_n$ the chemical production rate for the n -th species, respectively.

The unclosed term $\frac{\partial}{\partial x_j} \overline{\rho u_j'' Y_n''}$ is the turbulent transport of chemical species. Averages of the diffusion velocity contribution and of the source term are also unclosed. Passiatore *et al.*²⁸ found the former to be negligibly small in their DNS of a hypersonic boundary layer at Mach 10, supporting the idea that it can be removed from the equation. The system of Favre-averaged mixture/species transport equations is supplemented with thermodynamic and transport models, as well as with models for the reaction rates (see, e.g. Ref. 8). In addition, the unclosed terms arising from the Favre-averaging of the species equations must be modeled, as discussed in Section **VE**.

If the flow residence time becomes comparable to the characteristic relaxation times of energy pools of species, thermal nonequilibrium effects must be taken into account. In general, the energies associated with the internal degrees of freedom of molecules may be separated into rotational, vibrational, electronic and nuclear contributions^{1,31}, in addition to the energy associated with the molecule translational motion. The internal energies are denoted as e_m^{int} , where the superscript indicates an internal mode and the subscript m the internal mode “energy pool”. The latter may represent individual species in the mixture, but if the coupling between species is fast compared to the coupling with other internal modes, then it may be acceptable to assign the same energy to all species. For this case, subscript m is dropped. To fix ideas, we will consider in the following the so-called two-temperature (2T) model proposed by Park¹⁰⁰, which assumes equilibrium between the translational and the rotational modes of all molecules and vibrational non equilibrium, with all diatomic species sharing however the same vibrational temperature. Vibrational relaxation processes are then taken into account by adding a conservation equation for the vibrational energy e_V .

The Favre-averaged vibrational energy equation reads:

$$\begin{aligned}
 \frac{\partial \bar{\rho} \tilde{e}_V}{\partial t} + \frac{\partial (\bar{\rho} \tilde{e}_V \tilde{u}_j)}{\partial x_j} &= \frac{\partial}{\partial x_j} \left(\overline{\rho u_j'' e_V''} \right) \\
 &+ \frac{\partial}{\partial x_j} \left(-\bar{q}_{Vj} + \sum_{m=1}^{NM} \overline{\rho D_m \frac{\partial Y_m}{\partial x_j} e_{Vm}} \right) \\
 &+ \sum_{m=1}^{NM} \left(\overline{Q_{TVm}} + \bar{\omega}_m e_{Vm} \right),
 \end{aligned} \tag{25}$$

Here, NM is the number of molecular species, q_{Vj} the vibrational contribution of the heat flux and e_{Vm} the vibrational energy per unit of volume of the m -th species. Further, Q_{TV} and $\bar{\omega}_m e_{Vm}$ are source terms denoting translational-vibrational energy exchanges and the vibrational energy variations due to chemical production/depletion, respectively. Equation (25) contains the unclosed term $\frac{\partial}{\partial x_j} \left(\overline{\rho u_j'' e_V''} \right)$, corresponding to the turbulent transport of vibrational energy. Furthermore, the averaged source terms, described by non-linear expressions, also need an appropriate closure model. These aspects are discussed in Section **VE**.

IV. MODELING IMPROVEMENT STRATEGIES FOR HYPERSONIC FLOWS

Baseline turbulence models that are direct extensions of incompressible forms are generally insufficient for accurately predicting many hypersonic flows, especially in the presence of shock waves. Several modeling treatments and fixes are available to improve their performance, especially in the framework of the industry-favored two-equation family of $k-\varepsilon$ and $k-\omega$ models. We discuss key developments that have shown some success in predicting hypersonic flows in the two-equation modeling framework.

A. Dilatation dissipation modeling

Sarkar *et al.*¹⁰¹ and Zeman¹⁰² propose models for the dilatational dissipation ε_d (also referred to as compressible dissipation) using the DNS analysis for homogeneous turbulence. Wilcox¹⁰³ proposed an alternative form primarily applicable to the $k-\omega$ model and it has the same functional form as the Sarkar model. These approaches assume ε_d to be proportional to turbulent Mach number $M_T = \sqrt{2k}/\tilde{a}$, where $\tilde{a} = \sqrt{\gamma R \bar{T}}$ is the local speed of sound and γ is the ratio of specific heats. The turbulent Mach number represents a ratio of the propagation of information by turbulence to acoustic propagation, with the turbulent kinetic energy providing a characteristic velocity scale at which turbulent fluctuations transfer information. These models are given by

$$\varepsilon = \varepsilon_s (1 + F(M_T)), \quad (26)$$

with

$$F(M_T) = \begin{cases} M_T^2 \text{ (Ref. 101),} \\ \frac{3}{4} \left[1 - e^{-\frac{1}{2}(\gamma+1)[(M_T-M_{T0})/a]^2} \right] \mathcal{H}(M_T - M_{T0}) \\ \text{(Ref. 102),} \\ \frac{3}{2} [M_T^2 - M_{T0}^2] \mathcal{H}(M_T - M_{T0}) \text{ (Ref. 103),} \end{cases} \quad (27)$$

where $\mathcal{H}(\cdot)$ is the Heaviside function, $M_{T0} = 0.25$ for the Wilcox¹⁰³ model and $M_{T0} = b\sqrt{2/(\gamma+1)}$ in the Zeman¹⁰² model with $a = 0.66$, $b = 0.25$ for boundary layers and $a = 0.6$, $b = 0.1$ for free shear flows. The effect of these corrections is to enhance the destruction of TKE when M_T is large, resulting in an expected decrease in skin friction and wall heat transfer. Brown²¹ highlighted that the Sakar/Zeman/Wilcox corrections result in a significant reduction in wall shear stress (and heat transfer) for hypersonic boundary layers above Mach 5 and proposed a further correction to improve predictions for hypersonic boundary layers.

While dilatation-dissipation corrections have seen success in improving predictions for hypersonic flows, their underlying hypothesis remains in question. Wilcox⁸⁹ notes that DNS results indicate that dilatation dissipation is small, and while recent DNS results¹⁰⁴ highlight that dilatation-dissipation effects become non-negligible at high enough Mach numbers,

these Mach numbers are far in excess of those for which the Sakar/Zeman/Wilcox corrections were developed for and validated on.

B. Pressure work modeling

Hypersonic flows are generally characterized by large pressure gradients, especially in the regions of shock waves. The contribution due to the scalar product of the Favre-fluctuating velocity $\overline{u''}$ and the mean pressure gradient, i.e., pressure work, can thus become important. Turbulent mass flux $\overline{\rho' u_i'}$ is related to $\overline{u''}$ by

$$\overline{u''} = -\frac{\overline{\rho' u_i'}}{\bar{\rho}}, \quad (28)$$

and this flux can be approximated with the standard gradient transport hypothesis. The pressure work is modeled as^{105,106}

$$\overline{u_i'' \frac{\partial \bar{p}}{\partial x_i}} = \frac{\mu_T}{\bar{\rho}^2} \frac{1}{\sigma_p} \frac{\partial \bar{p}}{\partial x_j} \frac{\partial \bar{p}}{\partial x_j} \quad \text{where } \sigma_p = 0.5. \quad (29)$$

C. Pressure dilatation modeling

The pressure dilatation is an explicit compressibility term in the TKE transport equation (21) arising due to a non-divergent fluctuating velocity field. It refers to the work done due to simultaneous fluctuations in the volume of the fluid cell corresponding to the fluctuations in pressure. It can be either positive or negative and, when negative, represents an extra dissipation. Sarkar¹⁰⁷ analyzed the governing equations for pressure fluctuations using homogeneous turbulence to obtain a formal expression for the pressure-dilatation from which a model is deduced using scaling arguments,

$$\overline{p' \frac{\partial u''}{\partial x_i}} = \alpha_2 \tau_{ij} \frac{\partial \tilde{u}_i}{\partial x_j} M_T + \alpha_3 \bar{p} \varepsilon_s M_T^2, \quad (30)$$

where $\alpha_2 = 0.15$ and $\alpha_3 = 0.2$. The model has been calibrated using isotropic turbulence and homogeneous shear.

D. Length scale correction

Huang and Coakley¹⁰⁸ proposed a correction to remedy wall heat transfer overpredictions in the reattachment or shock impingement zone of SBLIs. The correction involves the use of an algebraic length scale which limits the length scale predicted by the two-equation turbulence models, which otherwise would become very large in these regions. For $k-\varepsilon$ and $k-\omega$ models, the correction is given by

$$l = \min\left(2.5y, \sqrt[3]{k/\varepsilon}\right) = \min\left(2.5y, \sqrt{k/\omega}\right) \quad (31)$$

where l is the turbulent length scale which is taken to be the smaller of an algebraic expression $\kappa C_\mu^{-3/4} y = 2.5y$ based on a

von Karman constant of $\kappa = 0.41$ and the conventional length scale given by the two-equation models. Here, y is the shortest distance from the wall. This relation is derived by bounding the turbulent viscosity by the k - ε or k - ω model by the turbulent viscosity as determined by Prandtl's model and by assuming Bradshaw's relation between shear stress and TKE and the logarithmic law for velocity to hold. Using this length scale, the value of ε or ω is recomputed and reset to be consistent with this value i.e. $\varepsilon = \sqrt[3]{k}/l$ or $\omega = \sqrt{k}/l$. This length-scale correction has proven effective for improving heat transfer predictions in the reattachment region in SBLIs¹⁰⁸. The correction, however, also impacts wall shear stress predictions and has seen minimal validation on this front.

Zhang *et al.*⁷⁷ recently proposed a new turbulent length scale correction for the ε -equation taking inspiration from the length-scale modification of Huang and Coakley¹⁰⁹. The correction is intended to control the growth of turbulence in the SBLI region. This involves the addition of an extra source term to the ε -equation,

$$S_{\varepsilon cm} = HY\lambda_l \frac{\varepsilon^2}{k}, \quad (32)$$

where $H = 3$ is the suggested value based on numerical experimentation of a fully separated hypersonic SBLI flow. It is to be noted that the model predictions for surface pressure and heat transfer rate were found to be sensitive to the values of H . Here, $\lambda_l = \max\left(\frac{k}{\varepsilon} \frac{\partial \tilde{u}_i}{\partial x_i}, -0.5\right)$ is designed to retain numerical stability and $Y = (\tanh(2(\eta - 3)) - 1)$, $\eta = \max(\widehat{S}, \widehat{\Omega})$ with $\widehat{S} = (k/\varepsilon)\sqrt{2S_{ij}^D S_{ij}^D}$ and $\widehat{\Omega} = (k/\varepsilon)\sqrt{2\Omega_{ij}\Omega_{ij}}$. This extra source term is specially designed for compressible flows and mainly remains effective in the near-wall or viscosity-dominated regions.

E. Rapid compression correction

Huang and Coakley¹⁰⁸ proposed a modification for k - ε and k - ω models to improve predictions for flow separation in SBLIs. This modification was made to increase the size of computed separation-bubble regions by ensuring that the turbulent length scale does not change too quickly when undergoing rapid compression. The basic principle of this correction is that the product of the density and turbulent length scale i.e. $\bar{\rho}l$ should remain constant in a uniaxial compression, such as a shock wave, where $l = k^{3/2}/\varepsilon = k^{1/2}/\omega$. Applying the continuity equation, the length scale equation can be written as

$$\frac{1}{l} \frac{dl}{dt} = \tilde{u}_{k,k}. \quad (33)$$

Comparison between the above equation and the length scale equation derived from the k - ε or k - ω model equations under rapid dilatation gives appropriate values of the coefficients of the dilatation part in the source term of the ε or ω equation. The corrected values of the dilatation coefficient for each model are

$$\alpha_\varepsilon = 2; \alpha_\omega = 4/3. \quad (34)$$

The net effect of this correction is to decrease the turbulent length-scale in regions of rapid compression, or shock waves, which reduces μ_T and enhances separation.

F. Shock-unsteadiness correction

Sinha *et al.*⁸⁴ propose modifications to the standard k - ε and k - ω models for high-speed shock-dominated flows to remedy the problem of excessive production obtained using standard models at shock waves. The modification is based on the physics of canonical STI and represents the damping effect of an unsteady shock oscillation due to interaction with the upstream vortical turbulence. The modeling approach replaces the TKE production term $P_k = \tau_{ij}\partial\tilde{u}_i/\partial x_j$ in the standard k - ε and k - ω models with a SU modified form in the vicinity of shock waves,

$$P_k^{SU} = -\frac{2}{3}\bar{\rho}kS_{ii}(1-b'_1) \quad (35)$$

with $b'_1 = \max[0, 0.4(1 - e^{-M_{1n}})]$.

The model parameter b'_1 represents the damping effect caused by the coupling between the shock unsteadiness and the upstream velocity fluctuations. Here, M_{1n} is the upstream shock-normal Mach number and it brings in the physical effect of the shock strength. The switching between the original TKE production and SU modified production term is done using a shock-detecting tanh function depending on the mean dilatation. Veera and Sinha¹¹⁰ modify the original SU model with the added effect of entropy fluctuations representative of hypersonic turbulent boundary layers. However, the effect of this model correction on hypersonic SBLIs has not been tested. The SU model is not Galilean invariant through the use of mean flow Mach number as a model parameter.

In recent works¹¹¹, the original SU model parameter b'_1 is approximated in terms of a shock function ψ given by

$$b'_1 = 0.4 \left(1 - \frac{\sqrt{(6\psi - 1)}}{5} \right). \quad (36)$$

The function ψ identifies the regions of the shock wave in a flow and brings in the history effect of the shock in the downstream flow. It is computed using a transport equation given by

$$\frac{\partial \bar{\rho}\psi}{\partial t} + \frac{\partial (\bar{\rho}\tilde{u}_i\psi)}{\partial x_i} = \bar{\rho}\psi S_{ii} - \frac{\bar{\rho}c(\psi - \psi_0)}{L}, \quad (37)$$

where c is the local speed of sound, $L = a\Delta(1 + b(\psi_0 - \psi))$ is the characteristic relaxation length with Δ is the representative grid size and the constants $a = 3$, $b = 15$, and $\psi_0 = 1$. The function ψ is set to 1 in the undisturbed boundary layer and takes a value of $1/r$ at shock waves with r being the local density ratio. A shock sensor is also devised based on ψ such that the SU model is only active in the vicinity of a shock wave.

G. Diffusion term corrections

Catris and Aupoix¹¹² propose corrections to the diffusion terms of the k - ε , k - ω , k - l , and SA models to account for the density variations and make these models consistent with the logarithmic law for high-speed compressible ZPG TBLs. These corrections are based on the analysis of the prediction of the logarithmic region of a compressible boundary layer by these Boussinesq hypothesis-based one- and two-equation models. The developments of these corrections assume equilibrium TBL and Bradshaw's assumption of shear stress proportional to TKE in a TBL. Their analysis shows that the diffused quantity should become $\bar{\rho}k$ in the TKE transport equation for k , while for the length scale determining equations, the diffused quantities should be $\sqrt{\bar{\rho}}\varepsilon$, $\sqrt{\bar{\rho}}\omega$, and l and $\bar{\rho}q^2$ for the transported quantities $\bar{\rho}\varepsilon$, ω , and $l/\sqrt{\bar{\rho}}$, respectively. Similarly, in the SA model, the diffused quantity becomes $\sqrt{\bar{\rho}}\nu_T$ for the transported quantity $\bar{\rho}\nu_T$. This results in additional terms linked to density variations in the transport equations of these models in their classical form.

More recently, Pecnik and Patel¹¹³ investigated variable-property scaling for non-adiabatic, low-Mach turbulent duct flows and obtained a new density scaling of the diffusion terms¹¹⁴ that carries similarities with that of Catris and Aupoix¹¹².

All of the above-mentioned corrections consist of rescaling the diffusion terms to account for local variations of the mean density. Such a phenomenon is not peculiar to compressible flows, and can also be found in incompressible variable-property flows. Hasan *et al.*¹¹⁵ discussed a velocity transformation based on the supposed universality of the total shear stress (sum of the viscous and turbulent stress) in the near-wall region of attached flows to infer modifications to the turbulence model that account for genuine compressibility effects (outward shift of the turbulent stresses in compressible flow cases).

H. Variable Pr_t modeling

The constant value of Pr_t used in the standard gradient-diffusion heat flux model generally results in good predictions of wall heat transfer for ZPG hypersonic TBLs at adiabatic wall conditions. However, inaccurate predictions are obtained at the practically relevant cold wall conditions and the standard turbulence models generally overpredict the reattachment point heat transfer rates in the case of SBLs. These inaccurate predictions can be attributed to a constant Pr_t assumption along with other reasons like inaccurate length scale characterizations. DNS studies reveal that Pr_t is not constant and varies in the near-wall region even though the average value across the TBL thickness is about 0.9–1 for highly cooled equilibrium TBLs. The strong Reynolds analogy breaks down especially at the non-adiabatic wall conditions^{118–122} and in SBLs^{104,123}, and we can expect a stronger near-wall variation of Pr_t with significant deviations from the nominally used value. Near-wall variation of Pr_t is also true

for air out of chemical equilibrium at high enthalpy conditions²⁸. Several modeling strategies that attempt to account for the variation of Pr_t in the flow field have thus been developed, and some of these key works are discussed below.

Variable Pr_t model of Roy and Sinha

Roy and Sinha¹²⁴ propose a variable Pr_t model based on the conservation of total enthalpy fluctuations across an unsteady oscillating shock wave interacting with incoming turbulence consisting of vorticity and temperature fluctuations. The model development based on Linear Interaction analysis (LIA) data and uses the SU model of Sinha *et al.*⁸⁴. The model is given by

$$Pr_t = \frac{3/4}{1 + b_1(r-1)} \quad (38)$$

$$\text{with } b_1 = 0.4 + 0.6 \left(\frac{6\psi - 1}{5\psi} \right)^{5.2} + 0.2(\gamma - 1)M_1^2.$$

Here, M_1 is the shock upstream mean flow Mach number, and ψ is a shock function computed using a transport equation to identify the regions of the shock wave in a flow. The model is not Galilean invariant because of the use of M_1 as a parameter. In the earlier version of the model¹²⁵, which neglects the shock-upstream temperature fluctuations while considering only the incoming vortical turbulence, the term depending on M_1 is effectively zero, and only the first two terms in Eqn. (38) for b_1 remain.

Variable Pr_t model of Xiao *et al.*

Xiao *et al.*⁶⁸ model the transport equations for enthalpy variance $\widetilde{h'^2}$ and its dissipation rate ε_h derived from the exact energy equation thereby accounting for the compressibility and dissipation terms. The modeled equations are free of damping and wall functions and are tensorially consistent and invariant under Galilean transformation. The modeled equations are

$$\begin{aligned} & \frac{\partial}{\partial t} (\bar{\rho} \widetilde{h'^2} / 2) + \frac{\partial}{\partial x_j} (\bar{\rho} \widetilde{u_j h'^2} / 2) = \\ & \frac{\partial}{\partial x_j} \left[\bar{\rho} (\gamma \alpha + \alpha_t C_{h,2}) \frac{\partial}{\partial x_j} (\widetilde{h'^2} / 2) \right] + \\ & 2\mu \gamma S_{ij} \left[\frac{\partial}{\partial x_j} (q_{T,i} / \bar{\rho}) + \frac{\partial}{\partial x_i} (q_{T,j} / \bar{\rho}) \right] - \frac{4}{3} \mu \gamma S_{kk} \frac{\partial}{\partial x_j} (q_{t,j} / \bar{\rho}) \\ & - (\gamma - 1) \bar{\rho} \widetilde{u_j h'^2} S_{kk} - q_{T,i} \frac{\partial \bar{h}}{\partial x_i} + 2C_{h,4} \gamma \mu \sqrt{\widetilde{h'^2}} \zeta - \gamma \bar{\rho} \varepsilon_h \end{aligned} \quad (39)$$

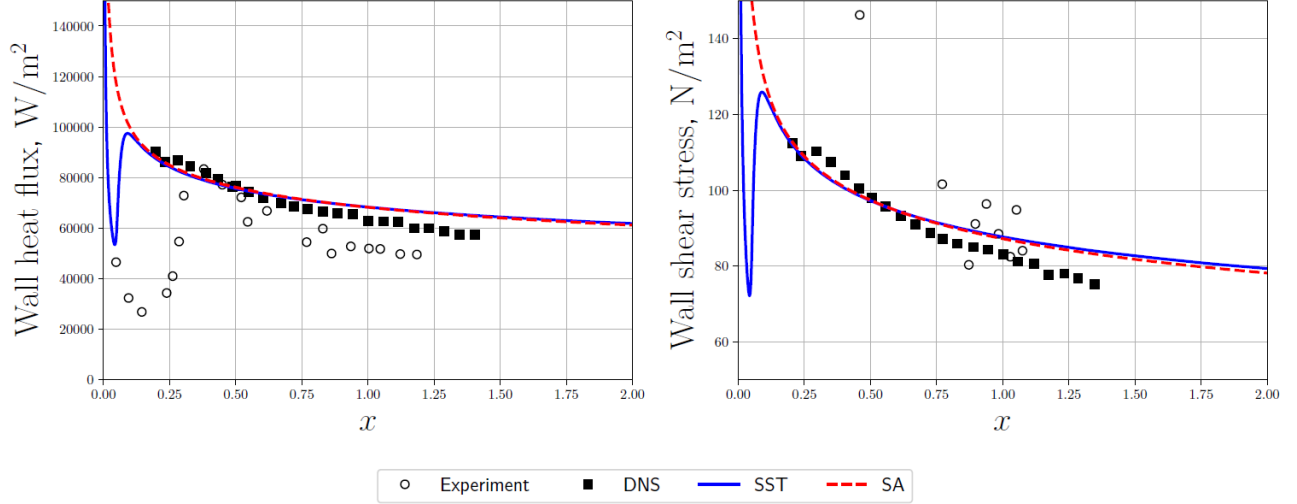


FIG. 2: Wall heat flux (left) and shear stress (right) predictions for a Mach 11 hypersonic boundary layer with $T_w/T_r = 0.20$. The DNS data are from Ref. 116 and the experimental data are from CUBRC^{20,117}.

$$\begin{aligned}
 \frac{\partial}{\partial t}(\bar{\rho}\varepsilon_h) + \frac{\partial}{\partial x_j}(\bar{\rho}\tilde{u}_j\varepsilon_h) &= \bar{\rho}\varepsilon_h \left(C_{h,5}a_{jk} + \frac{\delta_{jk}}{3} \right) \frac{\partial \tilde{u}_j}{\partial x_k} + \\
 C_{h,6}\bar{\rho}k \frac{\partial \sqrt{h'^2}}{\partial x_j} \frac{\partial \tilde{h}}{\partial x_j} + \frac{\partial}{\partial x_j} \left[\bar{\rho}(\gamma\alpha + \alpha_T C_{h,7}) \frac{\partial \varepsilon_h}{\partial x_j} \right] &+ \\
 C_{h,8} \frac{q_{T,j}}{\tau_h} \frac{\partial \tilde{h}}{\partial x_j} - \gamma \bar{\rho} \varepsilon_h \left[\frac{C_{h,9}}{\tau_h} \frac{C_{h,10}}{\tau_k} \right] &+ \\
 C_{h,11} \varepsilon_h \left[\frac{D\bar{\rho}}{Dt} + \frac{\bar{\rho}}{\bar{p}} \max \left(\frac{D\bar{p}}{Dt}, 0.0 \right) \right], &
 \end{aligned} \quad (40)$$

where D/Dt represents the substantial or material derivative and $\tau_k = \bar{\rho}k/(\mu\zeta)$. The turbulent Prandtl number is given in terms of μ_T and turbulent thermal diffusivity α_T i.e. $Pr_t = \mu_T/(\bar{\rho}\alpha_T)$ and α_T is modeled as

$$\alpha_T = 0.5(C_h k \tau_h + \mu_T / (0.89 \bar{\rho})), \quad \text{where } \tau_h = \tilde{h}'^2 / \varepsilon_h. \quad (41)$$

The modeling of α_T is based on experiments in simple shear flows which showed that the appropriate timescale for temperature fluctuations is proportional to the arithmetic average of τ_h and τ_k . The model constants are: $C_h = 0.0648, C_{h,2} = 0.5, C_{h,4} = -0.4, C_{h,5} = -0.05, C_{h,6} = -0.12, C_{h,7} = 1.45, C_{h,8} = 0.7597, C_{h,9} = 0.87, C_{h,10} = 0.25$, and $C_{h,11} = 0.575$.

V. MODELING CHALLENGES PERTINENT TO HYPERSONIC FLOWS

A. Flat plate boundary layers

Many one- and two-equation models struggle to accurately predict wall quantities of interest (wall shear stress and wall heat flux) for ZPG flat plate TBLs at hypersonic speeds^{22,24,126,127}, particularly for cold wall boundary layers at high Mach and Reynolds numbers²⁴. In general, RANS

models tend to over-predict both wall shear stress and wall heat flux at high Reynolds numbers. Figure 2 illustrates this challenge by showing predictions of two standard RANS models — the Menter SST model and the Spalart–Allmaras model — on a Mach 11 ZPG hypersonic TBL at a wall temperature-to-recovery ratio of $T_w/T_r = 0.20$, for which comparative DNS data are available from Ref. 116 and experimental data from the CUBRC facility^{20,117}. For both turbulence models, wall shear stress and heat flux predictions show discrepancies compared to the experiment and DNS that increase as the boundary layer spatially evolves.

Various compressibility corrections have been assessed (see Refs. 22 and 24) and proposed (see Refs. 126 and 127) to address these issues. Aiken *et al.*²² compared the predictions of the SA, SST, and BSL models to DNS data¹⁰⁴ for ZPG, cold-wall boundary layers for Mach numbers ranging from 2 to 8 with wall-to-recovery-temperature ratios of 0.18 to 1.0 and concluded that no model accurately predicts QoIs at the wall across this range of conditions. They further concluded that the Zeman compressibility correction tends to improve accuracy for wall QoIs, but does so at the expense of worse wall-normal temperature profiles. Rumsey²⁴ studies the performance of the $k-\omega$ model over a range of Mach numbers and wall-to-recovery-temperature ratios, and similarly shows degraded performance at high Mach number, cold-wall conditions. Rumsey notes an improved performance of algebraic models like Baldwin-Lomax over standard one- and two-equation models, and further shows that dilatation-dissipation corrections tend to bring $k-\omega$ predictions of wall QoIs more inline with the Baldwin-Lomax model. Danis and Durbin propose a compressibility correction for the $k-\omega$ model — which modifies the turbulent production in the ω equation — to improve wall QoI predictions in hypersonic boundary layers¹²⁶. The correction is local, is a function of a friction Mach number and a heat transfer parameter, and shows improved results over a range of boundary layers. Barone *et*

*al.*¹²⁷ propose several corrections to the SA model to improve performance in ZPG TBLs including a modified near-wall viscous damping function (informed by hypersonic boundary layer DNS datasets) and a normal Reynolds stress correction. Of note, Ref. 127 highlights that the wall-normal Reynolds stress has an appreciable impact on the wall-normal momentum balance for high-speed boundary layers; this aspect is neglected in traditional RANS models. Specifically, under the assumption that the wall-normal Reynolds stress scales with the freestream dynamic pressure, it is straightforward to show that the ratio of the wall-normal Reynolds stress to pressure scales with the Mach number squared, i.e.,

$$\frac{\tau_{22}}{p} \sim M_\infty^2.$$

For high Mach number flows, the contribution of the wall-normal Reynolds stress can be non-negligible; Barone confirmed this result with DNS. The resulting SA model gives improved performance for high Reynolds number boundary layers. While the aforementioned advancements have improved predictions, many are ad-hoc and, as Rumsey²⁴ concludes, there is a clear need for an increased understanding of zero pressure gradient hypersonic boundary layers.

B. Shock/turbulence interaction and compressibility effects

Shock waves, often embedded within a fully turbulent flow field, are an inevitable feature of high-speed applications. The interaction between turbulence and an oscillatory, corrugated, and sometimes broken shock wave causes a turbulence amplification and an increased anisotropy, which leads to increased dissipation and acoustic energy dispersion downstream of the shock. The physics of the shock turbulence interaction (STI) needs to be accurately modeled in the context of RANS. This is especially true for many applied problems, such as dual-bell nozzles, where incorrect modeling of the turbulence amplification directly impacts post-shock mixing effectiveness and thus the size of the recirculation regions characteristic under certain operating conditions. This, in turn, can influence the overall shock structure of the problem and have a first-order effect on the solution. The modeling of turbulence amplification in STI was first studied by Ribner¹²⁸ through linear interaction analysis (LIA); an approach that can capture many of the correct features of the STI problems, especially when the turbulent Mach number becomes small¹²⁹. STI was later re-examined using rapid distortion theory (RDT)^{130,131} but this approach leads to an over-amplification at high-Mach numbers as a result of the non-homogeneous compression of the shock due to unsteadiness and curvature, which is not modeled by RDT¹³². Despite their useful insight, analytical models generally provide an incomplete description of the turbulence amplification through shocks for direct use in RANS modeling.

Although LIA has been used for turbulence modeling (see e.g. Griffond and Soular¹³³) these analytical solutions require compatibility conditions that limit their applicability to weak turbulence. For greater generalizability, ad-hoc STI

models have been integrated into RANS solvers to correctly capture the TKE amplification across the shock. These ad-hoc models are necessary to address two important, yet related, problems when using the RANS equations for STI: (i) resolution of the shock structure, and (ii) shock unsteadiness and curvature.

The shock thickness in a viscous fluid scales with the mean free path of gas molecules¹³⁴ therefore, it represents a near discontinuity as observed from the relevant scales for typical RANS simulations. The turbulence causes instantaneous corrugation and unsteadiness of the shock structure. Thus, in a time-averaged sense, the shock will be significantly thicker than the instantaneous and local shock thickness. Despite its increased thickness, the shock still remains thin with respect to the typical scale of resolution of a RANS simulation. Therefore, high-speed RANS simulations will inevitably under-resolve the shock structure, which is problematic for most two-equation models. The TKE production in the classical turbulence transport equations (in standard two-equations models), takes the general form:

$$P_k = \tau_{ij} \frac{\partial u_i}{\partial x_j}, \quad (42)$$

where the production term is directly proportional to the velocity gradient and Reynolds stresses. As the shock thickness is effectively underresolved in applied, three-dimensional STI problems, the TKE production will effectively be tied to the mesh resolution at the shock; a significant problem for grid convergence. When the turbulence is high, thus a very diffusive shock, some models can reach grid convergence with sufficient resolution¹³⁵. However, this is not the case for most STI models.

A number of works^{129,136,137} have proposed a scaling to approximate the time-averaged shock thickness, which could be used to bound the TKE production. The integration of the ensemble-averaged shock thickness has been one of the core ideas behind some STI modeling paradigms¹³⁸. In the hypersonic regime, the time-averaged shock thickness becomes small, even sub-Kolmogorov, as the turbulent Mach numbers are typically smaller. Ryu and Livescu¹²⁹ showed that the LIA solutions are regained when the viscous and nonlinear effects become small across the shock when the laminar shock thickness over the Kolmogorov length scale tends toward zero; a condition which is met in most hypersonic flows. Therefore, the challenges of vortical turbulence interacting with a planar shock in the hypersonic regime are simpler as the solution will tend towards turbulence amplification predicted by LIA.

Despite the under-resolution of the shock thickness, most turbulence models over-predict the TKE amplification. To address this over-amplification and embed stronger physical modeling of the shock corrugation and unsteadiness, Sinha, Mahesh, and Candler¹³⁹, proposed a correction to the turbulence transport equations, discussed in greater depth in section IV F, which has become widely used and extended by others¹⁴⁰. Other works impose an upper bound on the production term to mitigate unphysical TKE production through the shock¹⁴¹. Zhang *et al.*¹⁴² relied on a combination of shock

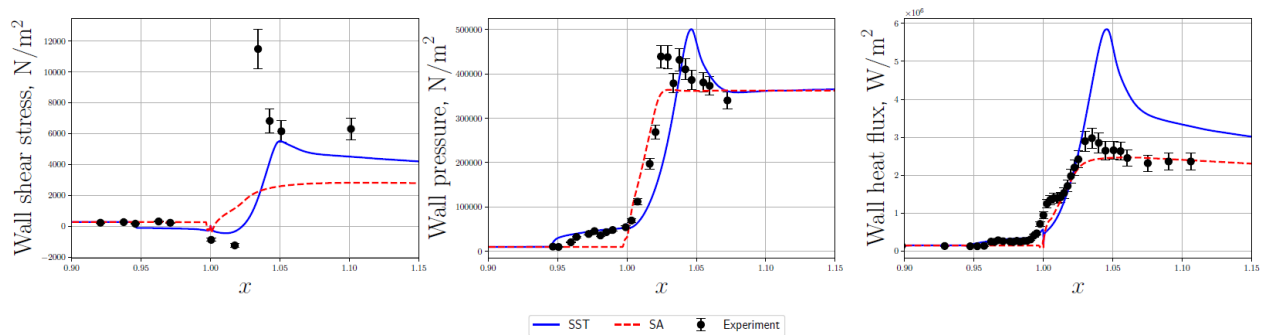


FIG. 3: RANS model predictions for wall shear stress (left), wall pressure (center), and wall heat flux (right) for a Mach 8, 33° compression ramp with $T_w/T_e = 0.29$.

sensors with locally applied damping functions to the TKE production term in $k-\omega$ SST to better match experimentally observed results, this model was recently extended to use a vorticity-based instead of a shear-based production term definition near the shock¹⁴³.

The two-equation models cannot directly account for the important anisotropy generated through STI, which plays a critical role in post-shock mixing, energy redistribution, and turbulence decay. To address the lack of anisotropy in two-equation models, RSTMs for STI have been proposed. Similar to the TKE, the Reynolds stresses are over-predicted using conventional RSTM models. A physics-based modification to RSTM was proposed by Vemula and Sinha¹⁴⁴ that accounts for the damping effect of the shock unsteadiness and showed some grid convergence properties. A number of works have integrated STI models within the transport equations for the Reynolds stresses by relying on two-length scale models which have shown good agreement with LIA^{135,138} but require a significant grid resolution. Karl, Hickey, and Lacombe¹⁴⁵ proposed a simple, but empirically derived correction method that adjusts the TKE jump, decay, and anisotropy; the generalizability of which, especially for oblique shocks has not been shown.

C. Shock/boundary layer interaction and wall heat-transfer

SBLIs occur when a turbulent boundary layer intersects with a shock wave and result in large peaks in wall heat flux, wall shear stress, and wall pressure. RANS modeling of SBLIs at hypersonic speeds is extremely difficult as the flow is largely anisotropic and standard modeling assumptions such as the Boussinesq relationship and constant turbulent Prandtl number break down. RANS predictions of SBLI flows are subject to erroneous predictions for flow separation, wall heat flux, and wall shear stress. Figure 3 illustrates this issue by presenting predictions from the Menter SST and Spalart-Allmaras RANS models for an SBLI emerging from a Mach 8, 33° compression ramp with $T_w/T_e = 0.29$ (T_e is the free-stream stagnation temperature) and comparing them to experimental data from Holden¹⁴⁶. The model predictions deviate significantly from each other and illustrate the challenges in

modeling SBLI flows. The SST model yields reasonable predictions for peak wall pressure but drastically over-predicts wall heat flux. The SA model fails to predict flow separation, under-predicts peak wall heat transfer and pressure, and massively under-predicts wall shear stress.

As seen above, two significant challenges RANS models encounter for SBLIs are (1) accurate prediction of flow separation and (2) the joint prediction of wall heat flux and wall shear stress. With respect to the prediction of flow separation, standard two-equation models without stress limiters, along with the Spalart-Allmaras model, tend to under-predict flow separation⁸⁹. A variety of fixes have been devised to address this issue. These fixes include, but are not limited to, rapid compression corrections (see Sec. IV E), stress limiters^{27,147}, and shock unsteadiness models (Sec. IV F). In general, these methods act by decreasing the eddy viscosity in regions near the SBLI, which in turn enhances separation. However, these corrections are typically calibrated for a flow regime of interest and a specific turbulence model; these models require further development for greater generalizability⁸⁹. Further, different turbulence models are subject to different systematic deficiencies. As an example, the 2003 variants of the SST model, which use the strain invariant instead of the vorticity invariant in the denominator of the eddy viscosity, systematically over-predict the size of the separation region in hypersonic SBLIs^{85,148}. Similar results exist with, e.g., the RNG $k-\epsilon$ model¹⁴⁹. A recent collaborative effort on RANS modeling of the hypersonic flared cone — using 11 different commercial, institutional, and open-source codes — revealed a large variation in the onset of flow separation¹⁵⁰. Thus, while progress has been made in predicting flow separation in SBLIs, challenges remain.

With respect to the joint prediction of wall heat flux and wall shear stress, standard two-equation models tend to massively over-predict wall heat flux near the point of reattachment. This over-prediction is typically worse for $k-\epsilon$ -based models than for $k-\omega$ -based models^{89,151}. Similar to ZPG TBLs, the over-prediction in peak heat flux appears to worsen as the Reynolds number grows¹⁴⁸. Length-scale corrections (Sec. IV D) and variable turbulent Prandtl number models (Sec. IV H) have shown promise for addressing this issue. Huang *et al.*¹⁰⁹ show that length-scale corrections result in

a dramatic improvement in wall heat flux predictions for a range of SBLI flows. It is worth highlighting, however, that length-scale corrections additionally reduce wall shear stress; this impact was not assessed in Ref. 109. The variable turbulent Prandtl number of Roy and Sinha (see Sec. IV H) similarly shows promise for addressing over-prediction in wall heat flux. Ref. 152 shows that an extension of the model for hypersonic flows results in improved predictions for wall heat flux on a variety of hypersonic compression ramps and impinging SBLI cases. Unlike length-scale limiting, the variable turbulent Prandtl number model decouples the turbulent thermal diffusivity from the eddy viscosity. This allows for a reduction in wall heat flux with a minimal impact on the wall shear stress, and vice versa. This approach is supported by experimental data, which suggests that the rate at which wall shear stress rises through an SBLI decouples from the rate at which wall heat flux rises as shock strength increases⁸¹. Lastly, we remark that the SA model does not result in the same type of over-predictions in wall heat flux in SBLIs as two-equation models, as seen above. However, the improved performance of the SA model for wall heat flux is at the expense of an under-prediction in wall shear stress¹⁴⁸.

D. Surface roughness and blowing effects

The development of roughness patterns and gasification during the ablation process (see Section V F 1) significantly alters the boundary layer state and affects SBLI properties. Modeling the transpired turbulent boundary layers over rough walls is a challenging task. Roughness effects tend to increase peak surface heat transfer compared to smooth wall conditions^{9,153}. On the other hand, blowing creates a cooler film in the near wall region and provides additional protection against the convective heat flux, referred to as the blockage effect of blowing, thus reducing the total heat load¹⁵⁴.

The distribution of Reynolds normal and shear stresses across a TBL is significantly affected due to the roughness effects^{47,155}. However, logarithmic behavior is preserved for the mean velocity and the outer region is independent of the wall conditions as per Townsend's hypothesis. A downward shift in the streamwise velocity is observed in the log region compared to ZPG TBLs over a smooth surface^{47,155,156}. The decreased momentum in the incoming TBL associated with the roughness effects before interaction with a shock wave results in an earlier separation and a delayed reattachment compared to a smooth wall case for identical flow conditions and shock strengths¹⁵³. In the RANS framework, the discrete element method has been widely used to describe the interaction between well-defined distributed roughness patterns and turbulent flow. This method involves directly including some roughness corrective terms in the form of sources and sinks into the RANS or boundary layer equations¹⁵⁷. However, it requires modification of the original system of RANS equations and thus it is not desirable.

A classical and the most commonly used method in industrial applications to describe the effect of any given roughness is the equivalent sand grain approach. Equivalent sand grain

roughness is defined as the height of Nikuradse's sand grain roughness that would be required to produce the same velocity defect. In the fully rough regime, it is characterized by the roughness parameter (also called roughness Reynolds numbers) k_s^+ , i.e. dimensionless equivalent sand grain height k_s

$$k_s^+ = \frac{\bar{\rho}_w k_s u_\tau}{\mu_w}. \quad (43)$$

Unlike the discrete element method, this method is not intrusive to an existing code and thus appears to be the most suitable for industrial purposes. It involves modification of the boundary conditions of a turbulence model using the sand grain roughness height as a new parameter to recover the expected law of the wall. The velocity shift is achieved by imposing an artificial increase of the eddy viscosity to increase turbulence levels at the wall. Several roughness corrections are available in the literature; however, they are developed for incompressible flows¹⁵⁸, and their application to hypersonic flows is limited. The extension of these corrections to compressible flows is based on the observations of Goddard^{159,160} which imply that the effect of roughness for compressible flow can be formulated in a fashion similar to that of the incompressible case if the pertinent parameters are evaluated based on local flow properties at the wall. These roughness corrections generally result in an over-prediction of the wall heat flux with a constant Pr_T value. A correction to Pr_T based on a large database of low-speed turbulent boundary layers over rough surfaces obtained using the discrete element method¹⁶¹ is found to improve wall heat flux predictions. Olazabal *et al.*^{162,163} applied the dynamic and thermal corrections of Aupoix^{158,161} to the SST $k-\omega$ model to compute 7° half-angle sharp and blunt cones at Mach 10 and 6° half-angle slender cone at Mach 11.3. Reasonable comparisons between the experiments and model predictions are obtained for skin friction and wall heat transfer, however, discrepancies remain. On the other hand, Marchenay *et al.*⁹ applied the Aupoix corrections to the SST $k-\omega$ model along with Sarkar and Zeman compressibility corrections and obtained excellent predictions for skin friction and Stanton number for a hemispherical model and 6° slender cone configuration at Mach 11 for which the standard SST model largely overestimated the surface heat transfer.

Similar to wall roughness effects, wall blowing also tends to decrease the viscous sublayer thickness and alters the velocity profile in the inertial region. Experimental investigations on the effects of blowing are generally motivated by turbulent flow control and transpiration cooling for thermal protection systems (TPS). The classical RANS models show an over-prediction of near-wall turbulence production, especially for the SA model, which results in a faster growing boundary layer over the blowing region¹⁶⁴. Blowing effects are introduced by altering the slope of the mean velocity profile in the inertial region through a blowing parameter $v_w^+ = v_w/u_\tau$, i.e. wall-normal velocity at the wall (also called blowing velocity). Wilcox's correction¹⁶⁵ to the $k-\omega$ model to account for the blowing effects has the same effect as the roughness corrections. It consists of a reduction of the specific dissipation

rate wall condition given by

$$\omega_w^+ = \frac{25}{v_w^+(1 + 5v_w^+)}. \quad (44)$$

However, the correction has not been tested for hypersonic flows.

The roughness and blowing corrections discussed above cannot be employed together since they play on the same wall boundary conditions. Recent works of Marchenay *et al.*^{9,166} model the combined effects of surface roughness and blowing due to the ablation process for k - ω based models. The modeling strategy relies upon the characterization of the velocity profile in the inertial region and the identification of the separate contributions of blowing and surface roughness on the velocity shift ΔU^+ of the logarithmic law,

$$u^+ = \frac{1}{\kappa} \ln y^+ + C - \Delta U^+ |_{app}(k_s^+, v_w^+). \quad (45)$$

Further, the apparent velocity shift is decomposed as

$$\Delta U^+ |_{app}(k_s^+, v_w^+) = U_r^+(k_s^+) + U_{rb}^+(k_s^+, v_w^+), \quad (46)$$

where U_r^+ is the velocity shift given by standard roughness corrections and U_{rb}^+ depicts the effect of the interaction between roughness elements and blowing on the skin friction. The apparent velocity shift is imposed by modifying the wall-boundary conditions for k and ω in the following manner,

$$k_w = k_w^+ u_\tau^2 \quad \text{and} \quad \omega_w = \bar{\rho} \omega_w^+ u_\tau^2 / \mu, \quad (47)$$

where

$$\begin{aligned} k_w^+ &= \max(0, k_0^+), \\ k_0^+ &= \frac{1}{\sqrt{\beta^*}} \tanh \left[\left(\frac{\ln(k_s^+ / 30)}{\ln(8)} + 0.5[1 - \tanh(k_s^+ / 100)] \tanh(k_s^+ / 75) \right) \right], \\ \omega_w^+ &= \frac{400000}{k_s^{+4}} \left(\tanh \frac{10000}{3k_s^{+3}} \right)^{-1} + \frac{70}{k_s^+} [1 - \exp(-k_s^+ / 300)]. \end{aligned} \quad (48)$$

The equivalent sand grain height, k_s , is given by

$$\begin{aligned} k_s^+ &= \max(k_1, k_2), \quad k_1 = k_s^+ (1 + f v_w^+), \\ k_2 &= \exp \left[\frac{\kappa(b_1 - C)}{1 - \kappa b_2} \right] (1 + f v_w^+)^{1/(1 - \kappa b_2)} \\ f &= 5.9 [1 + \tanh(k_s^+ - 7)] + 4.2, \end{aligned} \quad (49)$$

where $\kappa = 0.4$, $C = 0.55$, and the constants b_1 and b_2 are given by

$$\begin{aligned} k_s^+ < 3.5: & \quad b_1 = 5.5 \quad b_2 = 1/\kappa, \\ 3.5 \leq k_s^+ < 7: & \quad b_1 = 6.59 \quad b_2 = 1.52, \\ 7 \leq k_s^+ < 14: & \quad b_1 = 9.58 \quad b_2 = 0, \\ 14 \leq k_s^+ < 68: & \quad b_1 = 11.5 \quad b_2 = -0.7, \\ 68 \leq k_s^+: & \quad b_1 = 8.48 \quad b_2 = 0. \end{aligned} \quad (50)$$

The equivalent sand grain height estimation is difficult and relies on empirical roughness correlations. A correction to Pr_T is also proposed to account for the blowing thermal effects on smooth and rough surfaces. The turbulent mixing increase is represented by the roughness function ΔU^+ , the effect of surface topology or the geometry of roughness above the meltdown surface is parameterized using the corrected wetted surface ratio S_{corr} , and the correction is imposed only in the roughness sublayer via the mean physical height k_m of the rough surface.

A contribution that accounts for the effects as mentioned earlier is added to the constant turbulent Prandtl number used for smooth walls $Pr_{T,s}$

$$\begin{aligned} Pr_T &= Pr_{T,s} + \Delta Pr_T, \quad \Delta Pr_T = (A \Delta U^{+2} + B \Delta U^+) e^{-y/k_m} \\ A &= (0.0155 - 0.0035 S_{corr}) [1 - e^{-12(S_{corr}-1)}], \\ B &= -0.08 + 0.25 e^{-10(S_{corr}-1)} \\ \Delta U^+ &= \Delta U_r^+ + \Delta U_{rb}^+, \\ \Delta U_r^+ &= \frac{1}{\kappa} \ln(k_s^+) + C - b_1 - b_2 \ln(k_s^+), \\ \Delta U_{rb}^+ &= \frac{1}{\kappa} \ln(1 + f_T v_w^+) \\ f_T &= 8 [1 + \tanh(k_s^+ - 7)], \end{aligned} \quad (51)$$

where the parameters k_m and S_{corr} need to be estimated. The modification is designed to recover the turbulent Prandtl number's constant value above the roughness sublayer. These dynamic and thermal corrections when applied to the SST k - ω model along with the Zeman compressibility correction resulted in improved predictions for skin friction and Stanton number for a 10.5° slender cone configuration at Mach 11 for different blowing rates $F = (\bar{\rho}_w v_w) / (\bar{\rho}_e \tilde{u}_e)$ (see Ref. 9).

E. Thermochemical non-equilibrium effects

When thermochemical non-equilibrium effects are at stake, the governing equations for the gas are supplemented with additional transport equations describing the evolution of the chemical species (chemical non-equilibrium) and/or the modal energy(ies), see Section III A 5.

Favre-averaging of such equations introduces additional unclosed terms, which will be examined in the following.

We focus first on the unclosed terms in the species transport equations, and specifically on the turbulent mass transport term $\overline{\rho u_j'' Y_n''}$. The latter is usually modeled by introducing a ‘‘turbulent’’ Schmidt number, such that:

$$\overline{\rho u_j'' Y_n''} \simeq -\bar{\rho} D_{t,n} \frac{\partial \tilde{Y}_n}{\partial x_j} = -\frac{\mu_t}{Sc_{t,n}} \frac{\partial \tilde{Y}_n}{\partial x_j}, \quad (52)$$

where $D_{t,n}$ is a turbulent diffusivity coefficient for the n th species, and $Sc_{t,n} = \frac{\mu_t}{D_t}$ is the corresponding turbulent Schmidt number, representing the ratio of turbulent transport of momentum to turbulent transport of mass. Early CFD modeling of the turbulent mass transport of a passive scalar in

incompressible flow used $Sc_t = 0.7$, since “there is wall-authenticated evidence that the time–mean concentration profile is appreciable “fatter” than that of velocity”¹⁶⁷. On the other hand, Launder¹⁶⁸ pointed out that Sc_t shows the value of 0.9 for turbulence near the wall. Quoting from these results, the values 0.7 or 0.9 have been widely used to model turbulent mass diffusion in CFD codes. However, in the review paper of Tominaga and Stathopoulos¹⁶⁹ the turbulent Schmidt number providing the best fit to the experimental observations was found to vary in a range as large as $0.2 \leq Sc_t \leq 1.3$, depending on the flow problem. For compressible flows, experimental studies¹⁷⁰ have shown that Sc_t differs significantly from unity: in shock-free flows, the turbulent Schmidt number is found to be in the range $0.5 \leq Sc_t \leq 1.5$, and even larger variations are observed in case of SBLs. In addition to not having a well-defined value for all flows, Sc_t is also seen to vary across the flow, which invalidates the use of the linear constitutive relation (52) to model turbulent mass transport.

Sciacovelli *et al.*⁸ conducted *a priori* tests of the validity of the constant turbulent Schmidt number assumption for hypersonic boundary layers at Mach 10 and 12.48, under chemical nonequilibrium and adiabatic wall and thermochemical nonequilibrium and cooled wall conditions. For nearly parallel flows, the “exact” species Schmidt numbers can be computed from DNS data as:

$$Sc_{t,n} = \frac{\overline{\rho u'' v''} \partial \tilde{Y}_n / \partial y}{\overline{\rho v'' Y_n''} \partial \tilde{u} / \partial y}. \quad (53)$$

The results showed that, even for such relatively simple flows, $Sc_{t,n}$ is not constant but instead, like the turbulent Prandtl number, it exhibits a bump in the logarithmic region, more pronounced for the cooled wall case, and is below the average value in the outer region. The value of 0.9, often used in the literature for linear turbulent mass flux models, is only representative of the average across the boundary layer. The profiles for different chemical species were not found to be much different from each other, but their values and the position of the bump in the logarithmic region were clearly dependent on M_∞ and the wall conditions.

The influence of species mass fraction and temperature fluctuations on the species production rates, i.e. the intensity of turbulence-chemistry interactions (TCI), is evaluated through the quantity:

$$\hat{\omega}_n^I = \left[\overline{\hat{\omega}_n(T, \rho_n)} - \hat{\omega}_n(\bar{T}, \bar{\rho}_n) \right] \frac{\bar{\mu}}{\bar{\rho} \bar{\tau}_w}, \quad (54)$$

where $\overline{\hat{\omega}_n(T, \rho_n)}$ is a source term that represents the production or depletion of the n -th species in the mixture due to chemical reactions. This parameter represents the chemical production due to turbulent fluctuations, leading to $\overline{\hat{\omega}_n(T, \rho_n)} \neq \hat{\omega}_n(\bar{T}, \bar{\rho}_n)$ due to the strong nonlinearity of the chemical source term $\hat{\omega}_n$. A simplification often adopted in the RANS framework is to assume $\overline{\hat{\omega}_n(T, \rho_n)} \approx \hat{\omega}_n(\bar{T}, \bar{\rho}_n)$, which is an acceptable approximation only if the turbulence-chemistry interactions are limited. Less simplistic models ex-

ist for combustion applications¹⁷¹, based on the Eddy Dissipation Concept (EDC):

$$\overline{\hat{\omega}_n} \approx \gamma^* \hat{\omega}_n(\bar{T}, \bar{\rho}_n), \quad (55)$$

where $\gamma^* \approx 9.7(v\mathcal{E}/k^2)^{\frac{3}{4}}$ represents the fine-scale structure volume fraction, i.e. the fraction of the volume in which chemical reactions take place which is assumed to be in the region where the turbulent kinetic energy is quasi-steady. Direct extraction of $\hat{\omega}_n^I$ from DNS data shows that the indicator takes large values close to the wall for the adiabatic case M10C, and in the buffer region for the wall-cooled case M12, where turbulent fluctuations are significant.

A priori tests for the above-mentioned hypersonic boundary layers showed that the assumption $\overline{\hat{\omega}_n(T, \rho_n)} \approx \hat{\omega}_n(\bar{T}, \bar{\rho}_n)$ is reasonably accurate for adiabatic wall conditions, but underestimates the DNS value in the cooled case. On the contrary, the EDC model does not prove to be satisfactory, mainly due to the isotropic assumption in the formulation of γ^* causing the model to fail close to the wall. Further research is required on closures for this term, by leveraging, for instance, presumed PDF models typically used in turbulent combustion applications¹⁷².

The behavior of unclosed terms in the averaged vibrational energy equation was investigated in the DNS study of Passiatore *et al.*²⁹. They showed that the vibrational turbulent heat flux $\overline{\rho u_j'' e_v''}$ is a prominent term in the vibrational energy budget, and should be taken into account in RANS models. A simple gradient model, relying on the introduction of a vibrational turbulent Prandtl number Pr_t^V was introduced to model such term, by analogy with the rototranslational turbulent heat flux¹⁷³. For nearly parallel flows, an “exact” value can be extracted from DNS data:

$$Pr_t^V = \frac{\overline{\rho u'' v''} \partial \tilde{e}_v / \partial y}{\overline{\rho v'' e_v''} \partial \tilde{u} / \partial y}, \quad (56)$$

such that the model reads:

$$\overline{\rho u_j'' e_v''} = \frac{\mu_t}{Pr_t^V} \frac{\partial \tilde{e}_v}{\partial x_j}, \quad (57)$$

where Pr_t^V exhibits a behavior similar to that of Pr_t across the boundary layer height, with a bump in the logarithmic region. In this case, a value of 0.9 is reasonably well recovered only in the outer region.

Finally, the Favre-averaged source term in the vibrational energy equation also needs attention. Such a term measures the intensity of the interaction between turbulence and thermal relaxation, which can be considered as weak when $Q_{TV}(T, T_V, \rho, p, Y_n) \approx Q_{TV}(\bar{T}, \bar{T}_V, \bar{\rho}, \bar{p}, \bar{Y}_n)$, where Q_{TV} is a source term accounting for vibrational energy production/depletion due to translational-vibrational energy transfers. Deviation from such behavior can be measured using the indicator²⁹:

$$Q_{TV}^I = \frac{Q_{TV}(T, T_V, \rho, p, Y_n) - Q_{TV}(\bar{T}, \bar{T}_V, \bar{\rho}, \bar{p}, \bar{Y}_n)}{Q_{TV}^{\max}}, \quad (58)$$

with $\overline{Q_{TV}^{\max}}$ the maximum wall-normal value at the selected station. Differences up to $\approx 15\%$ in the inner layer, indicating a strong interaction between turbulence and thermal nonequilibrium, were observed for the thermochemical nonequilibrium boundary layer at Mach 12.48. Although a few models do exist for the chemistry source term $\dot{\omega}$, no models are found in the literature for $\overline{Q_{TV}}$, which is potentially critical for RANS modeling of hypersonic flows out of thermal equilibrium.

F. Multi-physics considerations

1. Catalysis and ablation phenomena

Catalysis and ablation are physical phenomena that occur at the interface between the hypersonic flow and the wall, typically as part of thermal protection system (TPS) used to reduce the heat transfer from the fluid to the vehicle.

Catalysis is a chemical gas/surface interaction, and it relates to a series of chemo-physical phenomena such as diffusion of reactants from the gas to the surface, chemical reactions at the interface, and diffusion of the products into the gas. In hypersonic flow models, catalysis is generally modeled by introducing a recombination coefficient (designated $\gamma = M_{rec}/M_{imp}$), corresponding to the ratio of recombining atoms M_{rec} over atoms that impinge on a wall M_{imp} . Such a ratio can be measured experimentally, but large uncertainties on its value exist¹⁷⁴.

Ablation of aerospace materials is a widely employed TPS solution used to protect vehicles from radiative heating. Convective heat-transfer rates are nearly zero because the outward flow of ablative products impedes the conductive heat flux to the wall. The product gas of ablation forms a layer, called ablation-product layer, which prevents the hot shock layer gas from reaching the wall¹⁷⁴. The ablation-product layer absorbs a portion of the radiative flux directed toward the wall. Lightweight ablative materials are characterized by high porosities, with pores being the site of chemical reactions¹⁷⁵. Turbulence models then largely borrow from pre-existing studies on incompressible flows on porous materials. Specific models for hypersonic flows are an open research topic.

Finally, ablation induces geometrical modifications of the surface and generates surface roughness, which plays a major role in transition and turbulence¹⁷⁶. This is another open topic (see Section **V D**) that needs attention for the development of improved models.

2. Conjugate heat transfer

Strong aerothermal heating of high-enthalpy flows represents a key consideration for thermal management systems in hypersonic vehicles. The predicted thermal loading characteristics dictate the material and TPS, which in turn has direct implications on vehicle weight and design. Both maximum and total integrated thermal loads are important design parameters

but their accurate prediction requires a two-way coupled, conjugate heat transfer (CHT) evaluation of the heat flux on the vehicle.

The main contribution to the heat flux at the solid-fluid interface is governed by the temperature gradient at the wall, which in turn depends on the near wall turbulence and heavily on the temperature of the wall. Whereas the heat flux shows a linear dependence on wall temperature for a perfect gas in the laminar regime¹⁷⁷, the effects of temperature are much more complex with turbulent flows for which temperature scaling has been recently proposed for high-speed, non-adiabatic boundary layer flows¹⁷⁸. The spatially and temporally varying wall temperature depends not only on the aerothermal heating and chemical kinetics of the gas but also on internal heat sources (propulsion system, combustion chamber, electronic equipment, etc.) and external heat transfer through radiation or other shock boundary layer interaction-induced heating. Furthermore, the wall temperature is influenced by the heat conduction within the vehicle structure, the convective and radiative losses, ablative effects, and active thermal protection system. The aggregate of these multiphysics effects will govern the time-varying heat flux in the vehicle.

The integration of CHT demands many algorithmic and computational changes to classical CFD solvers, readers can refer to a review of the recent studies on the topic¹⁷⁹. As the accuracy of the near-wall temperature and velocity gradients is central to CHT computations (especially in the turbulent regime), the compounding modeling challenges of high-speed near-wall flow, discussed earlier, take on even greater importance. Within the context of RANS, two modeling parameters are particularly important: turbulent Prandtl number¹⁸⁰ and the modeling of thermal fluctuations¹⁸¹. Within the context of higher fidelity simulations such as LES, the wall-modeling in the context of CHT is a particularly relevant topic. A good number of works have looked at wall-modeled LES (WM-LES) with CHT in lower speed application^{182,183} very few works have started to address this problem for high-speed flows^{184,185}.

VI. MODEL VALIDATION : AVAILABLE DATASETS

Experiments and DNS play an important role in the development and validation of turbulence models by providing data on the flow physics required to substantiate modeling assumptions. Comprehensive model validation requires assessment across a broad parameter space, encompassing diverse Mach numbers, Reynolds numbers, wall temperature and surface conditions, and geometric complexities. This extensive validation helps ensure the model's robustness and applicability to a wide range of operating conditions for a given design requirement. However, there is a serious lack of wind tunnel, flight, and high-fidelity simulation data in the hypersonic regime compared to the lower speeds.

Tables **I-VI** present the available experiments and DNS for TBL flows in the hypersonic regime for smooth as well as rough surfaces, and it excludes the experimental works that have not reported wall heat transfer. The experiments are gen-

TABLE I: Experiments – ZPG hypersonic TBL : Flat plate - FP; Nozzle Wall - NW; Wind tunnel wall - WTW; Cone/Ogive Cylinder - COC; Hollow cylinder - HC; Sharp circular cone - SCC; [®] high-enthalpy case; * ASCII datafile available on the NASA Turbulence Modeling Resource website¹⁸⁶.

Configuration	Experiments	Me	T_w/T_{aw}	H_e (MJ/kg)	Re_e/m $\times 10^6$	Quantities reported
FP	Winkler & Cha (Ref. 187) & Winkler (Ref. 188)	4.98 – 5.21	0.58 – 0.83	0.35 – 0.5	9.3 – 12.6	P_w, C_f, Q_w
	Danberg (Refs. 189 and 190)	6.7	0.41 & 0.87	0.5 & 0.5	8 & 19	P_w, Q_w
	Young (Ref. 191)	4.91	0.54 & 1	0.335 & 0.64	17.2 & 45.2	P_w, C_f, Q_w
	Neal (Ref. 192)	6.8	0.5	0.62	2 – 16	C_f, Q_w
	Wallace (Ref. 193)	7.4 – 10.7	0.16 – 0.33	1 – 2.12	29.5 – 265.7	P_w, C_f, Q_w
	Hopkins (Ref. 194)	6.5	0.32 – 0.51	0.69 – 1.09	1.7 – 4.07	C_f, Q_w
	Voisinet & Lee (Ref. 195)	4.9	0.25 – 1	0.4	9 – 25	C_f, Q_w
	Holden (Ref. 196)	7.4 – 12	0.16 – 0.34	0.99 – 2.07	15.1 – 191.8	P_w, C_f, Q_w
	Watson (Ref. 197)	9.5 – 10.1	1	0.3	7.769 – 34.544	P_w, C_f, Q_w
	Goynes (Ref. 198) [®]	5.3 – 6.7	0.022 – 0.11	3.2 – 13.1	0.43 – 16.1	P_w, C_f, Q_w
	Schulein (Ref. 81)*	5	0.8	0.41	37	P_w, C_f, Q_w
Holden (Ref. 146)*	8 – 11.4	0.195 – 0.325	1.02 – 1.71	36 – 205.2	P_w, C_f, Q_w	
NW	Hill (Ref. 199)	8.25 – 10.06	0.47 – 0.52	0.76 – 0.83	5.7 – 9.4	C_f, Q_w
	Wallace (Ref. 193)	6.6 – 8	0.1 – 0.33	1 – 3.2	1.2 – 36.1	P_w, C_f, Q_w
	Lee (Ref. 200)	4.91	0.52	0.61	5.06	P_w, C_f, Q_w
	Backx (Refs. 201 and 202) & Backx & Richards (Ref. 203)	15 & 19.8	*(T_w/T_{te} : 0.15 & 0.11)	1.7 & 2.3	27.9 & 11.2	P_w, Q_w
WTW	Hopkins (Ref. 194)	7.4	0.32 – 0.49	0.7 – 1.05	0.63 – 4.01	C_f, Q_w
COC	Horstman & Owen (Ref. 43) & Owen & Horstman (Ref. 44)	7.2	0.49	0.67	10.9	P_w, C_f, Q_w
HC	Samuels (Ref. 204)	6	0.55 & 0.49	0.49 & 0.54	32.6 & 28.6	P_w, C_f, Q_w
	Murray (Ref. 205)	8.9	0.27	1.2	48	P_w, Q_w
SCC	Kimmel (Ref. 206 and 207)	7.93	0.46	0.725	6.6	P_w, Q_w

TABLE II: DNS – ZPG hypersonic TBLs; * ASCII datafile available on the NASA Turbulence Modeling Resource website²⁰⁸.

Condition	DNS	Me	T_w/T_{aw}	Re_θ $\times 10^3$
Low enthalpy	Maeder <i>et al.</i> (Ref. 118)	6	1	2.945
	Xin-Liang <i>et al.</i> (Ref. 209)	6	0.94	109.5
	Martin (Ref. 210)	4.97 & 5.98	0.95	6.23 & 8.43
	Duan <i>et al.</i> (Ref. 119)	5	0.18 – 1	1.28 – 4.84
	Duan <i>et al.</i> (Ref. 120)	4.9 – 11.93	0.97 – 1.05	1.51 – 11.3
	Liang (Ref. 121) & Liang & Li (Ref. 122)	8	0.15 & 0.77	22 & 78
	Chu <i>et al.</i> (Ref. 211)	4.9	0.5 – 1.5	3.48 – 7.61
	Duan <i>et al.</i> (Ref. 212)	5.86	0.76	9.45
	Zhang <i>et al.</i> (Ref. 213)	5.86	0.25 & 0.76	2.121 & 9.455
	Zhang <i>et al.</i> (Ref. 104)*	5.84 – 13.64	0.18 – 0.76	2.12 – 14.4
	Huang <i>et al.</i> (Ref. 42) : (similar to CUBRC M11 FP experiments)	10.9 & 13.64	0.2 & 0.18	9.08 – 14.258
	Sciacovelli <i>et al.</i> (Ref. 214)	6	0.72	5.72
	Nicholson <i>et al.</i> (Ref. 215)	4.9	0.91	17.406
	Huang <i>et al.</i> (Ref. 116)	4.9 – 13.4	0.18 – 0.91	1.465 – 26.762
	Dang <i>et al.</i> (Ref. 216)	10	0.2	24.8
	Aultman <i>et al.</i> (Ref. 217)	5.84	0.25	2
	High enthalpy	Duan <i>et al.</i> (Ref. 218)	9 – 9.4	0.12 – 0.13
Passiatore <i>et al.</i> (Ref. 28) & Sciacovelli <i>et al.</i> (Ref. 8)		10	1	7.15
Passiatore <i>et al.</i> (Ref. 29)		12.48	0.1	18.66

TABLE III: Experiments – Two-dimensional planar SBLI : Compression Corner - CC; Impinging Shock - IS; θ = flow deflection (or shock generator) angle; * ASCII datafile available on the NASA Turbulence Modeling Resource website¹⁸⁶.

Configuration	Experiments	M_e	θ (degree)	T_w/T_{aw}	H_e (MJ/kg)	Re_e/m $\times 10^6$	Quantities reported
CC	Coleman & Stollery (Ref. 76)*	9	15-38	0.28	1.1	47	P_w, Q_w
	Holden (Ref. 196)	6.25 – 14.9	27 – 36	0.12 – 0.9	0.75 – 3.01	15.4 – 101.7	P_w, C_f, Q_w
	Appels (Ref. 219)	11.7	30 – 42	0.15	2.23	36.6	P_w, Q_w
	Coet (Ref. 220)	5	35	0.24 & 0.72	0.5	40	P_w, Q_w
	Holden (Ref. 146)*	8	27 – 36	0.34	0.97	145.7	P_w, C_f, Q_w
IS	Holden (Ref. 146)*	11.3	36	0.2	1.63	36	P_w, C_f, Q_w
	Schulein (Ref. 81)*	5	6 – 14	0.8	0.41	39.1	P_w, C_f, Q_w &
	Kussoy & Horstman (Ref. 221)*	8.18	5 – 11	0.29	1.1	4.87	P_w, Q_w
	Holden (Ref. 146)*	11.4	20	0.2	1.71	40.4	P_w, C_f, Q_w
	Holden (Ref. 196)	6.25 – 14.9	12.5 – 19.8	0.2 – 0.9	0.75 – 3.01	15.4 – 101.7	P_w, C_f, Q_w

TABLE IV: Experiments – Axisymmetric SBLI : Cone/Cylinder/Flare - CCF; Hollow Cylinder/Flare - HCF; Cone/Flare - CF; Hollow Cylinder/Cowl - HCC; hemisphere cylinder/flare - HemCF; Cone/ogive-cylinder - COC; Ogive Cylinder/Flare - OCFI; Ogive Cylinder/Fin - OCFi; θ = flow deflection (or shock generator) angle; Half-angle cone - HAC; Flare Angle - FA; * ASCII datafile available on the NASA Turbulence Modeling Resource website¹⁸⁶.

Configuration	Experiments	M_e	θ (degree)	T_w/T_{aw}	H_e (MJ/kg)	Re_∞/m $\times 10^6$	Quantities reported
CCF	Holden (Ref. 222)* : (HiFire I)	6.5 – 7.2	7 HAC; 33 FA	0.11 – 0.16	2.2 – 3.4	1.5 – 20	P_w, Q_w
	Coleman (Ref. 223–225)	9.22	10 HAC ; 15 – 40 FA	0.29	1.07	47	P_w, Q_w
HCF	Coleman (Ref. 223–225)	9.22	15-40	0.29	1.07	47	P_w, Q_w
	Murray (Ref. 205)*	8.9	36	0.27	1.2	48	P_w, Q_w
	Holden (Ref. 226 and 227)	5 – 8	36	0.13 – 0.25	1.27 – 2.54	4 – 22.3	P_w, Q_w
	Holden (Ref. 228)*	11 – 15.4	6 – 7 HAC ; 30 – 42 FA	0.15 – 0.21	1.7 – 2.6	5 – 15	P_w, Q_w
CF	Holden (Ref. 226 and 227)	4.96 – 8.21	7 HAC; 40 FA	0.12 – 0.67	0.47 – 2.38	4.4 – 49	P_w, Q_w
	Running (Ref. 229)	6.14	7 HAC; 34 – 43 FA	0.15	0.9	7.6 – 20	Q_w
HCC	Murray (Ref. 205)*	8.9	4.7 & 10	0.27	1.2	48	P_w, Q_w
HemCF	Coleman (Ref. 223–225)	9.22	15-40	0.29	1.07	47	P_w, Q_w
COC	Kussoy and Horstmann (Ref. 230)	7.2	7.5 & 15	0.45	0.7	7.1 & 7.7	P_w, C_f, Q_w
OCFI	Kussoy (Ref. 231)*	7	20 – 35	0.385	0.89	5.8	P_w, Q_w
OCFi	Kussoy (Ref. 231)*	7	10 – 20	0.385	0.89	5.8	P_w, Q_w

TABLE V: Three-dimensional SBLI : Single-fin SBLI - SFSBLI; crossing SBLI (double fin geometry) - CSBLI; θ = flow deflection angle; * ASCII datafile available on the NASA Turbulence Modeling Resource website¹⁸⁶.

Configuration	Experiments	M_e	θ (degree)	T_w/T_{aw}	H_e (MJ/kg)	Re_e/m $\times 10^6$	Quantities reported
SFSBLI	Kussoy (Ref. 221)*	8.18	5 – 15	0.29	1.1	4.87	P_w, C_f, Q_w
	Rodi (Ref. 232–234)*	4.9	6 – 16	0.8	0.42	38.1	P_w, Q_w
	Borovoy (Ref. 235–237)	5 & 6	10 – 20	0.62 & 0.59	0.53 & 0.57	10.9 & 7.7	P_w, Q_w
	Law (Ref. 238)*	5.85	6 – 16	0.51	0.6	32.8 & 98.4	P_w, Q_w
	Holden (Ref. 239)	11.3	5 – 12.5	0.2	1.66	31.6	P_w, Q_w
CSBLI	Schulein (Ref. 81 and 240)	5	2 – 27	0.8	0.41	37	P_w, C_f, Q_w
	Kussoy (Ref. 241)*	8.28	10, 15	0.269	1.2	5.3	P_w, C_f, Q_w
	Schulein (Ref. 81 and 240)	5	8 – 23	0.8	0.41	37	P_w, Q_w
	Borovoy (Ref. 235–237)	5 & 6	15	0.62 & 0.59	0.53 & 0.57	10.9 & 7.7	P_w, Q_w

TABLE VI: DNS - SBLLI : Impinging shock - IS; Compression corner - CC; BCC - Blunt Circular Cone; Cone/Flare - CF; Backward-facing curved wall - BFCW; Forward-facing curved wall - FFCW; θ - Flow deflection angle; Ramp angle - RA; Half-angle cone - HAC; Flare angle - FA; Sweep angle - SWA; * Re_θ based on μ_w ; na - not available; * ASCII datafile available on the NASA Turbulence Modeling Resource website⁹⁶.

Configuration	DNS	M_e	T_w/T_{aw}	θ (degree)	$Re_\theta \times 10^3$
IS : (based on Schuelein ⁸¹ experiments)	Volpiani <i>et al.</i> (Ref. 242)	5	0.8 & 1.9	6 – 14	3.8 & 5.4
CC : (based on Bookey ²⁴⁴ experiments)	Priebe & Martin (Ref. 243)	7.2	0.53	8	3.3
IS	Volpiani (Ref. 37) (3D simulation)	5.6	0.2	6	na ($Re_\tau = 190$)
Swept CC	Zhang <i>et al.</i> (Ref. 245) (3D simulation)	6	0.5	34 RA; 45 SWA	na ($Re_e/m = 10^6$)
CC	Dang <i>et al.</i> (Ref. 216)	6	0.5	34	4.9
BCC	Dang <i>et al.</i> (Ref. 216)	6	0.61	7 HAC	1.8
CC	Guo <i>et al.</i> (Ref. 246)	6	0.75	30	6.62
CF : (based on Running ²²⁹ experiments)	Fulin <i>et al.</i> (Ref. 247)	6	0.62	7 HAC; 34 FA	2.5
CC	Di Renzo <i>et al.</i> (Ref. 39)	5–6	0.4–0.714	15	(0.3–0.65)*
BFCW & FFCW	Nicholson <i>et al.</i> (Ref. 97)*	4.9	0.91	–	16.1–22.4

TABLE VII: Experimental studies on surface roughness effects : FP - Flat plate; CC - Compression Corner; na - not available.

Configuration	Experiment	M_e	T_w/T_{aw}	H_e (MJ/kg)	Re_e/m $\times 10^6$	Quantities reported
Flat plate (milled spanwise V-grooves)	Young (Ref. 191)	4.9	0.5–1	0.34–0.625	16.4–45.8	P_w, C_f, Q_w
Slender cones, biconic & hemispherical nosetips (sand grain & patterned roughnesses)	Holden (Ref. 248 and 249)	6–13	*($T_w/T_{te} : 0.2–0.4$)	0.69–2	15–125.6	P_w, C_f, Q_w
Rough cylinder with 15°, 20° flare (sawtooth and cavity shape roughnesses)	Babinsky & Edwards (Ref. 250)	5	na	0.4	13	P_w, Q_w
25°–38° CC (sand grains on FP & ramp)	Prince (Ref. 153)	8.2	0.24	1.3	9.3	P_w, Q_w
Sphere-cone and hemisphere (sand-grain and patterned roughnesses)	Hollis (Ref. 251)	6	0.7	0.5	9.95–27.4	Q_w
Sphere cone (sand-grain and patterned roughnesses)	Wilder (Ref. 252)	9–9.7	0.09–0.33	0.78–0.86	31	Q_w
Flat plate (patterned hemispheres, pseudomesh roughness, and their superposition)	Forsyth (Ref. 253)	4.9	0.74–0.85	0.38–0.44	22.3–37.3	Q_w

erally carried out using air, N_2 , or He as the working fluid. In the data, the subscript 'e' indicates quantities at the boundary layer edge or the freestream, and unit Reynolds number $Re_e = \bar{\rho}_e \tilde{u}_e / \mu_e$ with μ_e being the dynamic viscosity calculated using Sutherlands or Keyes law. The adiabatic wall temperature T_{aw} (or equivalently the recovery temperature T_r) is given by

$$\begin{aligned}
 T_{aw} &= \tilde{T}_e \left(1 + \frac{(\gamma-1)}{2} Pr_T M_e^2 \right) \\
 &= \tilde{T}_e \left(1 + \frac{(\gamma-1)}{2} M_e^2 \right)^{-1} \left(1 + \frac{(\gamma-1)}{2} Pr_i M_e^2 \right), \quad (59)
 \end{aligned}$$

where \tilde{T}_e is the total temperature at the edge of the boundary layer and unless specified otherwise Pr_i is taken to be 0.9.

Total enthalpy per unit mass is given by $H_e = C_p \tilde{T}_e + 0.5 \tilde{u}_e^2 = C_p \tilde{T}_{te}$. Note that, in some cases, wall heat transfer (Q_w) is given in terms of Stanton number S_t

$$S_t = \frac{Q_w}{\bar{\rho} \tilde{u}_e C_p (T_w - T_{aw})}. \quad (60)$$

All the available experimental data excluding the experiments of Goynes *et al.*¹⁹⁸ correspond to low enthalpy conditions, whereas a few DNS studies cover high enthalpy conditions. It is important to note that during a hypersonic flight, total (stagnation) enthalpies as large as 100 MJ/kg and higher can be experienced²⁵⁴.

The validation database for ZPG hypersonic smooth wall TBLs consists of flow over flat plates, wind tunnel walls, nozzle walls, and flow along model geometries with axisymmetric forebodies including hollow cylinders and sharp circular

cones at different wall temperature conditions. The available experimental database is given in Table I. Roy and Blottner¹² present a large number of available equilibrium hypersonic TBL experiments, however, many of these experiments were performed to establish the accuracy of the compressible engineering correlations (CECs) theories; a number of them are not well documented with many missing wall heat transfer measurements and they are not suitable for turbulence model validation studies.

On the other hand, Table II gives the available DNS studies for flat plate ZPG hypersonic TBLs. A majority of the DNS studies are based on perfect gas simulations while the works of Refs. 28, 29, and 218 consider real gas models with stagnation enthalpies ≈ 20 MJ/kg. Refs. 118–120, 209–211 consider adiabatic wall conditions whereas the works in Refs. 42, 104, 121, 122, 211–213, and 215 study the cold wall ZPG TBLs. Ref. 211 is the only work to consider heated wall condition at Mach 8 with $T_w/T_{aw} = 1.5$. A few DNS works study TCI⁴¹ while some works^{120,218,255} study the effects of radiation on hypersonic TBLs.

Compressible Engineering Correlations (CECs) are generally used for flat plate ZPG TBL comparisons of skin friction and wall heat transfer. The commonly used CECs include van Driest II²⁵⁶, White–Christoph²⁵⁷, and Spalding–Chi²⁵⁸ relations for skin friction estimation in terms of an equivalent incompressible TBL (see Appendix A). The correlations of van Driest II and White–Christoph generally give similar results for adiabatic as well as strongly cooled walls, but results using Spalding–Chi can differ significantly²⁴. Generally, these CECs give good results for adiabatic and moderately cold wall temperature ratios (T_w/T_{aw}). However, the accuracy of the results differs significantly depending on the Mach number, wall temperature ratio, and Reynolds numbers^{116,196,198,259}. Reynolds analogy factor R_{af} is classically used to predict wall heat flux from C_f obtained using the CECs,

$$S_t = \frac{1}{2} C_f R_{af}. \quad (61)$$

The commonly used approximation for R_{af} is $R_{af} = Pr^{-2/3}$ (with $Pr = 0.72$), $R_{af} = Pr_t^{-1}$ as per van Driest, and $R_{af} = 1$. The experimental data display a rather wide range of values for R_{af} ranging from 0.75 to 1.3.

A limited number of experimental studies are available for hypersonic SBLIs. Generally, complex configurations are broken down into simpler geometries to isolate different kinds of SBLIs. Experiments and DNS/LES studies are then performed on these canonical geometric configurations. These simplified geometries include 2D planar configurations consisting of compression corner and oblique shockwave impingement, axisymmetric configurations consisting of cone-cylinder-flare, cone-flare, etc. as given in Tables III and IV. Table V gives 3D SBLIs used for the model validation studies. The test geometry for the 3D configurations consists of one or two sharp or blunt fins that act as shock generators mounted on a flat plate. The two basic test models are the single fin and the symmetric double fin geometries. Surface flow visualization, surface streamline angles, flow field yaw angles, and mean profiles at various streamwise locations are

available for these experiments in addition to the surface pressure, skin friction, and wall heat transfer measurements.

DNS studies on SBLIs are limited (see Table VI) with most studies performing perfect gas simulations while only two works use a real gas model. LES studies are also limited with recent examples including the wall-resolved LES of BoLT-2 vehicle at Mach 6.11 flow conditions ($T_w/T_{aw} = 1&0.215$, $Re/m = 12.9 \times 10^6$) in the descent phase of the trajectory²⁶⁰; compression corner SBLIs at Mach 7.16 ($T_w/T_{aw} = 0.52$, $Re_\theta = 3300$) and Mach 9.05 TBLs with 33° and 34° ramp angles ($T_w/T_{aw} = 0.33$, $Re_\theta = 8000$)²⁶¹, respectively; Mach 10 axisymmetric 34° cylinder-flare configuration ($T_w/T_{aw} \approx 0.3$, $Re_\theta \approx 8000$)²⁶²; a hypersonic cold wall flat plate TBL at Mach 6 and 8 and several wall temperature ratios²⁶³; 31° – 34° compression ramps and 33° axisymmetric cylinder flare at Mach 10 ($T_w/T_{aw} \approx 0.3$, $Re_\theta \approx 8000$)²⁶⁴; and Mach 5 SBLI generated by a 23° single fin^{265,266}.

Hypersonic TBL experiments on rough wall conditions with surface heat transfer measurements are also limited as presented in Table VII. The test models use sand grain roughness and patterned roughness surfaces for these studies. Several experiments^{47,155,156,267} study the boundary layer characteristics in the presence of different roughness elements. These experiments verify the validity of the law of wall and wake for a rough wall which is given by

$$\frac{u_{VD}}{u_\tau} = \frac{1}{\kappa} \log\left(\frac{yu_\tau}{\nu_w}\right) + C - H(k_s^+) + \frac{2\Pi}{\kappa} \sin^2\left(\frac{\pi y}{2\delta}\right). \quad (62)$$

The function $H(k_s^+)$ gives the downward shift of the log region due to the roughness effect.

VII. CHALLENGES AND FUTURE DIRECTIONS

Accurate modeling and prediction of hypersonic TBL flows is one of the most difficult yet important problems in the aerothermal design of hypersonic vehicles. Equilibrium TBLs at cold wall conditions and the regions of SBLIs and separated flows present the greatest challenge for turbulence modeling. In these flows, turbulent as well as thermo-chemical non-equilibrium and compressibility effects are of major importance. Popular turbulence models like Baldwin-Lomax, Spalart-Allmaras, $k-\epsilon$, $k-\omega$, Menter SST $k-\omega$, etc., as well as advanced models like NLEVMs, EARSMS, and RSTMs, were primarily developed for incompressible or moderately compressible flows. These models are generally insensitive to compressibility effects and are tuned for non-hypersonic smooth wall turbulent boundary layers with conventional rates of heat transfer. The straightforward compressible extensions of these models generally fail to capture the intricate phenomena present in hypersonic regimes at different wall conditions. Over the years, a major focus of turbulence modeling has been the adaptation and extension of the traditional low-speed models to better handle the high-speed conditions relevant to hypersonic flows.

A. Current Limitations and Unresolved Issues

Turbulence modeling for hypersonic flows faces several critical limitations and unresolved issues, as discussed below, due to the extreme conditions and complex flow physics encountered at high Mach numbers. One of the main limitations, which echoes some of the previous recommendations by Roy and Blottner¹² from 2006, is the dearth of experimental data in the hypersonic regime. Additionally, many of the available experimental works reported in Roy and Blottner¹², especially on ZPG hypersonic TBLs, are poorly documented, including inadequate specifications of the boundary conditions and geometry details required to set up a CFD simulation for accurate one-on-one comparisons. Experiments generally do not include detailed measurements of Reynolds stresses and mean flow surveys are generally limited. DNS and wall-resolved LES works are also significantly limited in Reynolds numbers and geometric sophistication. Moreover, attempts to match DNS with experiments at similar conditions show disagreements for ZPG TBLs as well as SBLI characteristics²⁴². The scarcity of experimental and high-fidelity data makes it challenging to develop and calibrate turbulence models specifically for hypersonic flows, leading to uncertainty in their accuracy and reliability. Developing high-quality validation datasets and benchmarks for hypersonic turbulence models remains a critical issue.

Popular turbulence models generally do not correctly represent hypersonic cold-wall boundary layers. Reliable and accurate prediction of shock-induced separations and the associated wall pressure loads, surface heat-transfer rates, and skin-friction at different wall conditions remains an unsolved problem. Standard turbulence models generally lack sensitivity to adverse pressure gradients, often resulting in overestimated shear stresses and delayed flow separation predictions. Compressibility terms related to pressure fluctuations and dilatation dissipation are generally neglected due to a lack of information on these terms for wall-bounded flows even at lower speeds. The compressibility corrections in the form of dilatation dissipation and pressure dilatation of Sarkar or Zeman designed with some elegant theoretical framework, particularly with the compressible isotropic turbulence, are originally intended for improving mixing predictions in free shear layers. Their application to TBL flows with SBLIs is expected to adequately simulate the free shear layers over the separation bubbles. These compressibility corrections along with Wilcox's compressibility correction have been shown to improve model predictions for some hypersonic TBL flows involving SBLIs. However, improved separation length prediction generally results in significantly lower shear stress while the over-predicted peak heat transfer predictions remain largely unaffected. These corrections are also found to deteriorate model predictions for attached equilibrium TBLs in many cases. As a result, these compressibility corrections are not widely accepted. Further, the validity of the arguments underpinning dilatation-dissipation models are not substantiated by experimental or DNS data⁸⁹.

The length-scale determining equation remains a major limitation for the two-equation models including LEVMs,

NLEVMs, and EARSMs. Several ad-hoc fixes are proposed as discussed in Section IV to improve length scale predictions, especially aimed at improving heat transfer predictions. Other corrections including modification to the production terms, diffusion terms, and turbulent Prandtl number developed to date to improve SBLI predictions show promising results in some cases, however, model predictions generally depend on the flow conditions and geometry configurations.

In SBLIs, the average flow structure also results from shock motions with larger amplitude at very low frequencies, associated with large-scale bubble breathing. The compressible extensions of the standard turbulence models developed for low-speed flows cannot take into account the complex physical mechanisms driving the average shock position, separation length, surface pressure, skin friction coefficient, and wall heat transfer distributions. Attempts to incorporate the effects of small-scale high-frequency unsteady oscillations of shock waves upon interaction with upstream turbulence using LIA results based on canonical STI problems⁸⁴ have shown improvements over the standard models for a number of hypersonic test cases. However, these models lack a rigorous theoretical foundation as the physics of SBLIs and canonical STIs is considerably different and the scaling of turbulence quantities across a shock can differ significantly in the presence of wall effects. Studies using these models also do not offer an evolution of turbulence quantities like TKE or TKE budgets in comparison to DNS or experiments.

This review demonstrates that current turbulence models, while adequately predicting wall pressure distributions and separation zones, consistently overestimate heat flux at the wall surface. This discrepancy in heat flux prediction remains a significant challenge for accurate thermal analysis in hypersonic applications. Of note, while many modeling efforts have addressed the formulation of the constitutive equation for the Reynolds stresses and of the auxiliary transport equations, only a few studies have attempted to improve the turbulent heat flux formulation, which mostly relies on the over-simplistic constant turbulent Prandtl number hypothesis. Advanced turbulent heat flux models have been introduced with some success for incompressible, variable density flows²⁶⁸⁻²⁷⁰ and, recently, for hypersonic flows¹²⁴. Furthermore, data-driven turbulent heat flux models have been developed to improve the prediction of heat transfer effects in jet flows²⁷¹. Extension of such approaches to hypersonic flows should be pursued.

For flows with thermochemical non-equilibrium effects, only very rough models based on constant Schmidt or vibrational Prandtl numbers have been proposed. The validity of such models has only recently been assessed for simple hypersonic flow configurations such as flat plate boundary layers, showing a need for improvement. Furthermore, turbulence/chemistry and turbulence/vibrational energy interactions can be significant, especially in flows with shocks, making the approximation of evaluating chemical and vibrational source terms as a function of averaged flow properties inaccurate. Direct application of interaction models developed for combustion problems has proved unfruitful, pointing out the

necessity of developing specific models for hypersonic non-equilibrium flows.

The ablation process creates a complex interaction between the surface and TBL that must be properly modeled. Integration of rough wall effects into existing turbulence models should be a focus for improving overall prediction capabilities. Accurate modeling of blowing/surface roughness interactions in TBLs is necessary to correctly predict the aerothermal loads and efficiently design the ablative heat shield. Standard turbulence models fail to accurately estimate the velocity shift in the logarithmic law caused by roughness and blowing interactions. The development of sophisticated turbulence models that can accurately capture the combined effects of surface roughness/blowing in hypersonic conditions is an ongoing area of research.

B. Role of Machine Learning and Data-Driven Approaches

Data-driven modeling has emerged as a promising technique to improve RANS models. These methods combine high-fidelity and/or experimental data with more traditional phenomenological arguments to improve the predictive accuracy of turbulence models. There is a large body of work focused on data-driven turbulence modeling^{40,272,273} with the goal of developing improved augmentations in the transport equations for turbulence scalars, or directly for the Reynolds stress tensor, heat flux models, etc. These model augmentations are described over an appropriate feature space. Critical steps in this process include careful data preparation, choice of non-dimensional features, choice of learning algorithms, cross-validation strategies, and uncertainty quantification to assess model reliability across different flow regimes. While much of the early work on machine learning augmented turbulence modeling involved *a priori* learning, model consistency through inference²⁷³ is increasingly being adopted over the past few years by most practitioners. This step ensures that the learned augmentations are consistent with the RANS modeling environment. Validation against independent datasets is crucial to ensure generalizability, especially given the limited availability of hypersonic flow data. While still an emerging area, data-driven methods show potential for enhancing model performance across a range of conditions relevant to hypersonic vehicle design, provided challenges in data scarcity and extrapolation to extreme conditions can be overcome.

Refs. 274 and 275 demonstrate the use of machine learning to improve Reynolds stress predictions in hypersonic boundary layers. The approach was seen to significantly improve the accuracy of normal stress predictions. However, only *a priori* studies were performed, and the impact of the updated Reynolds stress predictions on the mean flow field was not assessed. In a similar vein, Parish *et al.*²⁷⁶ developed a tensor basis neural network trained on data from both subsonic and hypersonic flows, and showed that the resulting model improves wall shear stress and wall heat flux predictions in hypersonic TBL flows. Jordan²⁷⁷ developed a machine learning approach utilizing for predicting an improved structure factor in the SST turbulence model, which plays an important

role in hypersonic SBLIs. Jordan utilizes high-fidelity data to extract an “exact” structure factor, and then develops an equation learning neural network to learn the structure factor. The resulting model is seen to improve predictions for flow separation and peak heat transfer on a range of SBLI cases.

Parish *et al.*²⁷⁸ utilized field inversion^{279,280} to derive model consistent corrections and machine learning to develop a variable turbulent Prandtl number model to address over-prediction in peak heat flux in cold-wall hypersonic SBLIs. The approach resulted in a model that gave consistent improvements over baseline RANS models across a suite of SBLI cases. Chowdhary *et al.*²⁸¹ used surrogate-based Bayesian inference to calibrate the parameters of the SST $k - \omega$ model, using shock-tunnel data for the HIFiRE-1 vehicle. The authors found that the primary issues in estimating the SST model parameters are the limited information content of the heat flux and pressure measurements and the large model-form error encountered in a certain part of the flow. Barone *et al.*¹²⁷ utilized recent DNS simulation data of hypersonic boundary layers to develop modifications to the SA model to improve performance on hypersonic TBLs. The corrections include the development of a new near-wall damping function based on a novel eddy viscosity transformation as well as a normal stress correction to improve predictions for the wall-normal Reynolds stress. These corrections improved model performance for wall heat flux and wall shear stress in hypersonic SBLIs at sufficient Reynolds numbers. Zafar *et al.*²⁸² developed a data-driven turbulence modeling approach for cold-wall boundary layers that utilizes an ensemble Kalman filter to train improved models for the Reynolds stress and turbulent Prandtl number model with mixed degree of success.

Given the difficulty of obtaining abundant experimental datasets, the production and sharing of numerical ones should be encouraged and pursued, for instance via opendata repositories such as <https://blastnet.github.io> (mostly powered by the combustion research community for now). Furthermore, data-driven research should focus more on model-consistent (or CFD-in-the-loop) training methods, which have the potential of learning from sparse and noisy data. With sufficient data available, data-driven turbulent modeling approaches can facilitate the development of novel closures for turbulent heat or mass fluxes, vibrational energy fluxes, roughness and ablation models and much more.

1. Towards reliable data-driven models

Machine learning augmentations are generally developed as a functional map over a feature space. The underlying feature selection must balance both classical machine learning criteria and domain-specific requirements. From a classical machine learning perspective, features should provide unique and complementary information to prevent overfitting, even when dealing with correlated features. A parsimonious feature set is crucial, as it helps minimize overfitting risk, improves computational efficiency, and simplifies model interpretation. Features must also demonstrate robustness by being resistant to

noise and small data variations, ensuring model stability and generalizability. The computational cost of calculating features must be considered, especially when working with large datasets.

Domain-specific requirements add another layer of complexity to feature selection. Features must be locally non-dimensionalized to work effectively across different flow configurations. The selected features should respect important physical properties such as rotational, reflectional, and frame-invariance. Interpretability is another crucial aspect - features that are easily interpretable help avoid unphysical behavior and enable asymptotic analysis.

Generalization remains one of the most significant challenges in data-driven turbulence modeling. Model consistency is crucial for generalization, requiring careful consideration of the implicit relationship between state variables and augmentation values. Generalizable results in physical space can be achieved through careful interpolation over a well-designed feature space. However, this presents an important trade-off: while more features allow for more unique physical description, a lower-dimensional feature space is necessary for generalization with limited data. Model generalization to flows involving diverse physical processes is an active field of research, even for low-speed flows^{283–286}.

These insights suggest that successful data-driven turbulence modeling requires a delicate balance between physical understanding, mathematical rigor, and practical implementation considerations. The key to reliable data-driven models appears to lie in thoughtful feature design that captures essential physics while maintaining mathematical tractability complemented by a coordinated data generation process to adequately populate feature space.

VIII. CONCLUDING REMARKS AND PERSPECTIVES

It is realistic to expect that RANS methods will continue to be popular for computing practical industrial flows in the foreseeable future. In an industrial setting, it can be expected that further increases in computing power will be used to utilize advanced RANS models to shorten the design cycle rather than to yield the way to LES techniques. Turbulence modeling shortcomings remain a major limitation to the accuracy of hypersonic simulations, and this includes deficiencies in calculating the details of ZPG TBLs and SBLIs. Though there have been improvements, the concluding remarks of Marvin and Coakley¹¹ stating that “the status of turbulence modeling for hypersonic flows is still far from complete” remain mostly valid even after 35 years, partly because of a lack of concerted effort in developing Hypersonics-relevant models. The acquisition of reliable experimental data for hypersonic TBL flows remains challenging, especially at high enthalpy conditions. In the absence of experimental data at high-enthalpy conditions in the hypersonic regime, DNS and LES can be used to gain insight into flow physics and develop phenomenological models and novel turbulence modeling methodologies for chemically reacting boundary layers including radiation physics. We summarize key findings and discuss avenues for

further improvements.

A. Summary of Key Findings

The turbulence models routinely applied for hypersonic flow predictions are direct extensions of those developed originally for incompressible flows by invoking Morkovin’s hypothesis and using density-scaled variables. In simple applications, especially involving simple attached boundary-layer flows at near adiabatic smooth wall conditions, these incompressible model forms give satisfactory results with or without some adjustments to the model coefficients. However, the performance of standard forms of these turbulence models becomes unsatisfactory even for the TBL at equilibrium conditions when the wall temperature differs from the adiabatic conditions, especially at the realistically expected cold wall conditions. This is true even when the complexity of the model form is increased from linear eddy viscosity models to NLEVMs/EARSMS and RSTMs. In fact, although RSTMs have the natural potential to represent the dynamics of intercomponent energy transfer, additional modeling requirements coupled with more advanced numerical treatments in complex flow situations is a major disadvantage of these models. Also, as discussed in Section III A 3, thus far, RSTMs have not been shown to offer consistent predictive accuracy compared to EVMs for hypersonic SBLI predictions. On the other hand, there is evidence that the NLEVMs and EARSMS improve model predictions for hypersonic SBLIs compared to the corresponding LEVMs, however, validation studies for these models are limited compared to the LEVMs and extensive validation is needed against the available hypersonic test cases.

The choice and the form of the length scale determining equation for the turbulence models including LEVMs, NLEVMs, EARSMS, and RSTMs remains a major shortfall and investigations indicate ω is a better choice than ε for hypersonic flow predictions. Interestingly, modifications to the mixing-length hypothesis-based zero-equation models like Cebeci-Smith and Baldwin-Lomax can result in better predictions than the two-equation EVMs for equilibrium hypersonic TBLs at cold wall conditions and in some cases even for hypersonic SBLIs. We can consider current turbulence model choices as case-dependent and influenced by computational convenience. Overall, the performance of the standard turbulence models becomes increasingly unsatisfactory as the flow complexity and/or Mach number increase and the wall temperature ratio decreases.

Existing compressibility corrections generally do not satisfactorily overcome weaknesses seen in standard models when predicting flow separation or wall heat flux. Moreover, compressibility correction investigations are mainly confined within the context of LEVMs. Extending and testing these model corrections in the framework of more sophisticated NLEVMs and EARSMS remains unexplored.

The development of more sophisticated turbulence models that can accurately capture the effects of surface roughness in hypersonic conditions is an ongoing area of research. Velocity

shift in the log layer plays a key role in wall roughness modeling. The standard equivalent sand-grain approach is quite sensitive to the equivalent sand-grain height k_s estimate. A constant value of $Pr_t = 0.9$ gives inaccurate predictions of wall heat flux over rough surfaces even with dynamic corrections to correctly predict log-layer behavior. The existing thermal correction models aiming to accommodate Pr_t variation within the roughness sublayer are generally sensitive to the parameter S_{cor} for heat transfer predictions. In addition, there is a need for more experimental data on rough wall hypersonic flows to develop, validate, and improve the computational models.

Comparisons of turbulence model predictions with compressible engineering correlations (CECs) for ZPG TBLs require careful consideration, particularly when evaluating skin friction and wall heat transfer. The accuracy of these correlations diminishes significantly under cold wall conditions, necessitating additional validation against higher-fidelity data sources. The two most commonly used CECs of Van Driest II and Spalding–Chi for estimating the skin-friction give different results and studies reveal that their accuracy depends on the Mach number, wall temperature ratio, and Reynolds number along with the incompressible friction correlations used. At highly cooled wall conditions, these two theories result in inaccurate predictions. Moreover, heat transfer predictions using these CECs depend on the choice of the value of the Reynolds analogy factor R_{af} . At low enthalpy conditions with $Ma \gtrsim 5$, different studies draw different conclusions and it is unclear which theory should be favored, especially for cold-wall cases. For high-enthalpy hypersonic flows at cold-wall conditions, the study of Goyne *et al.*¹⁹⁸ found Spalding–Chi method to give better predictions than other correlations.

There is a great need to expand experimental databases and use rigorous validation methodologies for turbulence models in the hypersonic regime. Almost all of the experiments employ low enthalpy wind tunnels while none of the existing SBLI experiments match true flight conditions. Moreover, little attention has been directed toward DNS/LES studies considering real gas effects relevant to hypersonic conditions. Consequently, the majority of the RANS-based studies consider calorically perfect gas models in the absence of validation data at high enthalpy conditions. Sensitivity studies of real gas effects under potential flight conditions reveal that SBLI predictions obtained using the popular $k-\omega$ family of turbulence models (Menter SST and Wilcox $k-\omega$) are sensitive to the gas models. Real gas simulations for these models show a reduction in separation extent, an increase in peak pressure, and an increase in peak heating post-reattachment compared to the ideal gas scenario²⁸⁷. Moreover, the severity of the simulated real gas effect can be expected to depend on turbulence modeling in the vicinity of separation and reattachment, which are regions where the existing turbulence models have been demonstrated to exhibit the greatest deficiency in their performance.

Machine learning techniques appear poised to have a positive impact on model development. To develop robust and generalizable turbulence models, however, a synergistic ecosystem needs to be created that brings together modelers, experimentalists and high-fidelity simulation experts. While

existing datasets such as those described in this paper serve as a reasonable starting point, the development of generalizable models requires the data generation process to be consistent with the specific requirements of the underlying model and features. Further, measured quantities should be informative to the underlying model discrepancy, which can be assessed using inverse problems.

ACKNOWLEDGMENTS

E. Parish was supported by Sandia LDRD 226031, “Data-driven closure modeling for hypersonic turbulent flows”. K. Duraisamy was supported by OUSD(RE) Grant # N00014-21-1-295 titled “Physics-Aware Reduced Order Modeling for Nonequilibrium Plasma Flows: Implications in the Field of Hypersonic Aerothermodynamics.”

DECLARATION OF INTERESTS.

The authors report no conflict of interest.

Appendix A

Several correlations for compressible skin friction on a flat plate exist in the literature. The most commonly used models to estimate skin friction associated with a compressible boundary layer in terms of an equivalent incompressible boundary layer are van Driest II²⁵⁶, White–Christoph²⁵⁷, and Spalding–Chi²⁵⁸. These correlation theories use a compressibility transformation idea:

$$C_f = \frac{1}{F_c} C_{f,in}, \quad (A1)$$

$$Re_x = \frac{1}{F_x} Re_{x,in}, \quad (A2)$$

$$Re_\theta = \frac{1}{F_\theta} Re_{\theta,in},$$

where $C_{f,in}$, $Re_{x,in}$, and $Re_{\theta,in}$ are the equivalent ‘incompressible’ skin friction coefficient and surface distance Reynolds number, and momentum thickness Reynolds number, respectively. On the other hand, F_c is the skin friction transformation function whereas F_x and F_θ are surface distance and momentum thickness based Reynolds number transformation functions, respectively. The commonly used incompressible skin friction correlations are the $C_{f,in}$ vs $Re_{\theta,in}$ correlation by: Kármán–Schoenherr²⁵⁹:

$$C_{f,in} = \frac{1}{\log_{10}(2Re_{\theta,in})[17.075 \log_{10}(2Re_{\theta,in}) + 14.832]}, \quad (A3)$$

Smits *et al.*²⁸⁸ :

$$C_{f,in} = 0.024 Re_{\theta,in}^{-1/4}, \quad (A4)$$

Coles–Fernholz²⁸⁹ :

$$C_{f,in} = 2 \left[2.604 \log Re_{\theta,in} + 4.127 \right]^{-2}, \quad (\text{A5})$$

and $C_{f,in}$ vs $Re_{x,in}$ correlation by:

White²⁹⁰ :

$$C_{f,in} = \frac{0.455}{F_c \ln^2(0.06 Re_x F_x)}; F_x = \frac{F_\theta}{F_c}. \quad (\text{A6})$$

The transformation factor F_c for the van Driest II, Spalding-Chi, and White-Christoph theories can be written as²⁴

$$F_c = \frac{T_{aw}/T_e - 1}{(\sin^{-1} A + \sin^{-1} B)^2}, \quad (\text{A7})$$

where T_e refers to free stream or boundary layer edge temperature, and

$$T_{aw} = T_e \left(1 + r \frac{\gamma - 1}{2} M_e^2 \right). \quad (\text{A8})$$

The recovery factor r is taken to be 0.9. The A and B are given by

$$A = \frac{2a^2 - b}{(b^2 + 4a^2)^{1/2}}, \quad (\text{A9})$$

$$B = \frac{b}{(b^2 + 4a^2)^{1/2}}, \quad (\text{A10})$$

where

$$a = \left(r \frac{\gamma - 1}{2} M_e^2 \frac{T_e}{T_{aw}} \right), \quad (\text{A11})$$

$$b = \frac{T_{aw}}{T_w} - 1 = \frac{T_e}{T_{aw}} \left(1 + r \frac{\gamma - 1}{2} M_e^2 \right) - 1. \quad (\text{A12})$$

The transformation factor F_θ is different between the three theories and is given by van Driest II :

$$F_\theta = \frac{\mu_e}{\mu_w}, \quad (\text{A13})$$

Spalding-Chi :

$$F_\theta = \left(\frac{T_w}{T_e} \right)^{-0.702} \left(\frac{T_{aw}}{T_w} \right)^{0.772}, \quad (\text{A14})$$

White-Christoph :

$$F_\theta = \sqrt{F_c} \frac{\mu_e}{\mu_w} \left(\frac{T_e}{T_w} \right)^{1/2}. \quad (\text{A15})$$

³Y. Zhiyin, “Large-eddy simulation: Past, present and the future,” Chinese journal of Aeronautics **28**, 11–24 (2015).

⁴H. Choi and P. Moin, “Grid-point requirements for large eddy simulation: Chapman’s estimates revisited,” Physics of fluids **24** (2012).

⁵X. I. Yang and K. P. Griffin, “Grid-point and time-step requirements for direct numerical simulation and large-eddy simulation,” Physics of Fluids **33** (2021).

⁶S. T. Bose and G. I. Park, “Wall-modeled large-eddy simulation for complex turbulent flows,” Annual review of fluid mechanics **50**, 535–561 (2018).

⁷P. R. Spalart, “Detached-eddy simulation,” Annual review of fluid mechanics **41**, 181–202 (2009).

⁸L. Sciacovelli, A. Cannici, D. Passiatore, and P. Cinnella, “A priori tests of turbulence models for compressible flows,” International Journal of Numerical Methods for Heat & Fluid Flow (2023).

⁹Y. Marchenay, M. Olazabal Loumé, and F. Chedevigne, “Hypersonic turbulent flow reynolds-averaged navier–stokes simulations with roughness and blowing effects,” Journal of Spacecraft and Rockets **59**, 1686–1696 (2022).

¹⁰J. G. Marvin, “Turbulence modeling for computational aerodynamics,” AIAA Journal **21**, 941–955 (1983).

¹¹J. G. Marvin and T. J. Coakley, “Turbulence modeling for hypersonic flows,” Tech. Rep. (1989).

¹²C. J. Roy and F. G. Blottner, “Review and assessment of turbulence models for hypersonic flows,” Progress in aerospace sciences **42**, 469–530 (2006).

¹³P. Spalart and S. Allmaras, “A one-equation turbulence model for aerodynamic flows,” in *30th aerospace sciences meeting and exhibit* (1992) p. 439.

¹⁴G. Settles and L. Dodson, “Hypersonic shock/boundary-layer interaction database,” Tech. Rep. (NASA CR 177577, 1991).

¹⁵J. G. Marvin, J. L. Brown, and P. A. Gnoffo, “Experimental database with baseline cfd solutions: 2-d and axisymmetric hypersonic shock-wave/turbulent-boundary-layer interactions,” Tech. Rep. (2013).

¹⁶J. Bardina, T. Coakley, and J. Marvin, “Two-equation turbulence modeling for 3-d hypersonic flows,” in *AIAA 4th International Aerospace Planes Conference* (1992) p. 5064.

¹⁷J. Bardina, “Three-dimensional navier-stokes method with two-equation turbulence models for efficient numerical simulation of hypersonic flows,” in *30th Joint Propulsion Conference and Exhibit* (1994) p. 2950.

¹⁸L. Smits, P. Martin, and S. Girimaji, “Current status of basic research in hypersonic turbulence,” in *47th AIAA Aerospace Sciences Meeting including The New Horizons Forum and Aerospace Exposition* (2009) p. 151.

¹⁹N. J. Georgiadis, D. A. Yoder, M. A. Vyas, and W. A. Engblom, “Status of turbulence modeling for hypersonic propulsion flowpaths,” Theoretical and Computational Fluid Dynamics **28**, 295–318 (2014).

²⁰P. A. Gnoffo, S. A. Berry, and J. W. Van Norman, “Uncertainty assessments of hypersonic shock wave-turbulent boundary-layer interactions at compression corners,” Journal of Spacecraft and Rockets **50**, 69–95 (2013).

²¹J. Brown, “Turbulence model validation for hypersonic flows,” in *8th AIAA/ASME Joint Thermophysics and Heat Transfer Conference* (2002) p. 3308.

²²T. T. Aiken, I. D. Boyd, L. Duan, and J. Huang, “Assessment of reynolds averaged navier-stokes models for a hypersonic cold-wall turbulent boundary layer,” in *AIAA SciTech 2022 Forum* (2022) p. 0586.

²³J. Huang, J.-V. Bretzke, and L. Duan, “Assessment of turbulence models in a hypersonic cold-wall turbulent boundary layer,” Fluids **4**, 37 (2019).

²⁴C. L. Rumsey, “Compressibility considerations for kw turbulence models in hypersonic boundary-layer applications,” Journal of Spacecraft and Rockets **47**, 11–20 (2010).

²⁵A. Smith and T. Cebeci, *Numerical solution of the turbulent-boundary-layer equations* (Douglas Aircraft Company, Douglas Aircraft Division, 1967).

²⁶B. Baldwin and H. Lomax, “Thin-layer approximation and algebraic model for separated turbulentflows,” in *16th aerospace sciences meeting* (1978) p. 257.

²⁷F. R. Menter, “Two-equation eddy-viscosity turbulence models for engineering applications,” AIAA journal **32**, 1598–1605 (1994).

²⁸D. Passiatore, L. Sciacovelli, P. Cinnella, and G. Pascazio, “Finite-rate chemistry effects in turbulent hypersonic boundary layers: A direct nu-

¹J. D. Anderson, *Hypersonic and high temperature gas dynamics* (Aiaa, 1989).

²P. Moin and K. Mahesh, “Direct numerical simulation: a tool in turbulence research,” Annual review of fluid mechanics **30**, 539–578 (1998).

- merical simulation study,” *Physical Review Fluids* **6**, 054604 (2021).
- ²⁹D. Passiatore, L. Sciacovelli, P. Cinnella, and G. Pascazio, “Thermochemical non-equilibrium effects in turbulent hypersonic boundary layers,” *Journal of Fluid Mechanics* **941**, A21 (2022).
- ³⁰G. V. Candler, “Rate effects in hypersonic flows,” *Annual Review of Fluid Mechanics* **51**, 379–402 (2019).
- ³¹C. Park, “Nonequilibrium hypersonic aerothermodynamics,” (1989).
- ³²N. J. Georgiadis, M. R. Mankbadi, and M. A. Vyas, “Turbulence model effects on rans simulations of the hifire flight 2 ground test configurations,” in *52nd Aerospace Sciences Meeting* (2014) p. 0624.
- ³³R. D. Bowersox, “Extension of equilibrium turbulent heat flux models to high-speed shear flows,” *Journal of fluid mechanics* **633**, 61–70 (2009).
- ³⁴R. D. Bowersox and S. W. North, “Algebraic turbulent energy flux models for hypersonic shear flows,” *Progress in Aerospace Sciences* **46**, 49–61 (2010).
- ³⁵J. Urzay and M. Di Renzo, “Engineering aspects of hypersonic turbulent flows at suborbital enthalpies,” *Annual Research Briefs, Center for Turbulence Research*, 7–32 (2021).
- ³⁶M. Di Renzo and J. Urzay, “Direct numerical simulation of a hypersonic transitional boundary layer at suborbital enthalpies,” *Journal of Fluid Mechanics* **912** (2021).
- ³⁷P. S. Volpiani, “Numerical strategy to perform direct numerical simulations of hypersonic shock/boundary-layer interaction in chemical nonequilibrium,” *Shock Waves* **31**, 361–378 (2021).
- ³⁸D. Passiatore, L. Sciacovelli, P. Cinnella, and G. Pascazio, “Shock impingement on a transitional hypersonic high-enthalpy boundary layer,” *Physical Review Fluids* **8**, 044601 (2023).
- ³⁹M. Di Renzo, C. Williams, and S. Pirozzoli, “Stagnation enthalpy effects on hypersonic turbulent compression corner flow at moderate reynolds numbers,” *Physical Review Fluids* **9**, 033401 (2024).
- ⁴⁰K. Duraisamy, G. Iaccarino, and H. Xiao, “Turbulence modeling in the age of data,” *Annual review of fluid mechanics* **51**, 357–377 (2019).
- ⁴¹L. Duan and M. P. Martin, “Assessment of turbulence-chemistry interaction in hypersonic turbulent boundary layers,” *AIAA journal* **49**, 172–184 (2011).
- ⁴²J. Huang, G. L. Nicholson, L. Duan, M. M. Choudhari, and R. D. Bowersox, “Simulation and modeling of cold-wall hypersonic turbulent boundary layers on flat plate,” in *AIAA Scitech 2020 Forum* (2020) p. 0571.
- ⁴³C. Horstman and F. Owen, “Turbulent properties of a compressible boundary layer,” *AIAA Journal* **10**, 1418–1424 (1972).
- ⁴⁴F. Owen and C. Horstman, “On the structure of hypersonic turbulent boundary layers,” *Journal of Fluid Mechanics* **53**, 611–636 (1972).
- ⁴⁵F. Owen, C. Horstman, and M. Kussoy, “Mean and fluctuating flow measurements of a fully-developed, non-adiabatic, hypersonic boundary layer,” *Journal of Fluid Mechanics* **70**, 393–413 (1975).
- ⁴⁶V. Mikulla and C. C. Horstman, “Turbulence measurements in hypersonic shock-wave boundary-layer interaction flows,” *AIAA Journal* **14**, 568–575 (1976).
- ⁴⁷D. Sahoo, M. Schultze, and A. Smits, “Effects of roughness on a turbulent boundary layer in hypersonic flow,” in *39th AIAA Fluid Dynamics Conference* (2009) p. 3678.
- ⁴⁸M. L. Baumgartner, *Turbulence structure in a hypersonic boundary layer* (Princeton University, 1997).
- ⁴⁹C. McGinley, E. Spina, and M. Sheplak, “Turbulence measurements in a mach 11 helium boundary layer,” in *Fluid Dynamics Conference* (1994) p. 2364.
- ⁵⁰R. So, T. Gatski, and T. Sommer, “Morkovin hypothesis and the modeling of wall-bounded compressible turbulent flows,” *AIAA journal* **36**, 1583–1592 (1998).
- ⁵¹S. B. Pope, “A more general effective-viscosity hypothesis,” *Journal of Fluid Mechanics* **72**, 331–340 (1975).
- ⁵²J. Boussinesq, *Essai sur la théorie des eaux courantes* (Imprimerie nationale, 1877).
- ⁵³X. Chen, J. Gan, and L. Fu, “An improved baldwin–lomax algebraic wall model for high-speed canonical turbulent boundary layers using established scalings,” *Journal of Fluid Mechanics* **987**, A7 (2024).
- ⁵⁴A. D. Dilley and C. R. McClinton, “Evaluation of cfd turbulent heating prediction techniques and comparison with hypersonic experimental data,” *Tech. Rep.* (2001).
- ⁵⁵K. Hejranfar, V. Esfahanian, and R. Kamali-Moghadam, “Dual-code solution procedure for efficient computing equilibrium hypersonic axisymmetric transitional/turbulent flows,” *Aerospace Science and Technology* **21**, 64–74 (2012).
- ⁵⁶C. Horstman, “Prediction of hypersonic shock-wave/turbulent-boundary-layer interaction flows,” in *19th AIAA, Fluid Dynamics, Plasma Dynamics, and Lasers Conference* (1987) p. 1367.
- ⁵⁷N. Narayanswami, C. HORSTMAN, and D. KNIGHT, “Numerical simulation of crossing/turbulent boundary layer interaction at mach 8.3 comparison of zero and two-equation turbulence models,” in *31st Aerospace Sciences Meeting* (1993) p. 779.
- ⁵⁸A. G. Panaras, “Turbulence modeling of flows with extensive crossflow separation,” *Aerospace* **2**, 461–481 (2015).
- ⁵⁹J. Hu and A. Rizzi, “Turbulent flow in supersonic and hypersonic nozzles,” *AIAA journal* **33**, 1634–1640 (1995).
- ⁶⁰S. KIM and G. HARLOFF, “Hypersonic turbulent wall boundary layer computations,” in *24th Joint Propulsion Conference* (1988) p. 2829.
- ⁶¹H. McDonald and F. Camarata, “An extended mixing length approach for computing the turbulent boundary layer development,” in *Proceedings, Stanford Conference on Computation of Turbulent Boundary Layers*, Vol. 1 (1968) pp. 83–98.
- ⁶²W.-F. Ng, K. Ajmani, and A. Taylor III, “Turbulence modeling in a hypersonic inlet,” *AIAA journal* **27**, 1354–1360 (1989).
- ⁶³U. Goldberg, P. Batten, S. Palaniswamy, S. Chakravarthy, and O. Peromian, “Hypersonic flow predictions using linear and nonlinear turbulence closures,” *Journal of Aircraft* **37**, 671–675 (2000).
- ⁶⁴F. Menter, “Eddy viscosity transport equations and their relation to the $k-\epsilon$ model,” *Journal of Fluids Engineering* **119**, 876–884 (1997).
- ⁶⁵R. Paciorni, W. Dieudonne, G. Degrez, J.-M. Charbonnier, H. Deconinck, R. Paciorni, W. Dieudonne, G. Degrez, J.-M. Charbonnier, and H. Deconinck, “Validation of the spalart-allmaras turbulence model for application in hypersonic flows,” in *28th Fluid Dynamics Conference* (1997) p. 2023.
- ⁶⁶R. Nance and H. Hassan, “Turbulence modeling of shock-dominated flows with a k -zeta formulation,” in *37th Aerospace Sciences Meeting and Exhibit* (1999) p. 153.
- ⁶⁷X. Xiao, H. A. Hassan, and R. A. Baurle, “Modeling scramjet flows with variable turbulent prandtl and schmidt numbers,” *AIAA journal* **45**, 1415–1423 (2007).
- ⁶⁸X. Xiao, H. Hassan, J. Edwards, and R. Gaffney Jr, “Role of turbulent prandtl numbers on heat flux at hypersonic mach numbers,” *AIAA journal* **45**, 806–813 (2007).
- ⁶⁹D. Robinson and H. Hassan, “Further development of the $k-\zeta$ (enstrophy) turbulence closure model,” *AIAA journal* **36**, 1825–1833 (1998).
- ⁷⁰T. Coakley, “Turbulence modeling methods for the compressible navier-stokes equations,” in *16th fluid and plasmadynamics conference* (1983) p. 1693.
- ⁷¹B. Smith, “Prediction of hypersonic shock wave turbulent boundary layer interactions with the kl two equation turbulence model,” in *33rd Aerospace Sciences Meeting and Exhibit* (1995) p. 232.
- ⁷²M. Leschziner, “Modelling turbulent separated flow in the context of aerodynamic applications,” *Fluid dynamics research* **38**, 174–210 (2006).
- ⁷³T. SHIH, “A realisable reynolds stress algebraic equation model,” *NASA TM-105993* (1993).
- ⁷⁴F.-S. Lien, “Low-reynolds-number eddy-viscosity modelling based on non-linear stress-strain/vorticity relations,” in *Proc. 3rd Symposium On Engineering Turbulence Modelling and Measurements* (1996) pp. 1–10.
- ⁷⁵M. Holden, “Turbulent boundary layer development on curved compression surfaces,” *Calspan Report No*, 7724–1 (1992).
- ⁷⁶G. Coleman and J. Stollery, “Heat transfer from hypersonic turbulent flow at a wedge compression corner,” *Journal of Fluid Mechanics* **56**, 741–752 (1972).
- ⁷⁷H. Zhang, T. Craft, and H. Iacovides, “Application of linear and nonlinear two-equation turbulence models in hypersonic flows,” *AIAA Journal* **60**, 3472–3486 (2022).
- ⁷⁸T. Craft, H. Iacovides, and J. Yoon, “Progress in the use of non-linear two-equation models in the computation of convective heat-transfer in impinging and separated flows,” *Flow, Turbulence and Combustion* **63**, 59–80 (2000).
- ⁷⁹T. Craft, B. Launder, and K. Suga, “Development and application of a cubic eddy-viscosity model of turbulence,” *International Journal of Heat*

- and Fluid Flow **17**, 108–115 (1996).
- ⁸⁰S. Wallin and A. V. Johansson, “An explicit algebraic reynolds stress model for incompressible and compressible turbulent flows,” *Journal of fluid mechanics* **403**, 89–132 (2000).
- ⁸¹E. Schülein, “Skin friction and heat flux measurements in shock/boundary layer interaction flows,” *AIAA journal* **44**, 1732–1741 (2006).
- ⁸²I. Lindblad, S. Wallin, A. Johansson, R. Friedrich, R. Lechner, P. Krogmann, E. Schuelein, J.-C. Courty, M. Ravachol, and D. Giordano, “A prediction method for high speed turbulent separated flows with experimental verification,” in *29th AIAA, Fluid Dynamics Conference* (1998) p. 2547.
- ⁸³J. B. Vemula and K. Sinha, “Explicit algebraic reynolds stress model for shock-dominated flows,” *International Journal of Heat and Fluid Flow* **85**, 108680 (2020).
- ⁸⁴K. Sinha, K. Mahesh, and G. V. Candler, “Modeling shock unsteadiness in shock/turbulence interaction,” *Physics of fluids* **15**, 2290–2297 (2003).
- ⁸⁵P. Rajee and K. Sinha, “Anisotropic sst turbulence model for shock-boundary layer interaction,” *Computers & Fluids* **228**, 105072 (2021).
- ⁸⁶T. Rung, H. Lübcke, M. Franke, L. Xue, F. Thiele, and S. Fu, “Assessment of explicit algebraic stress models in transonic flows,” in *Engineering Turbulence Modelling and Experiments 4* (Elsevier, 1999) pp. 659–668.
- ⁸⁷T. B. Gatski and C. G. Speziale, “On explicit algebraic stress models for complex turbulent flows,” *Journal of fluid Mechanics* **254**, 59–78 (1993).
- ⁸⁸C. G. Speziale, S. Sarkar, and T. B. Gatski, “Modelling the pressure-strain correlation of turbulence: an invariant dynamical systems approach,” *Journal of fluid mechanics* **227**, 245–272 (1991).
- ⁸⁹D. C. Wilcox *et al.*, *Turbulence modeling for CFD*, Vol. 2 (DCW industries La Canada, CA, 1998).
- ⁹⁰A. Bosco, B. Reinartz, L. Brown, and R. Boyce, “Investigation of a compression corner at hypersonic conditions using a reynolds stress model,” in *17th AIAA International Space Planes and Hypersonic Systems and Technologies Conference* (2011) p. 2217.
- ⁹¹S. Frauholz, A. Bosco, B. U. Reinartz, S. Müller, and M. Behr, “Investigation of hypersonic intakes using reynolds stress modeling and wavelet-based adaptation,” *AIAA journal* **52**, 2765–2781 (2014).
- ⁹²B. Eisfeld and O. Brodersen, “Advanced turbulence modelling and stress analysis for the dlr-f6 configuration,” in *23rd AIAA Applied Aerodynamics Conference* (2005) p. 4727.
- ⁹³G. Gerolymos, C. Lo, I. Vallet, and B. Younis, “Term-by-term analysis of near-wall second-moment closures,” *AIAA journal* **50**, 2848–2864 (2012).
- ⁹⁴G. Gerolymos and I. Vallet, “Wall-normal-free near-wall reynolds-stress model for 3-d turbomachinery flows,” *AIAA Journal* **40**, 199208 (2002).
- ⁹⁵G. A. Gerolymos, E. Sauret, and I. Vallet, “Contribution to single-point closure reynolds-stress modelling of inhomogeneous flow,” *Theoretical and Computational Fluid Dynamics* **17**, 407–431 (2004).
- ⁹⁶L. Duan, “Nasa turbulence modeling resource,” https://turbmodels.larc.nasa.gov/Other_DNS_Data/highspeed_curvedwalls.html (2024), last accessed on December 18, 2024.
- ⁹⁷G. L. Nicholson, L. Duan, and N. J. Bisek, “Direct numerical simulation database of high-speed flow over parameterized curved walls,” *AIAA Journal* **62**, 2095–2118 (2024).
- ⁹⁸G. Colonna, M. Tuttafesta, and D. Giordano, “Numerical methods to solve euler equations in one-dimensional steady nozzle flow,” *Computer physics communications* **138**, 213–221 (2001).
- ⁹⁹C. Park, R. L. Jaffe, and H. Partridge, “Chemical-kinetic parameters of hyperbolic earth entry,” *Journal of Thermophysics and Heat transfer* **15**, 76–90 (2001).
- ¹⁰⁰C. Park, “Two-temperature interpretation of dissociation rate data for N₂ and O₂,” in *26th Aerospace Sciences Meeting* (1988) p. 458.
- ¹⁰¹S. Sarkar, G. Erlebacher, M. Y. Hussaini, and H. O. Kreiss, “The analysis and modelling of dilatational terms in compressible turbulence,” *Journal of Fluid Mechanics* **227**, 473–493 (1991).
- ¹⁰²O. Zeman, “Dilatation dissipation: the concept and application in modeling compressible mixing layers,” *Physics of Fluids A: Fluid Dynamics* **2**, 178–188 (1990).
- ¹⁰³D. C. Wilcox, “Dilatation-dissipation corrections for advanced turbulence models,” *AIAA journal* **30**, 2639–2646 (1992).
- ¹⁰⁴C. Zhang, L. Duan, and M. M. Choudhari, “Direct numerical simulation database for supersonic and hypersonic turbulent boundary layers,” *AIAA journal* **56**, 4297–4311 (2018).
- ¹⁰⁵F. Grasso and D. Falconi, “High-speed turbulence modeling of shock-wave/boundary-layer interaction,” *AIAA journal* **31**, 1199–1206 (1993).
- ¹⁰⁶C. G. Speziale and S. Sarkar, “A preliminary compressible second-order closure model for high speed flows,” *Tech. Rep.* (1989).
- ¹⁰⁷S. Sarkar, “The pressure–dilatation correlation in compressible flows,” *Physics of Fluids A: Fluid Dynamics* **4**, 2674–2682 (1992).
- ¹⁰⁸P. Huang and T. Coakley, “Calculations of supersonic and hypersonic flows using compressible wall functions,” in *Engineering Turbulence Modelling and Experiments* (Elsevier, 1993) pp. 731–739.
- ¹⁰⁹P. Huang and T. Coakley, “Turbulence modeling for complex hypersonic flows,” in *31st Aerospace Sciences Meeting* (1993) p. 200.
- ¹¹⁰V. K. Veera and K. Sinha, “Modeling the effect of upstream temperature fluctuations on shock/homogeneous turbulence interaction,” *Physics of fluids* **21** (2009).
- ¹¹¹H. Rathi and K. Sinha, “Simulation of hypersonic shock-boundary layer interaction using shock-strength dependent turbulence model,” *AIAA Journal*, 1–14 (2024).
- ¹¹²S. Catris and B. Aupoix, “Density corrections for turbulence models,” *Aerospace Science and Technology* **4**, 1–11 (2000).
- ¹¹³R. Pecnik and A. Patel, “Scaling and modelling of turbulence in variable property channel flows,” *Journal of Fluid Mechanics* **823**, R1–1–11 (2017).
- ¹¹⁴G. Otero, A. Patel, R. Diez, and R. Pecnik, “Turbulence modelling for flows with strong variations in thermo-physical properties,” *Journal of Heat and Fluid Flow* **823**, R1 (2018).
- ¹¹⁵A. M. Hasan, J. Larsson, S. Pirozzoli, and R. Pecnik, “Incorporating intrinsic compressibility effects in velocity transformations for wall-bounded turbulent flows,” *Physical Review Fluids* **8**, L112601 (2023).
- ¹¹⁶J. Huang, L. Duan, and M. M. Choudhari, “Direct numerical simulation of hypersonic turbulent boundary layers: effect of spatial evolution and reynolds number,” *Journal of Fluid Mechanics* **937**, A3 (2022).
- ¹¹⁷P. Gnoffo, S. Berry, and J. Van Norman, “Uncertainty assessments of 2d and axisymmetric hypersonic shock wave-turbulent boundary layer interaction simulations at compression corners,” in *42nd AIAA thermophysics conference* (2011) p. 3142.
- ¹¹⁸T. Maeder, N. A. Adams, and L. Kleiser, “Direct simulation of turbulent supersonic boundary layers by an extended temporal approach,” *Journal of Fluid Mechanics* **429**, 187–216 (2001).
- ¹¹⁹L. Duan, I. Beekman, and M. Martin, “Direct numerical simulation of hypersonic turbulent boundary layers. part 2. effect of wall temperature,” *Journal of Fluid Mechanics* **655**, 419–445 (2010).
- ¹²⁰L. Duan, I. Beekman, and M. Martin, “Direct numerical simulation of hypersonic turbulent boundary layers. part 3. effect of mach number,” *Journal of Fluid Mechanics* **672**, 245–267 (2011).
- ¹²¹X. Liang, “Dns and analysis of a spatially evolving hypersonic turbulent boundary layer over a flat plate at mach 8,” *SCIENTIA SINICA Physica, Mechanica & Astronomica* **42**, 282 (2012).
- ¹²²X. Liang and X. Li, “Dns of a spatially evolving hypersonic turbulent boundary layer at mach 8,” *Science China Physics, Mechanics and Astronomy* **56**, 1408–1418 (2013).
- ¹²³G. Nicholson, *Simulation and Modeling of Hypersonic Turbulent Boundary Layers Subject to Favorable and Adverse Pressure Gradients Due to Streamline Curvature*, Ph.D. thesis, Ohio State University (2024).
- ¹²⁴S. Roy and K. Sinha, “Turbulent heat flux model for hypersonic shock-boundary layer interaction,” *AIAA Journal* **57**, 3624–3629 (2019).
- ¹²⁵S. Roy, U. Pathak, and K. Sinha, “Variable turbulent prandtl number model for shock/boundary-layer interaction,” *AIAA Journal* **56**, 342–355 (2018).
- ¹²⁶M. E. Danis and P. Durbin, “Compressibility correction to k- ω models for hypersonic turbulent boundary layers,” *AIAA Journal* **60**, 6225–6234 (2022).
- ¹²⁷M. Barone, E. Parish, and C. Jordan, “Data-Driven Modifications to the Spalart–Allmaras Turbulence Model for Supersonic and Hypersonic Boundary Layers,” in *AIAA SciTech* (2024).
- ¹²⁸H. S. Ribner, *Convection of a pattern of vorticity through a shock wave*, Vol. 1164 (NACA, 1954).
- ¹²⁹J. Ryu and D. Livescu, “Turbulence structure behind the shock in canonical shock–vortical turbulence interaction,” *Journal of Fluid Mechanics* **756**, R1 (2014).
- ¹³⁰S. K. Lele, “Shock-jump relations in a turbulent flow,” *Physics of Fluids A: Fluid Dynamics* **4**, 2900–2905 (1992).

- ¹³¹G. P. Zank, Y. Zhou, W. H. Matthaeus, and W. Rice, "The interaction of turbulence with shock waves: A basic model," *Physics of Fluids* **14**, 3766–3774 (2002).
- ¹³²L. Jacquin, C. Cambon, and E. Blin, "Turbulence amplification by a shock wave and rapid distortion theory," *Physics of Fluids A: Fluid Dynamics* **5**, 2539–2550 (1993).
- ¹³³J. Griffond and O. Souldard, "Evolution of axisymmetric weakly turbulent mixtures interacting with shock or rarefaction waves," *Physics of Fluids* **24** (2012).
- ¹³⁴L. Howarth, *Modern developments in fluid dynamics : high speed flow*, The Oxford engineering science series (Oxford at the Clarendon Press, 1953).
- ¹³⁵J. D. Schwarzkopf, D. Livescu, J. R. Baltzer, R. A. Gore, and J. Ristorcelli, "A two-length scale turbulence model for single-phase multi-fluid mixing," *Flow, Turbulence and Combustion* **96**, 1–43 (2016).
- ¹³⁶C. H. Chen and D. A. Donzis, "Shock-turbulence interactions at high turbulence intensities," *Journal of Fluid Mechanics* **870**, 813–847 (2019).
- ¹³⁷F. Lacombe, S. Roy, K. Sinha, S. Karl, and J.-P. Hickey, "Characteristic scales in shock-turbulence interaction," *AIAA Journal* **59**, 526–532 (2021).
- ¹³⁸N. Braun and R. Gore, "On primitive variable behaviour near shocks in ensemble-averaged methods," *Journal of Turbulence* **19**, 868–888 (2018).
- ¹³⁹K. Sinha, K. Mahesh, and G. V. Candler, "Modeling shock unsteadiness in shock/turbulence interaction," *Physics of fluids* **15**, 2290–2297 (2003).
- ¹⁴⁰Z. Zhang, Z. Gao, C. Jiang, and C.-H. Lee, "A rans model correction on unphysical over-prediction of turbulent quantities across shock wave," *International Journal of Heat and Mass Transfer* **106**, 1107–1119 (2017).
- ¹⁴¹C. Prasad and D. V. Gaitonde, "Turbulence modeling of 3d high-speed flows with upstream-informed corrections," *Shock Waves* **33**, 99–115 (2023).
- ¹⁴²Z. Zhang, Z. Gao, C. Jiang, and C.-H. Lee, "A rans model correction on unphysical over-prediction of turbulent quantities across shock wave," *International Journal of Heat and Mass Transfer* **106**, 1107–1119 (2017).
- ¹⁴³Y. Tian, Z. Gao, C. Jiang, and C.-H. Lee, "A correction for reynolds-averaged-navier-stokes turbulence model under the effect of shock waves in hypersonic flows," *International Journal for Numerical Methods in Fluids* **95**, 313–333 (2023).
- ¹⁴⁴J. B. Vemula and K. Sinha, "Reynolds stress models applied to canonical shock-turbulence interaction," *Journal of Turbulence* **18**, 653–687 (2017).
- ¹⁴⁵S. Karl, J.-P. Hickey, and F. Lacombe, "Reynolds stress models for shock-turbulence interaction," in *31st International Symposium on Shock Waves 1: Fundamentals 31* (Springer, 2019) pp. 511–517.
- ¹⁴⁶M. Holden, T. Wadhams, M. MacLean, and E. Mundy, "Experimental studies of shock wave/turbulent boundary layer interaction in high reynolds number supersonic and hypersonic flows to evaluate the performance of cfd codes," in *40th fluid dynamics conference and exhibit* (2010) p. 4468.
- ¹⁴⁷M. Kandula and D. Wilcox, "An examination of k-omega turbulence model for boundary layers, free shear layers and separated flows," in *Fluid dynamics conference* (1995) p. 2317.
- ¹⁴⁸E. Parish, M. Barone, D. Ching, C. Jordan, N. Miller, G. Nicholson, K. Gitushi, S. Beresh, N. Gupta, and K. Duraisamy, "Data-driven closure modeling for hypersonic turbulent flows," *Tech. Rep.* (Sandia National Laboratories, 2024).
- ¹⁴⁹P. Huang, P. Bradshaw, and T. Coakley, "Turbulence models for compressible boundary layers," *AIAA journal* **32**, 735–740 (1994).
- ¹⁵⁰J.-J. Hoste, N. Gibbons, T. Ecker, C. Amato, D. Knight, A. Sattarov, O. Thiry, J.-P. Hickey, F. Hızir, T. Köktürk, N. Castelino, V. Viti, M. Roldan, S. Qiang, J. Coder, R. Baurle, and J. White, "A review of RANS modeling for hypersonic large cone-flares," *Physics of Fluids (under review)* (2024).
- ¹⁵¹T. Coakley, C. Horstman, J. Marvin, J. Viegas, J. Bardina, P. Huang, and M. Kossov, "Turbulence compressibility corrections," *Tech. Rep.* (1994).
- ¹⁵²S. Roy and K. Sinha, "Turbulent heat flux model for hypersonic shock-boundary layer interaction," *AIAA Journal* **57**, 3624–3629 (2019).
- ¹⁵³S. Prince, M. Vannahme, and J. Stollery, "Experiments on the hypersonic turbulent shock-wave/boundary-layer interaction and the effects of surface roughness," *The Aeronautical Journal* **109**, 177–184 (2005).
- ¹⁵⁴M. Holden, T. Wadhams, and E. Mundy, "A review of experimental studies of surface roughness and blowing on the heat transfer and skin friction to nosetips and slender cones in high mach numbers flows," in *40th Thermophysics Conference* (2008) p. 3907.
- ¹⁵⁵S. Peltier, R. Humble, and R. Bowersox, "Crosshatch roughness distortions on a hypersonic turbulent boundary layer," *Physics of Fluids* **28** (2016).
- ¹⁵⁶D. E. Berg, *Surface roughness effects on the hypersonic turbulent boundary layer*. (California Institute of Technology, 1977).
- ¹⁵⁷M. Finson and A. Clarke, "The effect of surface roughness character on turbulent re-entry heating," in *15th Thermophysics Conference* (1980) p. 1459.
- ¹⁵⁸B. Aupoix, "Roughness corrections for the k- ω shear stress transport model: Status and proposals," *Journal of Fluids Engineering* **137**, 021202 (2015).
- ¹⁵⁹F. E. Goddard Jr, "Effect of uniformly distributed roughness on turbulent skin-friction drag at supersonic speeds," *Journal of the Aerospace Sciences* **26**, 1–15 (1959).
- ¹⁶⁰T. Lin and R. Bywater, "Turbulence models for high-speed, rough-wall boundary layers," *AIAA Journal* **20**, 325–333 (1982).
- ¹⁶¹B. Aupoix, "Improved heat transfer predictions on rough surfaces," *International Journal of Heat and Fluid Flow* **56**, 160–171 (2015).
- ¹⁶²M. Olazabal-Loumé, F. Danvin, J. Mathiaud, B. Aupoix, and O. Toulouse, "Study on k- ω shear stress transport model corrections applied to rough wall turbulent hypersonic boundary layers," in *Seventh European Conference for Aeronautics and Space Sciences* (2017).
- ¹⁶³M. Olazabal-Loumé, F. Chedevergne, F. Danvin, and J. Mathiaud, "Roughness corrections applied to the simulation of turbulent hypersonic flows," in *EUCASS 2019* (2019).
- ¹⁶⁴A. Bukva, K. Zhang, N. Christopher, and J.-P. Hickey, "Assessment of turbulence modeling for massively-cooled turbulent boundary layer flows with transpiration cooling," *Physics of Fluids* **33** (2021).
- ¹⁶⁵D. C. Wilcox, "Reassessment of the scale-determining equation for advanced turbulence models," *AIAA journal* **26**, 1299–1310 (1988).
- ¹⁶⁶Y. Marchenay, F. Chedevergne, and M. Olazabal Loumé, "Modeling of combined effects of surface roughness and blowing for reynolds-averaged navier-stokes turbulence models," *Physics of Fluids* **33** (2021).
- ¹⁶⁷D. Spalding, "Concentration fluctuations in a round turbulent free jet," *Chemical Engineering Science* **26**, 95–107 (1971).
- ¹⁶⁸B. E. Launder, "Heat and mass transport," *Turbulence*, 231–287 (2005).
- ¹⁶⁹Y. Tominaga and T. Stathopoulos, "Turbulent schmidt numbers for cfd analysis with various types of flowfield," *Atmospheric Environment* **41**, 8091–8099 (2007).
- ¹⁷⁰P. Marquardt, M. Klaas, and W. Schröder, "Experimental investigation of the turbulent schmidt number in supersonic film cooling with shock interaction," *Experiments in Fluids* **61**, 160 (2020).
- ¹⁷¹Z. Xiang, S. Yang, S. Xie, J. Li, and H. Ren, "Turbulence-chemistry interaction models with finite-rate chemistry and compressibility correction for simulation of supersonic turbulent combustion," *Engineering Applications of Computational Fluid Mechanics* **14**, 1546–1561 (2020).
- ¹⁷²K. Bray, M. Champion, P. Libby, and N. Swaminathan, "Finite rate chemistry and presumed pdf models for premixed turbulent combustion," *Combustion and Flame* **146**, 665–673 (2006).
- ¹⁷³A. Baranwal, D. A. Donzis, and R. D. Bowersox, "Vibrational turbulent prandtl number in flows with thermal non-equilibrium," in *AIAA Scitech 2020 Forum* (2020) p. 2052.
- ¹⁷⁴J. Longo, "Modelling of hypersonic flow phenomena," *Critical Technologies for Hypersonic Vehicle Development Technology-RTO/AVT/VKI Lecture Series*, 10–14 (2004).
- ¹⁷⁵N. N. Mansour, F. Panerai, J. Lachaud, and T. Magin, "Flow mechanics in ablative thermal protection systems," *Annual Review of Fluid Mechanics* **56**, 549–575 (2024).
- ¹⁷⁶S. P. Schneider, "Hypersonic boundary-layer transition with ablation and blowing," *Journal of Spacecraft and Rockets* **47**, 225–237 (2010).
- ¹⁷⁷Z. Yang, S. Wang, and Z. Gao, "Studies on effects of wall temperature variation on heat transfer in hypersonic laminar boundary layer," *International Journal of Heat and Mass Transfer* **190**, 122790 (2022).
- ¹⁷⁸C. Cheng and L. Fu, "Mean temperature scalings in compressible wall turbulence," *Physical Review Fluids* **9**, 054610 (2024).
- ¹⁷⁹M. T. Lewis and J.-P. Hickey, "Conjugate heat transfer in high-speed external flows: A review," *Journal of Thermophysics and Heat Transfer* **37**, 697–712 (2023).

- ¹⁸⁰D. A. Yoder, "Comparison of turbulent thermal diffusivity and scalar variance models," in *54th AIAA aerospace sciences meeting* (2016) p. 1561.
- ¹⁸¹G. Yang, H. Iacovides, T. Craft, and D. Apsley, "RANS model development on temperature variance in conjugate heat transfer," *Journal of Turbulence* **22**, 180–207 (2021).
- ¹⁸²N. Maheu, V. Moureau, and P. Domingo, "Large-eddy simulations of flow and heat transfer around a low-mach number turbine blade," in *THMT-12. Proceedings of the Seventh International Symposium On Turbulence Heat and Mass Transfer* (Begel House Inc., 2012).
- ¹⁸³M. Gelain, *Aerothermal characterisation of a surface heat exchanger implemented in a turbofan by-pass duct*, Ph.D. thesis, Université Paris-Saclay (2021).
- ¹⁸⁴J. A. Muller, M. Dutta, J. Boisvert, and J. C. Oefelein, "Investigation of conjugate heat transfer in wall-modeled large eddy simulation of high-speed compressible wall-bounded flows," in *Turbo Expo: Power for Land, Sea, and Air*, Vol. 88094 (American Society of Mechanical Engineers, 2024) p. V013T13A034.
- ¹⁸⁵J. Muller, J. Boisvert, M. Dutta, and J. Oefelein, "Investigation of loosely-coupled conjugate heat transfer with wall-modeled large eddy simulation in a mach 2.5 flow," in *AIAA AVIATION FORUM AND ASCEND 2024* (2024) p. 4175.
- ¹⁸⁶J. Marvin, "Nasa turbulence modeling resource," https://turbmodels.larc.nasa.gov/Other_exp_Data/sbli_various_marvin_exp.html (2024), last accessed on December 18, 2024.
- ¹⁸⁷A. M. Winkler and M. H. Cha, *Investigation of flat plate hypersonic turbulent boundary layers with heat transfer at a Mach number of 5.2* (NAVORD, 1959).
- ¹⁸⁸E. M. Winkler, "Investigation of flat-plate hypersonic, turbulent boundary layers with heat transfer," *Journal of Applied Mechanics* **28**, 323 (1961).
- ¹⁸⁹J. E. Danberg, "Characteristics of the turbulent boundary layer with heat and mass transfer at $m=6.7$," (1964).
- ¹⁹⁰J. E. Danberg, "Characteristics of the turbulent boundary layer with heat and mass transfer: data tabulation," *NOLTR 675-6* (1967).
- ¹⁹¹F. L. Young, "Experimental investigation of the effects of surface roughness on compressible turbulent boundary layer skin friction and heat transfer," Tech. Rep. (Technical Report DLR-532, CR- 21 Defense Research Laboratory, University of Texas, Austin, 1965).
- ¹⁹²L. Neal Jr, "A study of the pressure, heat transfer, and skin friction on sharp and blunt flat plates at mach 6.8," Tech. Rep. (1966).
- ¹⁹³J. Wallace, "Hypersonic turbulent boundary layer studies at cold wall temperatures," *Proceedings of the 1967 Heat Transfer and Fluid Mechanics Institute held at the University of California, San Diego, La Jolla, California* (1967).
- ¹⁹⁴E. J. Hopkins, *Summary and correlation of skin-friction and heat-transfer data for a hypersonic turbulent boundary layer on simple shapes*, Vol. 5089 (National Aeronautics and Space Administration, 1969).
- ¹⁹⁵R. Voisinot and R. E. Lee, "Measurements of a mach 4.9 zero-pressure-gradient turbulent boundary layer with heat transfer. part 1: Data compilation," Tech. Rep. (Technical Report NOLTR 72-232 (White Oak, Silver Spring, MD: United States Naval Ordnance Laboratory), 1972).
- ¹⁹⁶M. HOLDEN, "Shock wave-turbulent boundary layer interaction in hypersonic flow," in *10th Aerospace Sciences Meeting* (American Institute of Aeronautics and Astronautics, 1972).
- ¹⁹⁷R. Watson, J. Harris, and J. ANDERS, JR, "Measurements in a transitional/turbulent mach 10 boundary layer at high-reynolds numbers," in *11th Aerospace Sciences Meeting* (1973) p. 165.
- ¹⁹⁸C. Goyne, R. Stalker, and A. Paull, "Skin-friction measurements in high-enthalpy hypersonic boundary layers," *Journal of Fluid Mechanics* **485**, 1–32 (2003).
- ¹⁹⁹F. Hill, "Turbulent boundary layer measurements at mach numbers from 8 to 10," *The Physics of Fluids* **2**, 668–680 (1959).
- ²⁰⁰R. E. Lee, W. J. Yanta, and A. C. Leonas, *Velocity Profile, Skin-friction Balance and Heat-transfer Measurements of the Turbulent Boundary Layers at Mach 5 and Zero-pressure Gradient*, Vol. 69 (United States Naval Ordnance Laboratory, 1969).
- ²⁰¹E. Backx, "Measurements in the mach 15 turbulent boundary layer on the wall of the longshot conical nozzle," in *EUROMECH, Colloquium on Heat Transfer in Turbulent Boundary Layers with Variable Fluid Properties, Goettingen, West Germany* (1973).
- ²⁰²E. Backx, "Experimental study of the turbulent boundary layer at mach 15 and 19.8 in a conical nozzle," (1974).
- ²⁰³E. Backx and B. Richards, "A high mach number turbulent boundary-layer study," *AIAA Journal* **14**, 1159–1160 (1976).
- ²⁰⁴R. D. Samuels, J. B. Peterson, and J. B. Adcock, *Experimental investigation of the turbulent boundary layer at a Mach number of 6 with heat transfer at high Reynolds numbers*, Vol. 3858 (National Aeronautics and Space Administration, 1967).
- ²⁰⁵N. Murray, R. Hillier, and S. Williams, "Experimental investigation of axisymmetric hypersonic shock-wave/turbulent-boundary-layer interactions," *Journal of Fluid Mechanics* **714**, 152–189 (2013).
- ²⁰⁶R. Kimmel, "Experimental transition zone lengths in pressure gradient in hypersonic flow," *ASME-PUBLICATIONS-FED* **151**, 117–117 (1993).
- ²⁰⁷R. KIMMEL, "The effect of pressure gradients on transition zone length in hypersonic boundary layers," *Journal of fluids engineering* **119**, 36–41 (1997).
- ²⁰⁸L. Duan, "Nasa turbulence modeling resource," https://turbmodels.larc.nasa.gov/Other_DNS_Data/supersonic_hypersonic_flatplate.html (2024), last accessed on December 18, 2024.
- ²⁰⁹L. Xin-Liang, F. De-Xun, and M. Yan-Wen, "Direct numerical simulation of a spatially evolving supersonic turbulent boundary layer at $ma=6$," *Chinese Physics Letters* **23**, 1519 (2006).
- ²¹⁰M. P. Martin, "Direct numerical simulation of hypersonic turbulent boundary layers. part 1. initialization and comparison with experiments," *Journal of Fluid Mechanics* **570**, 347–364 (2007).
- ²¹¹Y.-B. Chu, Y.-Q. Zhuang, and X.-Y. Lu, "Effect of wall temperature on hypersonic turbulent boundary layer," *Journal of Turbulence* **14**, 37–57 (2013).
- ²¹²L. Duan, M. M. Choudhari, and C. Zhang, "Pressure fluctuations induced by a hypersonic turbulent boundary layer," *Journal of Fluid Mechanics* **804**, 578–607 (2016).
- ²¹³C. Zhang, L. Duan, and M. M. Choudhari, "Effect of wall cooling on boundary-layer-induced pressure fluctuations at mach 6," *Journal of Fluid Mechanics* **822**, 5–30 (2017).
- ²¹⁴L. Sciacovelli, X. Gloerfelt, D. Passiatore, P. Cinnella, and F. Grasso, "Numerical investigation of high-speed turbulent boundary layers of dense gases," *Flow, Turbulence and Combustion* **105**, 555–579 (2020).
- ²¹⁵G. Nicholson, J. Huang, L. Duan, and M. M. Choudhari, "Simulation and modeling of hypersonic turbulent boundary layers subject to adverse pressure gradients due to streamline curvature," in *AIAA Aviation 2021 Forum* (2021) p. 2891.
- ²¹⁶G. Dang, S. Liu, T. Guo, J. Duan, and X. Li, "Direct numerical simulation of compressible turbulence accelerated by graphics processing unit: An open-source high accuracy accelerated computational fluid dynamic software," *Physics of Fluids* **34** (2022).
- ²¹⁷M. T. Aultman, D. Roy, and L. Duan, "Asymptotic near-wall behavior of a mach 6 cold-wall turbulent boundary layer," in *AIAA SCITECH 2024 Forum* (2024) p. 2733.
- ²¹⁸L. Duan and M. Martin, "Direct numerical simulation of hypersonic turbulent boundary layers. part 4. effect of high enthalpy," *Journal of Fluid Mechanics* **684**, 25–59 (2011).
- ²¹⁹C. Appels, "Turbulent boundary layer separation at mach 12," VKI TN-90 (1973).
- ²²⁰M. COET, "Experiments on shock wave/boundary layer interaction in hypersonic flow," *La Recherche Aérospatiale(English Edition)*, 61–74 (1993).
- ²²¹M. I. Kussoy and K. Horstman, "Documentation of two-and three-dimensional shock-wave/turbulent-boundary-layer interaction flows at mach 8.2," NASA Ames Research Center Technical Report (1991).
- ²²²T. Wadhams, E. Mundy, M. MacLean, and M. Holden, "Ground test studies of the hifire-1 transition experiment part 1: experimental results," *Journal of Spacecraft and Rockets* **45**, 1134–1148 (2008).
- ²²³G. Coleman, "A study of hypersonic boundary layers over a family of axisymmetric bodies at zero incidence: preliminary report and data tabulation," Imperial College Aero Report 73-06 Imperial College of Science and Technology, London, UK (1973).
- ²²⁴G. T. Coleman, *Hypersonic turbulent boundary layer studies*, Ph.D. thesis, Imperial College London (1973).
- ²²⁵G. Coleman and J. Stollery, "Incipient separation of axially symmetric hypersonic turbulent boundary layers," *AIAA Journal* **12**, 119–120 (1974).

- ²²⁶M. Holden, T. Wadhams, and M. MacLean, "Measurements in regions of shock wave/turbulent boundary layer interaction on double cone and hollow cylinder/flare configurations for open and," Blind" Code Evaluation/Validation," Tech. rep., American Institute of Aeronautics and Astronautics (2014).
- ²²⁷M. Holden, "Measurements in regions of shock wave/turbulent boundary layer interaction from mach 4 to 7 at flight duplicated velocities to evaluate and improve the models of turbulence in cfd codes," in *2018 Fluid Dynamics Conference* (2018) p. 3706.
- ²²⁸M. Holden, "Studies of the mean and unsteady structure of turbulent boundary layer separation in hypersonic flow," in *22nd Fluid Dynamics, Plasma Dynamics and Lasers Conference* (1991) p. 1778.
- ²²⁹C. L. Running, T. J. Juliano, J. S. Jewell, M. P. Borg, and R. L. Kimmel, "Hypersonic shock-wave/boundary-layer interactions on a cone/flare," *Experimental Thermal and Fluid Science* **109**, 109911 (2019).
- ²³⁰M. Kussoy and C. Horstmann, "An experimental documentation of a hypersonic shock-wave turbulent boundary layer interaction flow: With and without separation," Tech. Rep. (1975).
- ²³¹M. I. Kussoy, *Documentation of two-and three-dimensional hypersonic shock wave/turbulent boundary layer interaction flows*, Vol. 101075 (National Aeronautics and Space Administration, Ames Research Center, 1989).
- ²³²P. Rodi, D. Dolling, and D. Knight, "An experimental/computational study of heat transfer in sharp fin induced turbulent interactions at mach 5," in *22nd Fluid Dynamics, Plasma Dynamics and Lasers Conference* (1991) p. 1764.
- ²³³P. Rodi and D. Dolling, "An experimental/computational study of sharp fin induced shock wave/turbulent boundary layer interactions at mach 5-experimental results," in *30th Aerospace Sciences Meeting and Exhibit* (1992) p. 749.
- ²³⁴P. Rodi and D. Dolling, "Behavior of pressure and heat transfer in sharp fin-induced turbulent interactions," *AIAA journal* **33**, 2013–2019 (1995).
- ²³⁵V. Y. Borovoy, V. Mosharov, A. Y. Noev, and V. Radchenko, "Laminar-turbulent flow over wedges mounted on sharp and blunt plates," *Fluid Dynamics* **44**, 382–396 (2009).
- ²³⁶V. Y. Borovoy, I. V. Egorov, A. Y. Noev, V. N. Radchenko, A. S. Skuratov, and I. V. Struminskaya, "3d shock/turbulent boundary layer interaction on the plate near a wedge in presence of an entropy layer," *TsAGI Science Journal* **43** (2012).
- ²³⁷V. Borovoy, I. Egorov, V. Mosharov, V. Radchenko, A. Skuratov, and I. Struminskaya, "Entropy-layer influence on single-fin and double-fin/boundary-layer interactions," *AIAA Journal* **54**, 443–457 (2016).
- ²³⁸C. H. Law, *Three-dimensional shock wave-turbulent boundary layer interactions at Mach 6*, Vol. 75 (Aerospace Research Laboratories, Air Force Systems Command, United States . . . , 1975).
- ²³⁹M. Holden, "Experimental studies of quasi-two-dimensional and three-dimensional viscous interaction regions induced by skewed-shock and swept-shock boundary layer interaction," in *17th Fluid Dynamics, Plasma Dynamics, and Lasers Conference* (1984) p. 1677.
- ²⁴⁰E. Schülein and A. Zheltovodov, "Documentation of experimental data for hypersonic 3-d shock waves," Report IB 223-99 A 26 Deutsches Zentrum für Luft- und Raumfahrt e.V. (DLR), Institut für Strömungsmechanik, Göttingen, Germany (2001).
- ²⁴¹M. Kussoy, K. Horstoman, and C. Horstman, "Hypersonic crossing shock-wave/turbulent-boundary-layer interactions," *AIAA journal* **31**, 2197–2203 (1993).
- ²⁴²P. S. Volpiani, M. Bernardini, and J. Larsson, "Effects of a nonadiabatic wall on hypersonic shock/boundary-layer interactions," *Physical Review Fluids* **5**, 014602 (2020).
- ²⁴³S. Priebe and M. P. Martín, "Turbulence in a hypersonic compression ramp flow," *Physical Review Fluids* **6**, 034601 (2021).
- ²⁴⁴P. Bookey, C. Wyckham, A. Smits, and P. Martin, "New experimental data of stbl at dns/les accessible reynolds numbers," in *43rd AIAA Aerospace Sciences Meeting and Exhibit* (2005) p. 309.
- ²⁴⁵J. Zhang, T. Guo, G. Dang, and X. Li, "Direct numerical simulation of shock wave/turbulent boundary layer interaction in a swept compression ramp at mach 6," *Physics of Fluids* **34** (2022).
- ²⁴⁶T. Guo, J. Zhang, F. Tong, and X. Li, "Amplification of turbulent kinetic energy and temperature fluctuation in a hypersonic turbulent boundary layer over a compression ramp," *Physics of Fluids* **35** (2023).
- ²⁴⁷T. Fulin, D. Junyi, L. Jiang, S. Dong, and Y. Xianxu, "Hypersonic shock wave and turbulent boundary layer interaction in a sharp cone/flare model," *Chinese Journal of Aeronautics* **36**, 80–95 (2023).
- ²⁴⁸M. Holden, "Experimental studies of surface roughness, entropy swallowing and boundary layer transition effects on the skin friction and heat transfer distribution in high speed flows," in *20th Aerospace Sciences Meeting* (1982) p. 34.
- ²⁴⁹M. Holden, "Studies of surface roughness and blowing effects on hypersonic turbulent boundary layers over slender cones," in *27th Aerospace Sciences Meeting* (1989) p. 458.
- ²⁵⁰H. Babinsky and J. Edwards, "Large-scale roughness influence on turbulent hypersonic boundary layers approaching compression corners," *Journal of spacecraft and rockets* **34**, 70–75 (1997).
- ²⁵¹B. R. Hollis, "Distributed roughness effects on blunt-body transition and turbulent heating," in *52nd Aerospace Sciences Meeting* (2014) p. 0238.
- ²⁵²M. C. Wilder and D. K. Prabhu, "Rough-wall turbulent heat transfer experiments in hypersonic free flight," in *AIAA Aviation 2019 Forum* (2019) p. 3009.
- ²⁵³P. R. Forsyth, C. Hambidge, and M. McGilvray, "Experimental assessment of hypersonic convective heat transfer augmentation due to surface roughness," *Journal of Thermophysics and Heat Transfer* , 1–10 (2024).
- ²⁵⁴P. Collen, L. J. Doherty, S. D. Subiah, T. Sopek, I. Jahn, D. Gildfind, R. Penty Gerats, R. Gollan, C. Hambidge, R. Morgan, *et al.*, "Development and commissioning of the t6 stalker tunnel," *Experiments in Fluids* **62**, 1–24 (2021).
- ²⁵⁵L. Duan, M. Martin, A. Feldick, M. Modest, and D. Levin, "Study of turbulence-radiation interaction in hypersonic turbulent boundary layers," *AIAA journal* **50**, 447–453 (2012).
- ²⁵⁶E. VAN DRIEST, "The problem of aerodynamic heating," *Aeronaut. Eng. Rev.* **15**, 26–41 (1956).
- ²⁵⁷F. White and G. Christoph, "A simple theory for the two-dimensional compressible turbulent boundary layer," *Journal of Fluids Engineering, Transactions of the ASME* **94**, 636 (1972).
- ²⁵⁸D. Spalding and S. Chi, "The drag of a compressible turbulent boundary layer on a smooth flat plate with and without heat transfer," *Journal of Fluid Mechanics* **18**, 117–143 (1964).
- ²⁵⁹E. J. Hopkins and M. Inouye, "An evaluation of theories for predicting turbulent skin friction and heat transfer on flat plates at supersonic and hypersonic mach numbers," *AIAA Journal* **9**, 993–1003 (1971).
- ²⁶⁰V. A. Bhagwandin and P. Martin, "Wall-resolved les of mach 6 bolt-2 hypersonic vehicle," in *AIAA AVIATION 2023 Forum* (2023) p. 3848.
- ²⁶¹C. M. Helm and M. Martín, "Large eddy simulation of two separated hypersonic shock/turbulent boundary layer interactions," *Physical Review Fluids* **7**, 074601 (2022).
- ²⁶²V. A. Bhagwandin and P. Martin, "Les of shock-turbulent boundary layer interaction over a mach 10 hollow cylinder with flare," in *AIAA AVIATION 2021 FORUM* (2021) p. 2820.
- ²⁶³N. Kianvashrad and D. D. Knight, "Large eddy simulation of hypersonic cold wall flat plate," in *AIAA AVIATION 2021 FORUM* (2021) p. 2882.
- ²⁶⁴V. A. Bhagwandin, C. M. Helm, and P. Martin, "Shock-turbulent boundary layer interactions in separated compression corners at mach 10," in *AIAA Scitech 2019 Forum* (2019) p. 1129.
- ²⁶⁵J. Fang, Y. Yao, A. Zheltovodov, and L. Lu, "Large-eddy simulation of a three-dimensional hypersonic shock wave turbulent boundary layer interaction of a single-fin," in *53rd AIAA Aerospace Sciences Meeting* (2015) p. 1062.
- ²⁶⁶J. Fang, Y. Yao, A. A. Zheltovodov, and L. Lu, "Investigation of three-dimensional shock wave/turbulent-boundary-layer interaction initiated by a single fin," *AIAA Journal* **55**, 509–523 (2017).
- ²⁶⁷D. Neeb, D. Saile, and A. Gülhan, "Experimental flow characterization and heat flux augmentation analysis of a hypersonic turbulent boundary layer along a rough surface," in *Proceedings of the 8th European Symposium on Aerothermodynamics for Space Vehicles*, 89873 (2015) pp. 1–15.
- ²⁶⁸B. J. Daly and F. H. Harlow, "Transport equations in turbulence," *Physics of fluids* **13**, 2634–2649 (1970).
- ²⁶⁹K. Abe and K. Suga, "Towards the development of a reynolds-averaged algebraic turbulent scalar-flux model," *International Journal of Heat and Fluid Flow* **22**, 19–29 (2001).
- ²⁷⁰J. K. Shin, J. S. An, Y. D. Choi, Y. C. Kim, and M. S. Kim, "Elliptic relaxation second moment closure for the turbulent heat fluxes," *Journal of*

- Turbulence, N3 (2008).
- ²⁷¹J. Weatheritt, Y. Zhao, R. D. Sandberg, S. Mizukami, and K. Tanimoto, “Data-driven scalar-flux model development with application to jet in cross flow,” *International Journal of Heat and Mass Transfer* **147**, 118931 (2020).
- ²⁷²Y. Zhao, H. D. Akolekar, J. Weatheritt, V. Michelassi, and R. D. Sandberg, “Rans turbulence model development using cfd-driven machine learning,” *Journal of Computational Physics* **411**, 109413 (2020).
- ²⁷³K. Duraisamy, “Perspectives on machine learning-augmented reynolds-averaged and large eddy simulation models of turbulence,” *Physical Review Fluids* **6**, 050504 (2021).
- ²⁷⁴J. Huang, L. Duan, J. Wang, R. Sun, and H. Xiao, “High-mach-number turbulence modeling using machine learning and direct numerical simulation database,” in *55th AIAA Aerospace Sciences Meeting* (2017) p. 0315.
- ²⁷⁵J.-X. Wang, J. Huang, L. Duan, and H. Xiao, “Prediction of Reynolds stresses in high-Mach-number turbulent boundary layers using physics-informed machine learning,” *Theoretical and Computational Fluid Dynamics* **33**, 1–19 (2019).
- ²⁷⁶E. Parish, D. S. Ching, N. E. Miller, S. J. Beresh, and M. F. Barone, “Turbulence modeling for compressible flows using discrepancy tensor-basis neural networks and extrapolation detection,” in *AIAA SciTech 2023 Forum* (2023) p. 2126.
- ²⁷⁷C. Jordan, *Turbulence Model Development for Hypersonic Shock Wave Boundary Layer Interactions*, Ph.D. thesis, North Carolina State University (2023).
- ²⁷⁸E. Parish, D. S. Ching, C. Jordan, G. Nicholson, N. E. Miller, S. Beresh, M. Barone, N. Gupta, and K. Duraisamy, “Data-driven turbulent prandtl number modeling for hypersonic shock–boundary-layer interactions,” *AIAA Journal*, 1–22 (2024).
- ²⁷⁹A. P. Singh, S. Medida, and K. Duraisamy, “Machine-learning-augmented predictive modeling of turbulent separated flows over airfoils,” *AIAA journal* **55**, 2215–2227 (2017).
- ²⁸⁰E. J. Parish and K. Duraisamy, “A paradigm for data-driven predictive modeling using field inversion and machine learning,” *Journal of computational physics* **305**, 758–774 (2016).
- ²⁸¹K. Chowdhary, C. Hoang, K. Lee, J. Ray, V. G. Weirs, and B. Carnes, “Calibrating hypersonic turbulence flow models with the hifire-1 experiment using data-driven machine-learned models,” *Computer Methods in Applied Mechanics and Engineering* **401**, 115396 (2022).
- ²⁸²M. I. Zafar, X. Zhou, C. J. Roy, D. Stelter, and H. Xiao, “Data-driven turbulence modeling approach for cold-wall hypersonic boundary layers,” arXiv preprint arXiv:2406.17446 (2024).
- ²⁸³Y. Fang, Y. Zhao, F. Waschkowski, A. S. Ooi, and R. D. Sandberg, “Toward more general turbulence models via multicase computational-fluid-dynamics-driven training,” *AIAA Journal* **61**, 2100–2115 (2023).
- ²⁸⁴M. J. Rincón, A. Amarloo, M. Reclari, X. I. Yang, and M. Abkar, “Progressive augmentation of reynolds stress tensor models for secondary flow prediction by computational fluid dynamics driven surrogate optimisation,” *International Journal of Heat and Fluid Flow* **104**, 109242 (2023).
- ²⁸⁵S. Cherroud, X. Merle, P. Cinnella, and X. Gloerfelt, “Space-dependent aggregation of stochastic data-driven turbulence models,” arXiv preprint arXiv:2306.16996 (2023).
- ²⁸⁶M. Oulghelou, S. Cherroud, X. Merle, and P. Cinnella, “Machine-learning-assisted blending of data-driven turbulence models,” arXiv preprint arXiv:2410.14431 (2024).
- ²⁸⁷J. L. Brown, “Hypersonic shock wave impingement on turbulent boundary layers: computational analysis and uncertainty,” *Journal of Spacecraft and Rockets* **50**, 96–123 (2013).
- ²⁸⁸A. Smits, N. Matheson, and P. Joubert, “Low-reynolds-number turbulent boundary layers in zero and favorable pressure gradients,” *Journal of ship research* **27**, 147–157 (1983).
- ²⁸⁹H. M. Nagib, K. A. Chauhan, and P. A. Monkewitz, “Approach to an asymptotic state for zero pressure gradient turbulent boundary layers,” *Philosophical Transactions of the Royal Society A: Mathematical, Physical and Engineering Sciences* **365**, 755–770 (2007).
- ²⁹⁰F. M. White and J. Majdalani, *Viscous fluid flow*, Vol. 3 (McGraw-Hill New York, 2006).